UNIVERSITÀ DEGLI STUDI DI PADOVA

DIPARTIMENTO DI INGEGNERIA INDUSTRIALE

CORSO DI LAUREA MAGISTRALE IN INGEGNERIA CHIMICA E DEI PROCESSI INDUSTRIALI

Tesi di Laurea Magistrale in
Ingegneria Chimica e dei Processi Industriali

SYNTHESIS AND CHARACTERIZATION OF PRINTABLE BIOINKS: GELATIN METHACRYLATE COMPOSITE HYDROGELS FOR 3D CULTURE

Relatore: Prof.ssa Elisa Cimetta
Correlatore: Dott. Lorenzo Bova
Ing. Sara Micheli

Laureando: DARIO FALCONE

ANNO ACCADEMICO 2020 – 2021

Riassunto

Il Neuroblastoma è una forma tumorale pediatrica che ha origine da alcune cellule del sistema nervoso periferico. Rappresenta circa il 10% dei tumori solidi nei neonati e nei bambini entro i 15 anni. Nel 90% dei casi il neuroblastoma viene diagnosticato prima dei 5 anni. Alcuni studi fatti su cellule di Neuroblastoma in colture bidimensionali (2D) hanno permesso di ipotizzare che nella progressione metastatica del tumore abbiano un ruolo fondamentale gli esosomi, nano-vescicole rilasciate dalle cellule per scambiarsi informazioni anche a grandi distanze. Per cercare di comprenderli al meglio, un approccio può essere quello di ricreare un microambiente di coltura tridimensionale (3D), molto più simile a quello *"in vivo"*, all'interno del corpo umano. Tale microambiente, dopo essere stato ottimizzato nella forma e nelle dimensioni, può essere utilizzato per studiare il comportamento del Neuroblastoma e il ruolo degli esosomi.

Questo lavoro è focalizzato sulla sintesi, caratterizzazione e validazione di hydrogels semisintetici a base di gelatina di origine animale funzionalizzata con gruppi metacrilici. È stata inoltre esaminata la combinazione di gelatina metacrilata con diversi materiali, di origine sia naturale che sintetica. Tali materiali saranno utilizzabili come inchiostri biocompatibili per la stampa di strutture tridimensionali al fine di studiare l'interazione tra esosomi e cellule tumorali di Neuroblastoma in ambiente 3D.

È stato messo a punto un protocollo di sintesi e purificazione del metacrilato di gelatina che ha permesso di ottenere un prodotto finale sterile e con caratteristiche meccaniche e chimiche compatibili con le applicazioni biologiche. Ne è seguita la caratterizzazione degli hydrogel compositi a base di gelatina metacrilata, per studiare come la combinazione di diversi materiali influisca sulle proprietà finali del materiale, e per ottimizzarne la composizione in conformità con biostampa ed applicazioni biologiche. Infine, la biocompatibilità degli hydrogel è stata testata con successo tramite test di vitalità cellulare.

Abstract

Neuroblastoma is a pediatric cancer that originates from cells of the peripheral nervous system. It accounts for about 10% of solid tumors in infants and children below 15 years of age. In 90% of cases, Neuroblastoma is diagnosed before the age of 5. Preliminary studies on Neuroblastoma cells in two-dimensional (2D) cultures allowed to hypothesize that exosomes, nanosized vesicles released by cells to exchange information even at great distances, play a fundamental role in the metastatic progression of the tumor. To improve our knowledge, a possible approach would be to recreate a three-dimensional (3D) culture microenvironment, resembling more closely what happens *in vivo* within the human body.

This work is focused on the synthesis, characterization and validation of semisynthetic hydrogels with a gelatin base of animal origin, functionalized with methacrylic groups. A combination of different materials, both natural and synthetic, with gelatin methacrylate is also investigated. These composite materials will be used as biocompatible inks for printing three-dimensional structures in order to study Neuroblastoma tumor cells in a 3D environment. Initially, a synthesis and purification protocol of gelatin methacrylate was developed, allowing to obtain a sterile final product with mechanical and chemical characteristics compatible with biological applications. Gelatin methacrylate-based hydrogels are then characterized to investigate how the combination of different materials allows to produce hydrogels with selected properties, according to bioprinting and biological applications. Hydrogels biocompatibility was successfully tested through cell viability tests.

Table of Contents

INTRODUCTION **1**

CHAPTER 1 ..... **3**

1.1 INTRODUCTION TO HYDROGELS **3**

1.1.1 Classification of hydrogels 5

1.1.2 Application fields 7

1.1.3 Neuroblastoma 9

1.2 THREE-DIMENSIONAL BIOPRINTING **10**

1.2.1 Microextrusion 12

1.2.2 Bio-ink 13

1.2.3 Gelatin Methacrylate (GelMA) 14

1.3 AIM OF THE THESIS **16**

CHAPTER 2 ..... **17**

1.1 GELATIN METHACRYLATE SYNTHESIS **17**

2.1.1 Preparation method 18

2.1.2 Purification method 19

2.1.3 Proton Nuclear Magnetic Resonance (H NMR) 20

2.2 GELMA-BASED HYDROGELS: PREPARATION **21**

2.2.1 GelMA 23

2.2.2 Agarose 24

2.2.3 Pluronic F127 25

2.3 GELMA-BASED HYDROGELS: CHARACTERIZATION **27**

2.3.1 Swelling 27

2.3.2 Scanning Electron Microscope 29

2.3.3 Image processing 32

2.4 THREE-DIMENSIONAL BIOPRINTING **33**

2.4.1 G-Code generation 34

2.4.2 3D printing 34
2.4.3 3D printing protocol 36
2.4.4 3D bioprinting with encapsulated cells 39

2.5 BIOLOGICAL VALIDATION 40
2.5 3D cell culture 40
2.5.2 Fluorescent imaging 42

CHAPTER 3 45

3.2 GELMA-BASED HYDROGELS 46
3.2.1 Swelling 47
3.2.2 Porosity evaluation 49

3.3 3D BIOPRINTING 55

3.4 BIOLOGICAL TESTS 58

CONCLUSION 65

APPENDIX 67

A.1 H NMR SPECTRA 67

BIBLIOGRAPHY 71

Introduction

Most research on cancer biology is based on experiments performed with two-dimensional (2D) cell cultures or experiments that involve animal testing; in particular, more than 80% of cancer biologists still rely on results obtained with 2D cell cultures before *in vivo* testing [1]. Of course, 2D cell cultures provide several advantages, such as highly controlled culture conditions, high reproducibility, easy cell observation, established protocols for quantitative measurements, but are also characterized by several limitations. Two-dimensional cell cultures do not faithfully reproduce real cellular conditions in human tissues, since cells are flattened in a single layer, cell-cell and cell-environment contacts are limited, cells migration is constrained and cells polarization is abnormal.

The solution to the low representativeness of 2D models and to the necessity of avoiding test on animals for cancer studies, for tissue engineering and also drug discovery, was identified in the development of three-dimensional (3D) structures for cell culture. Three-dimensional cell cultures (made of natural, synthetic or semisynthetic polymers) are certainly more expensive and laborious, but allow to grow cells in 3D environments, well mimicking the *in vivo* microenvironment of the human body. The aim of this work of thesis, proposed to be the continuation of a previous research [2], concerns the development of 3D polymeric cultures through micro extrusion bioprinting technologies. The biological field of application of this research is Neuroblastoma, a malignant childhood tumor of the sympathetic nervous system that develops from immature nerve cells. In this context, the main objective was to realize 3D cultures of Neuroblastoma cells in order to reproduce cells' movement and clustering phenomena.

Gelatin methacrylate hydrogels were selected as suitable materials for 3D scaffolds realization, according to the defined goals and based on the wide use of the material for similar purposes, as reported in the literature. Gelatin methacrylate hydrogels are semisynthetic materials obtained from porcine gelatin molecules, modified with the introduction of methacrylic groups, and that can swell and retain large amount of water or biological fluids without dissolving and maintaining their original network structure. Gelatine methacrylate hydrogels are conveniently modified with the addition of blending materials, with the aim to combine different properties and therefore tune hydrogel morphology and behaviour. Such materials, chosen according to the final biological applications, are: *i.* agarose, a natural polysaccharide; *ii.* Pluronic F127, a synthetic triblock copolymer.

The thesis is structured in four main sections. In Chapter 1, a brief introduction about hydrogels is provided, involving the main properties, classification and application fields, followed by a brief description of Neuroblastoma. 3D bioprinting technologies are then introduced, and gelatin methacrylate hydrogels are described as suitable materials for 3D bioprinting applications. The goals of the proposed research are finally described.

In Chapter 2, procedures and methods used for project development are described and discussed. Synthesis and purification protocols of gelatin methacrylate and gelatin methacrylate hydrogels are reported, and all the tests used to characterize these materials are explained. Printing and bioprinting protocols developed are reported, and cellular experiments performed are described.

In Chapter 3, results of all the tests performed to characterize both gelatin methacrylate and gelatin methacrylate hydrogels are reported and discussed. Subsequentially, designed structures for 3D bioprinting are shown and discussed, together with the results of all cellular tests performed.

In the final section, general conclusions about the methods applied and the results obtained are drawn, and improvements on the performed procedures are suggested for the continuation of the project.

Chapter 1

State of the art

In this Chapter some fundamental arguments are introduced in order to better understand the project developed in this work of thesis. The subjects treated include a general introduction about hydrogels and their application fields, in particular the biomedical one; a brief description of Neuroblastoma and the tumor microenvironment; the introduction of 3D bioprinting technologies for printing cellular constructs; lastly, an overview on microextrusion bioprinting and bioinks materials. Particular focus will be given to gelatin methacrylate, thanks to its properties that elect it as suitable materials for 3D bioprinting applications.

1.1 Introduction to hydrogels

Hydrogels are solid-based three-dimensional materials composed by a network of polymeric chains, capable of both retaining large amounts of water or biological fluids and of preserving their structure in aqueous conditions. The water retention property is due to the presence of cross-linking points between the polymeric chains, obtained during the gelification process: hydrogels are crosslinked via covalent bonds or physical attraction, either intra- or intermolecular. In chemical hydrogels, covalent bonds connect polymeric chains, while physical hydrogels are characterized by the presence of molecular entanglements or secondary forces (i.e., hydrogen bonds, ionic interactions, Van Der Waals forces). Physical hydrogels are reversible and can be dissolved by varying specific properties of the solvent (i.e., by changing temperature and pH, or with the application of an appropriate stress [3]. Chemical hydrogels are instead irreversible, and the presence of covalent bonds ensures a higher mechanical stability of materials.

The ability of hydrogels to absorb water arises from hydrophilic functional groups attached to the polymeric backbone, while their resistance to dissolution arises from cross-links between network chains [3]. The hydrophilicity of the network is due to the presence of chemical residues such as hydroxylic (-OH), carboxylic (-COOH), amidic (-CONH-), primary amidic (-CONH2), sulphonic (-SO3H), and others that can be found within the polymer backbone or as

lateral chains. Nevertheless, it is also possible to produce hydrogels containing a significant portion of hydrophobic polymers, by blending or copolymerizing hydrophilic and hydrophobic polymers [4].

An important parameter that affects the properties of hydrogels is the degree of crosslinking (X), which is related to the molecular weight of the polymer chain between cross-linking points [4], defined as [5]:

$$X = \frac{M_0}{2\overline{M_c}}$$

where, M_0 is an estimate of the molecular weight of the repeating units, $\overline{M_c}$ is the molecular weight of the polymer chains between cross-links.

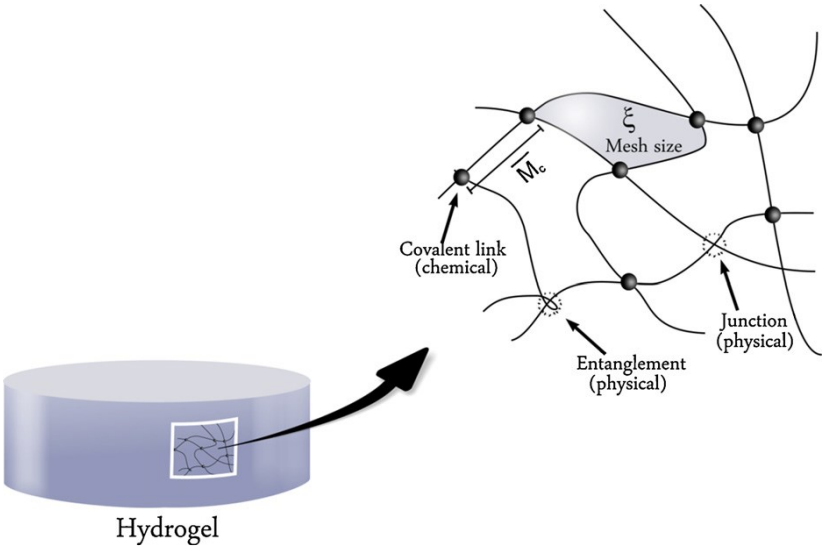

Figure 1.1. *Schematic representation of the cross-linked structure of a hydrogel. M_c is the molecular weight of the polymer chains between cross-links and ξ is the molecular mesh size; adapted from Buenger et al., 2012.*

The degree of crosslinking is responsible for the hydrogel structure, which is made of a mesh network of size ξ (Figure 1.1), whose value returns an estimation of porosity. The mesh contains the solvent and is responsible for the overall elastic forces, which allow both expansion and shrinkage of the gel, within certain limits (i.e., the water content inside hydrogels ranges from at least 10% of the total weight or volume, up to and even beyond 90% [3]. The network deformation allows the solvent to migrate in the gel. The concurrent deformation of the network and migration of the solvent is known as poroelasticity [6]. According to the Flory-Rehner theory [7], a crosslinked polymer gel, which is immersed in a fluid and allowed to reach equilibrium with its surroundings, is subject only to two opposing forces, the thermodynamic

force of mixing and the retractive force of the polymer chains. At equilibrium, these two forces are equal [8]. The adjustments of three-dimensional crosslinked hydrophilic polymer networks make hydrogels capable of the so-called swelling or de-swelling, reversibly in water and retaining large volume of liquid in swollen state. In general, hydrogels are particularly suitable for biomedical and tissue engineering applications [9–12] because of their ability to simulate biological tissues [13,14], and gained increased applications in bioseparations, agriculture and enhanced oil recovery [15–17].

Hydrogels can be designed with controllable responses as to shrink or expand with changes in external environmental conditions. They may perform dramatic volume transition in response to a variety of physical and chemical stimuli (Figure 1.2). Physical stimuli include temperature, electric or magnetic field, light, pressure, and sound, while chemical stimuli include pH, solvent composition, ionic strength, and molecular species [3].

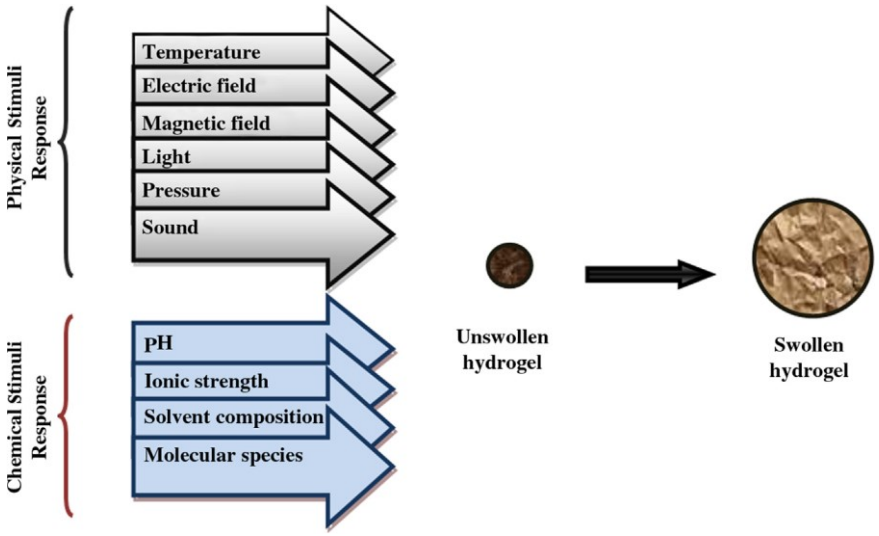

Figure 1.2. *Stimuli response swelling hydrogel; adapted from Enas M. Ahmed, 2015.*

1.1.1 Classification of hydrogels

The classification of hydrogels depends on several factors, such as physical properties, swelling capability, preparation method, origin, ionic charge, biodegradability, cross-linking type.

As previously stated, the origin of a polymer is a factor that allows the distinction between natural and synthetic hydrogels. Hydrogel-forming natural polymers include proteins such as collagen and gelatine and polysaccharides such as starch, alginate, and agarose [3]. Despite biocompatibility and biodegradability, they present some disadvantages, such as the possible presence of pathogenic agents, human immune response and limited properties replicability

among different production batches. Synthetic polymers that form hydrogels are traditionally prepared using chemical polymerization methods; they present well-defined properties due to a fine-tuned synthesis, which allows an accurate control of hydrogel properties; they are characterized by the absence of pathogenic agents, although they present low biodegradability and can include toxic chemicals because of the synthesis.
The method of preparation leads to formation of some important classes of hydrogels. These can be exemplified by the following:

(a) Homopolymeric hydrogels are referred to polymer network derived from a single species of monomer, which is a basic structural unit comprising of any polymer network [3]. Homopolymers may have cross-linked skeletal structure depending on the nature of the monomer and polymerization technique;
(b) Copolymeric hydrogels are comprised of two or more different monomer species with at least one hydrophilic component, arranged in a random, block or alternating configuration along the chain of the polymer network [18];
(c) Multipolymer Interpenetrating polymeric hydrogel (IPN), an important class of hydrogels, is made of two independent cross-linked synthetic and/or natural polymer component, contained in a network form. In semi-IPN hydrogel, one component is a cross-linked polymer and other component is a non-cross-linked polymer [3,19].

Hydrogels may be further categorized into four groups depending on the presence or absence of electrical charge located on the crosslinked chains:

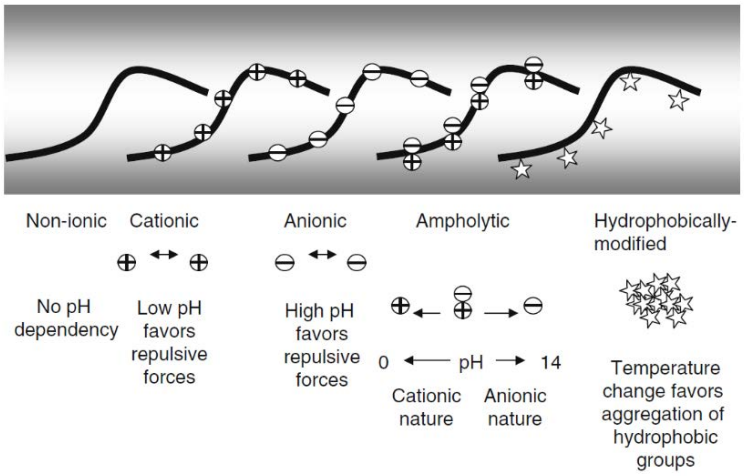

Figure 1.3. *Electrical charge influence on hydrogel structures, adapted from Omidian et al., 2010.*

(a) Non-ionic (neutral);
(b) Ionic (including anionic or cationic).
(c) Amphoteric electrolyte (ampholytic) containing both acidic and basic groups.
(d) Zwitterionic (polybetaines) containing both anionic and cationic groups in each structural repeating unit.

Non-ionic hydrogels, such as poly(*N*-vinyl pyrrolidone) and poly(ethylene oxide), swell in aqueous medium solely due to water–polymer interactions. The cationic hydrogels swelling is dependent on the pH of the aqueous medium, which determines the degree of dissociation of the ionic chains. Cationic hydrogels display superior swelling at acidic media since their chain dissociation is favored at low pHs. Similarly, anionic hydrogels dissociate more in higher pH media, and hence, display superior swelling in neutral to basic solutions. Ampholytic hydrogels possess both positive and negative charges that are balanced at a certain pH (their iso-electric point). A change in pH can change the overall ionic (cationic or anionic) properties. For example, ampholytic gelatin dissolves in water at low pHs due to its cationic nature in an acidic medium. The hydrophobic modified hydrogels contain a hydrophilic backbone with pendant hydrophobic groups. In an aqueous solution, the balance between the hydrophilic and hydrophobic interactions changes with temperature. Therefore, depending on the nature of these groups, hydrophobic association occurs at a specific temperature, which results in gelation as depicted in Figure 1.3.

1.1.2 Application fields

Hydrogels find application in several fields, depending on some key properties, including the swelling capability. Hydrogels can be used as a swelling agent or as a delivery platform for active compounds. Hydrogels with high swelling capacity are mostly used in hygiene and agriculture fields where retention of water and aqueous solutions, of say urine and tap water, is expected, respectively. For the delivery of drugs, pesticides, proteins, colorants, for example, hydrogels with lower swelling capacity are generally used [20].
Hydrogels for hygiene products, such as baby diapers, are disposable short-term products; therefore, they are required to offer high and fast swelling properties as well as moderate stability. These should be safe, non-toxic and be able to function in solutions containing urine and salts while loaded. As far as the purity is concerned, hygiene hydrogels must have very limited amounts of residual monomers and other reagents. In agriculture, while high swelling capacity is very desirable, the fast-swelling rate is not needed in most applications. Agricultural hydrogels should absorb ion-containing aqueous solutions, while being stable to UV irradiation, oxygen, ozone, acidic rains, temperature variation, microorganisms, and soil composition.

The interest in the use of hydrogels for biological applications arises from the possibility of using them for the realization of bi-dimensional or three-dimensional scaffolds that mimic the extracellular environment and that can be used to study the behavior of different cells. Reticulated structures of cross-linked polymer chains can retain and absorb biological fluids and allow for easy transportation of oxygen, nutrients and waste (all soluble factors). In hydrogels scaffolds, cells can therefore be supported (both mechanically and in terms of nutrition) and can follow their normal life cycle, so they can maintain a high viability and their natural behavior with the possibility to grow, migrate, proliferate, differentiate, and eventually die [21]. Hydrogels try to mimic the physiological extracellular matrix (ECM), in which the growth of the desired tissue takes place. Scaffolds should provide mechanical strength; allow cellular proliferation; stimulate the generation of cells matrix upon which new tissue can grow; avoid cell outflow because of structural imperfections. Hydrogels constitute optimal scaffold for tissue engineering, by means of high water retention and enabling the flow - across the structure - of fundamental nutrients, for cells growth and proliferation. Upon growth phase completion inside the bioreactor, the hydrogel with cells can be inserted in the human body through implantation or direct injection (Figure 1.4).

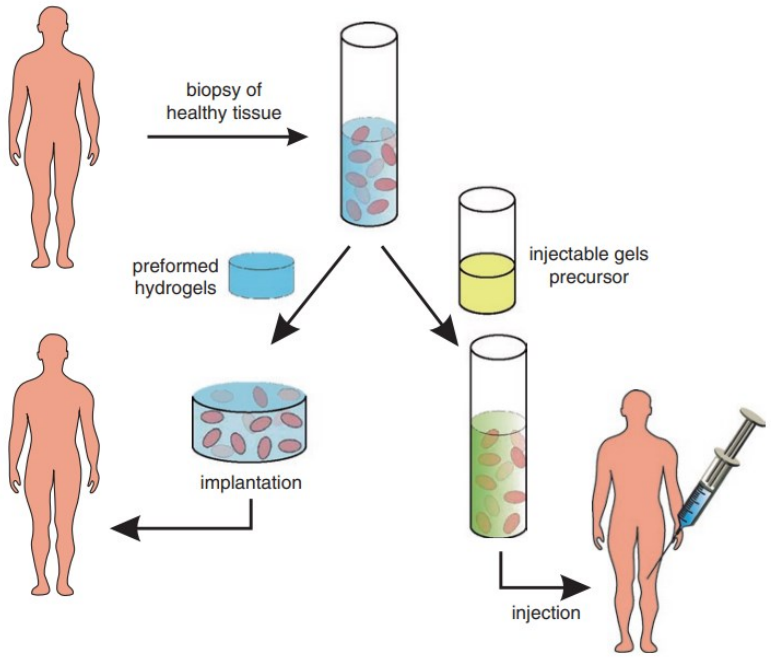

Figure 1.4. *Tissue engineering strategies using preformed and injectable hydrogels in combination with cells; adapted from Rong Jin and Pieter J. Dijkstra, 2010.*

Not all hydrogel materials are suitable for biological applications; cells can follow their normal life cycle only when encapsulated in inherently biocompatible and bioactive environments. The biocompatibility and bioactivity of hydrogel materials directly depends on the nature of

polymeric chains and, according to the origin of their polymeric chains, hydrogels can be classified as natural based, partially synthetic or completely synthetic [22].
Synthetic hydrogels are obtained through flexible and replicable processes. The main advantage in the synthesis of synthetic hydrogels is the high degree of control over the properties of the material, especially over mechanical properties and the degradation velocity; this is possible through molecular scale control of the polymeric structure. Synthetic hydrogels are however characterized by the absence of bioactive molecules that can promote cell behavior in terms of adhesion, growth, proliferation, differentiation, and secretion of molecules in the surrounding environment. Moreover, synthetic hydrogels lack the cell-binding and protease-cleavage motifs that are naturally found in ECM. This limitation can be overcome by adding cell-responsive sites, such as integrin cell-binding motifs, to synthetic polymers, therefore engineering biomimetic materials. Natural based hydrogels are composed of ECM natural proteins such as collagen, hyaluronic acid, or Matrigel, or can be obtained from other biological sources such as chitosan, alginate, or silk fibrils [21]. Natural based materials are inherently biocompatible and bioactive and are able to promote several cellular functions because of the presence of endogenous factors, which are useful for the viability, proliferation and the development of different types of cells. These materials are however affected by low batch to batch consistency, that result in the inevitable variability in terms of cell proliferation, differentiation and migration inside the same types of hydrogel. The control over mechanical and biochemical properties in natural hydrogels is not high and time of degradation could be inconsistent with experimental time [22]. In natural materials, the risk of contamination is very high due to the presence of impurities.

1.1.3 Neuroblastoma

Neuroblastoma is a malignant tumor of the sympathetic nervous system, which is part of the autonomic nervous system and that is responsible of the activation of the so-called fight or flight response. It is an extracranial tumor that originates from neuroblasts, primitive neuroepithelial cells of the embryonic neural crest, and it is the most common form of embryonal tumor. It can develop anywhere along the sympathetic nervous system and is mainly seen in very young children. Bone marrow is the main site where Neuroblastoma metastasizes. Indeed, cancer cells are not only able to proliferate against the normal rules of growth but, in malignant cases, can also invade and colonize other areas of the body, since they can move by entering blood or lymphatic vessels.
Cancers are complex systems, closely associated with a dynamic biological landscape, which is mainly composed of fibroblast, myofibroblasts, neuroendocrine cells, adipose cells, immune and inflammatory cells, blood and lymphatic vascular networks, and extracellular matrix. Cancer development and progression require extensive reorganization of the extracellular

matrix [23]. Cancer cells interact with their extracellular matrix through a combination of mechanical interactions, enzymatic manipulation of the matrix structure, or signalling interactions, leading to changes in the degree of inflammation and hypoxia of the tumor microenvironment as well as its levels of intracellular signalling [24]. Cancer cells interact with the immune system, causing both pro-tumorigenic and anti-tumorigenic behaviours. The immune system helps maintaining a continuous state of inflammation in the tumor microenvironment, promoting cancer cell growth and metastasis as well as angiogenesis in the tumor microenvironment. The tumor microenvironment is therefore the first promoter of tumor growth and supports the formation of metastasis. It also ensures the protection of the tumor from the immune system of the host organism, and it reinforces the resistance to chemotherapy.

1.2 Three-Dimensional Bioprinting

Three-dimensional bioprinting technologies allow for the additive manufacturing of 3D constructs by printing multiple biomaterials, cells and biochemicals in predesigned spatial positions, with high resolution, accuracy and reproducibility [25]. Biodegradable 3D cellular constructs with intricate architectures and heterogeneous composition are printed through the layer-by-layer deposition of bioinks. High structural complexity can be achieved, making 3D bioprinting technologies relevant in the field of tissue engineering, for applications in tissue repair and regeneration, and for the development of in vitro models for cell biology, drug development and study of several diseases.

Independently of the mechanism used to assist the deposition of cells and biomaterials, all bioprinters include a reservoir containing the bioink to print, a system to generate the ejection of bioink from the reservoir and a receiving stage that collects the printed material. Computer-aided design and computer-aided manufacturing tools allow to generate personalized constructs, organized at different length scales [25]. The main technologies used for deposition and patterning of biological materials are inkjet, microextrusion and laser-assisted printing.

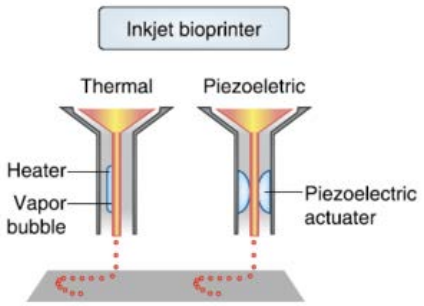

Figure 1.6. *Schematic illustration of 3D inkjet bioprinting process; adapted from Biogelx.*

Inkjet bioprinting (Figure 1.6) is a non-contact technology based on the deposition of small droplets of a bioink, with diameters on the order of tens of microns (with corresponding volumes in the range of 1-100 picolitres) onto a receiving platform with micrometer resolution [25]. Inkjet printers, also known as drop-on-demand printers, are widely used for both non-biological and biological applications. Thermal or acoustic forces are used to eject drops of liquid onto a substrate, which can support or form part of the final construct. In the first case, the printer head is electrically heated to produce pulses of pressure that force droplets from the nozzle. In the second case, the inkjet printer is characterized by the presence of a piezoelectric crystal that, when subjected to a voltage, shows a rapid change in shape and creates an acoustic wave inside the printer head that breaks the liquid into droplets at regular intervals [26]. Alternatively, an acoustic radiation force, associated with an ultrasound field, can be used to eject liquid droplets from an air-liquid interface.

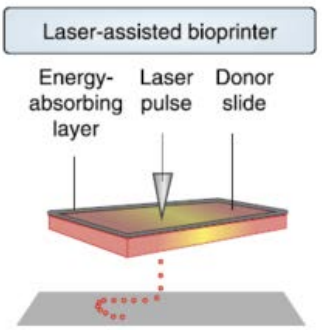

Figure 1.5. *Schematic representation of laser assisted bioprinting (LAB) approach; adapted from Biogelx.*

Laser-Assisted Bioprinting (LAB) technology, shown in Figure 1.5, has emerged from the initial work and patents of researchers at the Naval Research Laboratory [27], as a promising method for engineering artificial tissues. This latter method is based on the laser-induced

forward-transfer (LIFT) effect. LIFT Assisted Bioprinters or LAB are composed of three main constituents: a pulsed laser source; a target, or ribbon, serving as a support for the printing material; a support to collect the printed material. Briefly, the ribbon is composed by a support, that is non absorbing to the laser (e.g. glass or quartz), coated by a thin laser absorbing layer of metal (e.g. gold or titanium). The organic components (cells or molecules) are prepared inside a liquid phase (e.g. culture medium or collagen), and deposited on the surface of the metal-coated support. Then, the laser pulse induces the vaporization of the metal film, resulting in the formation of a droplet, which is then deposited on the receiving substrate [27].

1.2.1 Microextrusion

The most common and affordable biological 3D printers use microextrusion. It is the most used method to fabricate 3D cell-laden constructs for tissue regeneration. The great success of this technology is related to the possibility of printing viscous biomaterials, containing relatively high cell densities, into 3D structures with clinically relevant dimensions within a realistic time frame, that is not obtainable using inkjet or laser-assisted bioprinting. The ability to deposit very high cell densities achieving physiological values in tissue-engineered organs is a major goal for the bioprinting field.

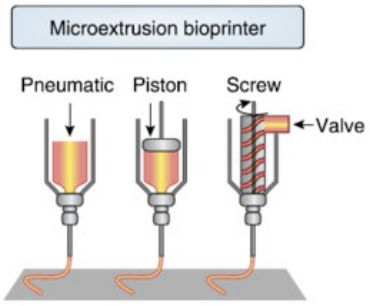

Figure 1.7. *Illustration of 3D micro extrusion bioprinting and of its main components; adapted from Biogelx*

As schematically illustrated in Figure 1.7, by using this technology, a polymeric solution is loaded within disposable medical grade syringes or reservoirs, and subsequently dispensed via either pneumatic, piston driven, or rotating screw-driven force on a building platform. Pneumatic systems are more effective when working with highly viscous molten polymer, however they are associated with a delay in dispensing due to the compressed gas. The piston driven deposition often allows for more direct control over the flow of the biomaterial from the nozzle. Screw based extrusion systems ensure more spatial control and are suitable for the dispensing of polymers with higher viscosities. Bioink viscosity and the induction of *in situ*

gelation of temperature-sensitive polymers can be controlled with the inclusion of temperature-controlled modules that continuously allow to adjust the temperature of both the bioink and the construction platform. Cells can be incorporated as suspended in prepolymer solutions, and then printed with high viability using pneumatic and piston-driven systems. Screw driven extrusion systems can also be used, however it is necessary to consider that larger pressure drops at the nozzle can be generated, with detrimental consequences for the encapsulated cells; this problem can be solved by specifically designing the screw for bioprinting applications. Cell viability after microextrusion bioprinting is anyway lower than the one obtained with inkjet-based bioprinting. Cell survival rates stand between 40-86%, with the rate decreasing while increasing extrusion pressure and increasing nozzle gauge [28]. The decreased viability of deposited cells results from the shear stresses inflicted on cells in viscous fluids. Dispensing pressure may have a more substantial effect on cell viability than the nozzle diameter, and therefore higher cell viability could be obtained with lower pressures and larger nozzle sizes, however obtaining lower resolution and print speed. Actually, the resolution that can be achieved with extrusion-based printers is in the order of 200 μm, that is considerably lower than the one achievable by using laser-based or inkjet-based systems.

1.2.2 Bio-ink

Bioprinting derives from the concept of additive manufacturing, where a 3D architecture can be fabricated by a predesigned and sequential deposition of layers of a *bioink*, which is a material - usually a hydrogel - containing cells. Bioprinting aims to accurately dispense cells, hydrogels, or cell-laden materials, to achieve spatially controlled 3D constructs, to mimic the structures of native tissues and lead to the direct manufacturing of mature artificial tissue *in vitro* that are suitable for transplantation [29]. While there are several bioprinting modalities commonly used for tissue fabrication, the bioink consisting of a mixture of biomaterial(s) and cell(s) is the unanimously vital component serving as the building block of bioprinted 3D tissue structures [26,30,31]. The bioprinted cell-laden constructs featuring arbitrary shapes and architectures finally form 3D tissue-like structures after a period of culture [30,32]. The selection of the bioink depends on the specific application (i.e., target tissue) and the type of cells as well as the bioprinter to be used [33]. Biomaterials commonly used in combination with cell populations for cell-laden printing include natural, synthetic and hybrid (combination of natural and synthetic) bioinks [28].

An ideal bioink should possess the desired physicochemical properties, such as proper mechanical, rheological, chemical, and biological characteristics [33,34]. These properties should lead to:

a) the generation of tissue constructs with adequate mechanical strength and robustness, while retaining the tissue-matching mechanics, preferably in a tunable manner;
b) adjustable gelation and stabilization to aid the bioprinting of structures with high shape fidelity;
c) biocompatibility and, if necessary, biodegradability mimicking the natural microenvironment of the tissues;
d) suitability for chemical modifications to meet tissue-specific needs;
e) the potential for large-scale production with minimum batch-to-batch variations [33,35].

Cells can be encapsulated in modified-composite bioinks that enable shape fidelity post-printing even at low polymeric concentrations, preserving cell viability and sustaining proliferation [28]. Additionally, hydrogels selected for bioprinting should demonstrate stable gelation conditions to enable uniform deposition and ensure shape fidelity [28,36,37]. Blending materials can be applied to create optimize inks for encapsulating and printing living cells as they combine the natural and the synthetic components to produce highly printable bioinks [28,38–40]. Numerous hydrogel-based bioink formulations such as gelatin methacryloyl (GelMA) [30,41–43], acrylate-functionalized poly(ethylene glycol) [30,44,45], alginate [30,46,47], agarose [30,48] collagen [30,49], and Pluronic [33] have been adopted, either used alone or in combinations, as bioinks. Taking extrusion bioprinting as an example, the bioinks play key roles in dispersing the cells prior to bioprinting, in maintaining the integrity of the structures during bioprinting, and in supporting the adhesion, spreading, and functionality of encapsulated cells post-bioprinting [30,50,51]. To produce hydrogel constructs through extrusion bioprinting, it is necessary to control the viscosity of the bioink as an important rheological parameter [30,52]. High viscosity of the bioink is essential to maintain the structural fidelity of the extruded filaments deposited layer by layer in 3D.

1.2.3 Gelatin Methacrylate (GelMA)

Among the different types of hydrogel bioinks, those based on GelMA hold good promise attributed to the superior biocompatibility, on-demand photocrosslinkability, and broadly tunable physicochemical properties of this biomacromolecule denatured from collagen [30,48]. Gelatin is a natural protein extract, obtained through heat denaturation and partial hydrolysis of collagen extracted from skin, bones and connective tissue of animals [53]. Gelatin can be obtained by performing acid or basic treatment of collagen, it is biodegradable and highly biocompatible. Contrarily to collagen, gelatin exhibits lower antigenicity due to heat denaturation, and it retains cell-binding motifs such as arginylglycylaspartic acid (RGD) and matrix metalloproteinase (MMP)-sensitive degradation sites, fundamental for cell encapsulation.

Gelatin is also an interesting base material for engineering hydrogels for drug delivery [43]. The blending of hydrophilic/hydrophobic polymers produce phase-separated composite hydrogels. The advantages of polymer blend systems for controlled release applications may include easy fabrication of devices, manipulation of device properties (hydration, degradation rate, and mechanical strength), drug loading, and utilization of the dispersed phase domains as a micro-reservoir for enhanced release properties.

However, gelatin can be chemically modified to enable chemical crosslinking between macromolecules, and therefore to obtain chemical hydrogels, irreversible and stable under a wider range of temperature. Several chemical strategies can be applied. One possibility is the addition of small molecule chemical reagent to cross-link gelatin macromolecules. Another possibility is methacrylation of the amino groups of gelatin macromolecules, with different degrees of functionalization, to obtain a photoreactive product known as gelatin methacrylate [54]. Actually, the addition of functional groups to gelatin backbone is a crosslinking strategy characterized by higher control over hydrogel design and properties if compared to direct crosslinking techniques. Moreover, photopolymerizable gelatin derivatives undergo quicker and more homogeneous crosslink compared to other derivatives obtained through the addition of small molecules [29]. What is crucial is that chemical, physical and mechanical properties of GelMA can be easily tuned by manipulating the ratio of its components.

GelMA polymers can therefore be used to prepare hydrogel-based 3D cell culture models for cancer and stem cell research, as well as for tissue engineering applications. Using photolithography and 3D bioprinting, it is feasible to fabricate micropatterned 3D cell-laden GelMA hydrogel containing single or multiple cell lines for engineering different tissues. Direct bioprinting of pure GelMA hydrogel as the bioink has been a challenge because of its generally low viscosity at room or higher temperatures. Yet, GelMA could still be directly bioprinted through adjusting several parameters to reach appropriate viscosity: the concentration of the polymer, the temperature, and the degree of crosslinking [29,30].

The fabrication and use of GelMA hybrids with other biopolymers have been explored for diverse purposes, including enhancing mechanical properties [29,55,56], tuning characteristics such as porosity, swelling ratio and degradability [29,56], or imparting a particular property such as electrical conductivity [29,57,58]. In general, GelMA possesses many relevant characteristics to serve as tissue engineering scaffolds. GelMA-based hydrogels are biocompatible, biodegradable, non-cytotoxic, and nonimmunogenic [29].

1.3 Aim of the thesis

Starting from previous results [2], the target of the original research described in this thesis referred to the production of gelatin methacrylate hydrogels for the realization of three dimensional scaffolds, through microextrusion bioprinting, for cancer cells studies. Within this goal, the following sub-targets were set and pursued:

(a) Optimization of the synthesis and purification protocol to obtain a sterile product;

(b) Realization of GelMA-blended hydrogels, employing both natural and synthetic blending polymers, in order to obtain scaffolds with fine-tuned properties;

(c) Study how both GelMA degree of functionalization and the concentration ratio of different blended-materials affect swelling, porosity, printability and therefore cell viability;

(d) Development of a MATLAB algorithm for image processing, computing important hydrogel parameters, such as the average pore radius and percent porosity.

Chapter 2

Materials and methods

This Chapter illustrates all the protocols adopted to pursue the final goal of this work. Synthesis and purification methods for gelatin methacrylate are described, along with the material characterization analyses. Accordingly, the preparation of gelatin methacrylate hydrogels-based is discussed, as well as the procedures for the material characterization. Finally, three-dimensional (bio)printing applications using gelatin methacrylate hydrogels-based bioinks are considered and biologically validated via cellular tests.

1.1 Gelatin methacrylate synthesis

The traditional preparation method of gelatin methacrylate (GelMA) was proposed by Van Den Bulcke et al. in 2000 [59]: it is based on the reaction between lysine and hydroxy-lysine groups of gelatin and methacrylic anhydride (MAA) [60] and returns methacrylic acid as by-product (Figure 2.1).

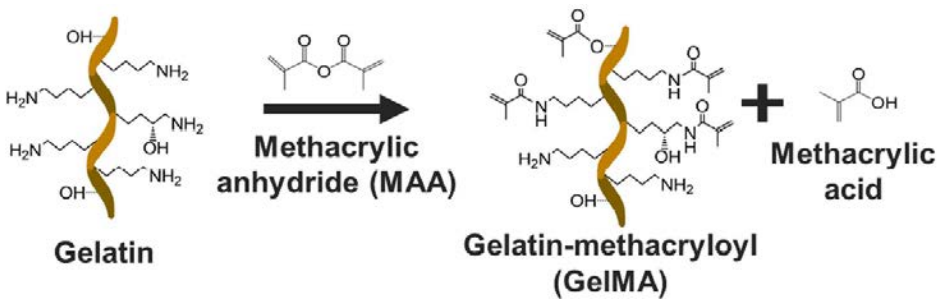

Figure 2.1. *Gelatin methacrylation using methacrylic anhydride (MAA). The resulting gelatin methacrylate (GelMA) contains methacrylate and methacrylamide groups, which can be photocrosslinked with the assistance of a photoinitiator; adapted from Shirahama et al and from Modaresifari et al.*

In literature, gelatin from porcine skin is dissolved in 0.25 M carbonate-bicarbonate (CB) buffer in 10% w/v concentration. Gelatin concentration is an important parameter for the reaction promotion: if concentration is lower than 10% w/v, phase separation occurs with the formation of both aqueous and organic phases, preventing the homogeneous dispersion of MAA and therefore the gelatin functionalization; for concentrations at least equal to 10% w/v, the reaction effectively takes place; at 20% w/v gelatin concentration provides the best reaction efficiency. Since the reaction is strongly pH-dependent, during the synthesis a pH control and adjustment

is mandatory. In fact, keeping the free amino groups of lysine neutral allows them to properly react with MAA. The neutrality is preserved if the reaction solution pH is above the isoelectric point (IEP) of gelatin [60]. For type A gelatin, the IEP value is at pH = 8÷9 [61]. The upper limit is at a pH value between 10 and 11, where methacrylation is prevented due to MAA hydrolysis. Accordingly, a 0.25 M CB buffer is close to the optimal buffer concentration [60] and provides a pH = 9.59, which is adjusted with hydrochloric acid until a pH ≅ 9.2 value, before the MAA addition. To effectively carry out the methacrylation reaction, several studies set a lower and an upper temperature limits (i.e., T = 35÷50 °C), which correspond to gelatin gelation point and possible denaturation, respectively. An optimal solution mixing is also recommended, both to homogeneously dissolve gelatin and to ensure an effective MAA molecules dispersion. Reaction generally occurs in 1 up to 2 hours. Several studies confirmed that the reaction between gelatin and MAA takes place in an hour: studying the pH variation in the reaction solution, high pH reduction is measured in the first half hour, while moderate pH variation is observed in the second half hour; no substantial pH changes are seen in the next hour. Therefore, reaction mostly occurs in the first half hour, which expresses the need to accurately control the solution pH over that time. However, reaction time is extended up to 2 hours to ensure the desired degree of functionalization (DoF).

2.1.1 Preparation method

The protocol has been optimized in a previous thesis work [2]. Briefly, type A gelatin from porcine skin (G1890, gel strength ~300g bloom, Sigma-Aldrich, St. Louis, MO) is completely dissolved in 0.25 M carbonate (PanReac AppliChem, ITW Reagents) and bicarbonate (PanReac AppliChem, ITW Reagents) buffer, at a 10% w/v concentration, under vigorous magnetic stirring (~600 rpm) and in a water bath at 45 °C. After complete gelatin dissolution, the solution pH is measured and adjusted - if necessary- with hydrochloric acid (ACS reagent, 37%, Sigma-Aldrich) up to a value of ~ 9.2. Depending on the desired DoF to achieve, different MAA (94%, Sigma-Aldrich) concentrations are added dropwise to the solution (15, 25 or 50 µl per gram of gelatin). The reaction is considered completed after 2 hours from the first MAA drop addition. Again, the solution pH is measured and adjusted with hydrochloric acid up to a value of ~ 7.4, in order to stop the reaction. Finally, it is important to underline the threat of some reagents, such as methacrylic anhydride and hydrochloric acid: the former is a volatile and toxic organic compound, which may cause skin irritation, serious eye damage and respiratory irritation if inhaled; the latter is a corrosive and irritant chemical compound, which generates severe skin burns and eye damage and may cause respiratory irritation. Hence, the synthesis takes place under chemical fume hood. GelMA synthesis main parameters are summarized in Table 2.1:

Buffer type	Carbonate-Bicarbonate
Buffer Molarity [M]	0.25
Buffer pH (25 °C) [-]	9.59
Gelatin/Buffer [% w/v]	10
Reaction initial pH [-]	~ 9.2
Reaction temperature [°C]	45
MAA/gelatin [µl/g]	15, 25, 50
Reaction time [h]	2
Reaction final pH [-]	~ 7.4
Magnetic stirring [rpm]	600
Heat transfer	Water bath
pH adjustments	Hydrochloric acid (37%)

Table 2.1. *Main parameters related to GelMA synthesis.*

After the synthesis, GelMA is recovered and purified. Furthermore, the product must preserve sterility since it is used for biological applications.

2.1.2 Purification method

The purification method is based on dialysis and involves several steps:

(a) Depending on the reaction volume, the solution is withdrawn with a sierological pipette (up to 50 ml) and transferred in one or two flexible cellulose acetate tubing dialysis membrane (molecular weight cut-off of 12÷14 kDa, Sigma-Aldrich), previously sterilized in boiling water (100 °C) for up to 5 minutes. The dialysis is performed to remove unreacted reagents (MAA), by-products (methacrylic acid) and to desalt the solution. It is carried out in a 2 liters volume of milli-Q water for 5 days and changed twice-daily, at constant magnetic stirring (~300 rpm) and temperature (40 °C). Additionally, GelMA solution is protected from light, due to its photosensitivity. Dialysis is considered concluded as GelMA solution in the membrane appears clear at sight;

(b) The solution is withdrawn from the membrane and filter-sterilized using 0.22 µm cellulose acetate membrane - both vacuum bottle caps and syringe - filter units. This

step is carried out under biological hood to remove potential biological contaminants and to preserve sterility;

(c) The sterile solution is transferred in test tubes (up to 30 ml volume solution per tube) and sealed with vented screw-top caps (CELLTREAT Bio-Reaction Centrifuge Vented Tube Cap, Cole-Parmer);

(d) The caps are then wrapped in parafilm tape to further reduce the contamination risk, taken out the biological hood and frozen at -80 °C for at least one hour;

(e) The solution is freeze-dried in a lyophilizer under vacuum condition ($\leq$ 6.1 mbar) and at -60 °C, until GelMA is completely dried (up to 7 days);

(f) The purified and dried product can be stored at -20 °C, protected from light and moisture until final use.

2.1.3 Proton Nuclear Magnetic Resonance (H NMR)

An important and indicative parameter for the synthesis reaction success is the degree of functionalization (DoF) of gelatin amino groups, which also represents the degree of the methacrylamide groups substitution. It can be determined with the Proton Nuclear Magnetic Resonance (H NMR) and it also verifies the method replicability for GelMA synthesis.
Nuclear Magnetic Resonance Spectroscopy is an analytical technique that allows to obtain detailed information on the molecule structure: its nucleus is placed in an external magnetic field to determine its behaviour. NMR can only detect nuclei with a non-zero spin since they are forced to rotate and align with an external electromagnetic field. Notably, it is necessary to consider that:

(a) when the number of protons and neutrons are even and equal, the nucleus has no spin, resulting in no magnetic resonance phenomena;

(b) if an odd number is obtained by summing the nucleus protons and neutrons number, then the nucleus has a half-integer spin, equal to (or a multiple of) ½;

(c) if the sum of protons and neutrons returns an odd number, the atomic nucleus has an integer spin (i.e., 1, 2, 3).

Accordingly, the nucleus of ^{12}C has no magnetic spin, as the protons and neutrons number are even and equal. Considering instead ^{1}H and ^{13}C, the resulting spin is different from zero, with a half-integer spin. When ^{1}H is subjected to an external electromagnetic field, there are two possible orientations: one corresponding to m (magnetic quantum number), equal to -½; the other corresponding to -m, equal to +½. The nuclear magnetic moment is not perfectly aligned with the external magnetic field; it oscillates, simply performing a precession motion. The two possible nucleus states are not characterized by the same energy, since the state with positive magnetic quantum number corresponds to a slightly lower energy with respect to the one with

negative magnetic quantum number. The precession motion of nuclear magnetic moments occurs with a frequency proportional to this energy difference, that increases as the external applied field increases; this is known as Larmor frequency. The equilibrium between the two possible states is quickly reached and, on average, only 50% of the nuclei immersed in the magnetic field are oriented; the other half assumes the opposite orientation. It is possible to excite these nuclei into the highest energy level with electromagnetic radiation, characterized by a specific frequency. The radiation frequency depends on the external magnetic field, on the nucleus examined and on the chemical environment of single protons. According to their chemical environment, the protons of a molecule are shielded in different ways, and thus the NMR signal of a certain nucleus is displaced in the spectrum at higher or lower frequencies. This happens because the electrons that belong to the neighboring atoms, when immersed in the external magnetic field, generate a small magnetic field with their movement, opposite to the applied one. This secondary magnetic field shields the examined nucleus from the full strength of the applied field; the greater the electron density, the greater the corresponding shielding from the external field, and the neighboring nuclei undergo the transition at a lower frequency than the ones placed in other areas (characterized by limited presence of electrons). The resulting displacement in NMR signal for a given nucleus is known as chemical displacement. In general, protons (^{1}H) or carbons (^{13}C) adjacent to electronegative atoms are unshielded, resulting in a more intense magnetic field; since the transition occurs at higher frequencies, higher chemical displacement is found in the spectrum.
GelMA synthesis replicability is therefore studied with the NMR spectra analysis, kindly performed by Professor Sgarbossa: 20 mg samples of dried GelMA are dissolved in 0.7 ml of deuterium oxide; for each batch synthesis, two GelMA samples are analysed. However, for the interpretation of H NMR signals, it has to be considered that:

(a) the number of signals corresponds to the types of protons that are present;
(b) the position of signals is related to the shielding;
(c) the strength of signals is directly related to the number of specific types of protons;
(d) signal splitting shows the number of protons that are present on adjacent atoms.

2.2 GelMA-based hydrogels: preparation

Hydrogels of different properties can be obtained by varying selected synthesis parameters, such as MAA, dried GelMA and photoinitiator concentrations. Methacrylic anhydride is related to the degree of functionalization (DoF) of amino groups, which can bind together the macromolecules in different ways, resulting in three-dimensional polymer networks with different properties. In this work, three different MAA concentrations are used during the synthesis (15, 25, 50 µl per gram of gelatin), according to the desired DoF obtainable. As

already mentioned, also the dried GelMA concentration affects the final properties of hydrogels. In this work, GelMA concentration was fixed on a value of 8% w/v, based on Santi G. [2] previous results. Although several crosslinking methods can be applied to crosslink functional groups, only a few are suitable for both crosslinking and cell encapsulation. Since GelMA is a photosensitive material, photo-polymerization is an option; crosslinking can be achieved with the combination of a suitable photoinitiator and an appropriate exposure time to ultraviolet radiation. GelMA crosslinking process occurs through free radical generation by light exposure and in the presence of a photoinitiator: it is a radical addition polymerization, resulting in a network of gelatin chains connected by poly-methacryloyl chains, as shown in. Figure 2.2.

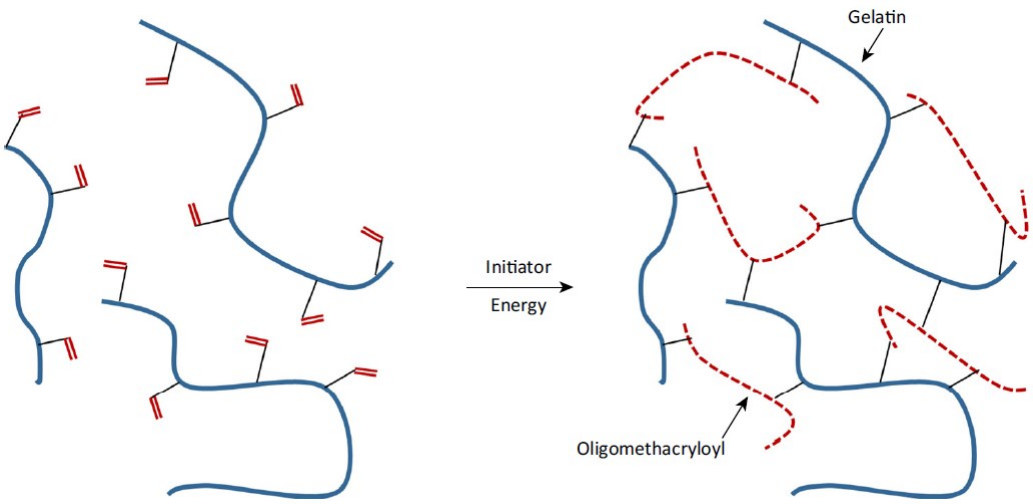

Figure 2.2. *Schematic crosslinking process between GelMA and a photoinitiator, adapted from Klotz et al., 2016.*

For biological applications, biocompatible initiators are the most indicated among all available photoinitiators. Photo-polymerization with 2-hydroxy-4'-(2-hydroxyethoxy)-2-methylpropiophenone (Irgacure 2959, 98%, Sigma-Aldrich, St. Louis, MO) is the most used for its relative low cytotoxicity, it can be activated with UV-A radiation exposure and it is water-soluble, allowing a quick crosslinking even at ambient temperature. The reaction mechanism of Irgacure 2959 is schematized in Figure 2.3, where UV-light generates benzoyl and ketyl-free radicals, through an α-cleavage reaction.

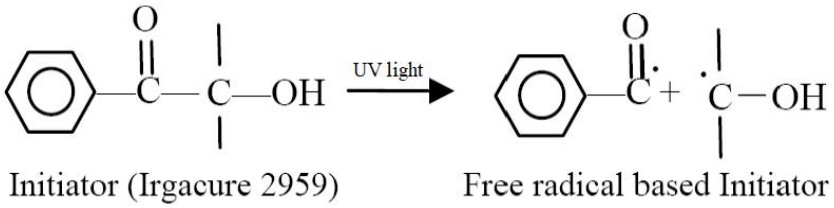

Figure 2.3. *Benzoyl and ketyl-free radical generation through UV-light irradiation, adapted from Wang S., 2011.*

In this work, hybrid hydrogels are also formed from blends of different components, which are selected to possess specific properties. Blending is a simple method to combine the advantages of different materials; the resulting polymer blends sometimes show synergistic properties [62]. Although GelMA is a cell-responsive material with wide-spectrum of tunable properties, tailored design of blending materials has been a useful strategy to improve some characteristics of GelMA for certain applications [29], such as the development of bioinks for three-dimensional bioprinting, as explained in 2.4. The fabrication and use of GelMA hybrids with other biopolymers have been explored for diverse purposes, including enhancing mechanical properties [29,55,56], tuning characteristics such as porosity, swelling ratio and degradability [29,56], or imparting a particular property such as electrical conductivity [29,57,58] GelMA-based hydrogels are therefore biocompatible, biodegradable, non-cytotoxic, and nonimmunogenic [29]. The materials tested, together with GelMA, as blended hydrogels are agarose and Pluronic F127.

2.2.1 GelMA

The protocol for GelMA-based hydrogels preparation and casting can be synthetized as follows:

(a) Prepare a precursor solution in a 40 °C water bath at constant stirring (~ 300 rpm), by dissolving 0.5% w/v Irgacure 2959 in 1x PBS solution (pH ≅ 7.4);
(b) Add 0.8% w/v dried GelMA (stored at -20 °C) and wait until mixing;
(c) Withdraw the solution containing PBS, GelMA and Irgacure (namely pure GelMA) and filter-sterilize with 0.2-µm syringe filter units, in order to prevent biological contamination;
(d) Cast the solution in PDMS anulus molds and light-cure with UV LED at 365 nm for 60 seconds;
(e) A three-dimensional crosslinked structure is obtained (Figure 2.4)

Note that all the steps are carried out under biological hood to preserve sterility.

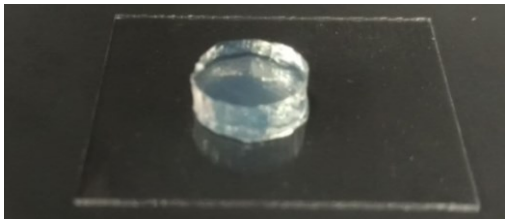

Figure 2.4. *Three-dimensional hydrogel structure obtained with casting method.*

Photo-crosslinking parameters influence the hydrogel properties; a fine-tuning of photoinitiator concentration, light intensity and light exposure time is necessary to obtain hydrogels with specific properties. These parameters are optimized for biological applications, and the exposure time is limited up to 60 s, in order to avoid cellular apoptosis.

2.2.2 Agarose

Agarose is a linear polysaccharide derived from red algae consisting of β-1,3-linked-D-galactose and α-1,4-linked 3,6-anhydro-L-galactose units [63] and used as a matrix to encapsulate cells [64]. Agarose is an attractive platform for cell encapsulation because it undergoes mild gelation through the formation of extensive intermolecular hydrogen bonds resulting in double helical structures that aggregate into thick bundles [65]. The gelling mechanism of agarose resides in the formation and aggregation of double helices by intermolecular hydrogen-bonds upon cooling [63]. The gelation process is divided into three stages: induction, gelation, and quasi-equilibrium [66–68]. Several agarose nuclei are formed in the first step followed by the growing of nuclei, which gradually form agarose-rich networks (Figure 2.5). In agarose, the formation of gel is related to the agarose molecule twisting linked to the transplantation of hydrogen and electrostatic penetration [66,69]. In the end, it is essential to note that the concentration of the agarose gel determines its permeability [66,70].

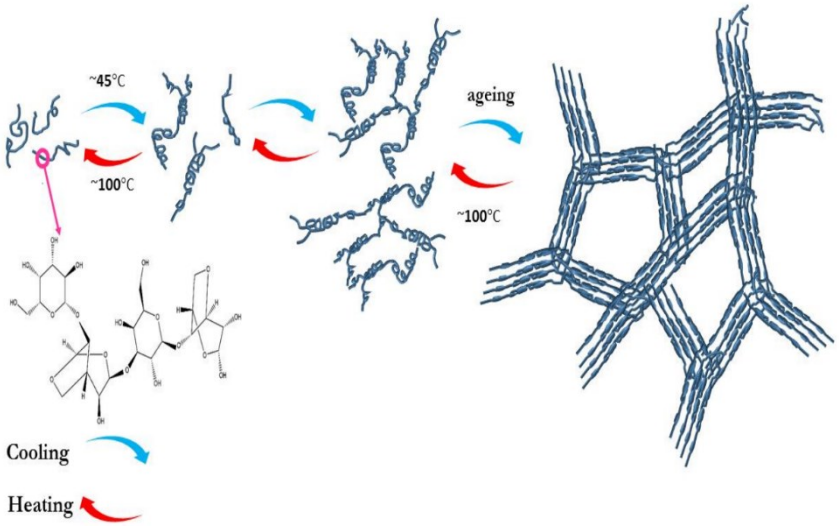

Figure 2.5. *The molecular structure of agarose and schematic of its gelling process (adapted from Amin Salati et al 2020).*

Agarose offers biocompatibility, retention of round cell morphology, homogeneity and strong mechanical properties [71]. However, agarose is bio-inert and does not present any cell adhesion motifs. A blend consisting of 8% w/v GelMA and 0.7% w/v agarose has been set up to enhance the biofunctionality of agarose. The protocol for this blend requires the same steps for pure GelMA hydrogels, where a precursor solution of agarose is prepared and added to pure GelMA before light-curing. The precursor solution preparation follows:

(a) Dissolve 3.5% w/v agarose in 1X PBS at constant stirring (~ 600 rpm) and in a 70 °C water bath;
(b) Autoclave the solution at 120 °C to remove potential biological contaminants and mix it to pure GelMA solution to obtain 8% w/v GelMA, 0.7% w/v agarose and 0.5% w/v Irgacure in 1X PBS.

It is important to underline that all the steps are carried out under biological hood as for pure GelMA-based hydrogels. In this case, it is extremely important to preserve biological sterility, as agarose allows bacterial colonies or bacteriophage plaques to spread and increases the chances of cross-contamination.

2.2.3 Pluronic F127

Copolymers of poly(ethylene oxide)-poly(propylene oxide)-poly(ethylene oxide) (PEO-PPO-PEO, commercially known as Pluronics, generic name poloxamers) are water soluble and exhibit low toxicity. Certain molecular weight classes of Pluronics have been approved by the

Food and Drug Administration (FDA) for clinical use [72,73] including Pluronic F127 (poloxamer 407). Pluronic F127 (poloxamer 407) is a thermo-responsive hydrogel (Figure 2.6) which has been used as a mold, track patterning and sacrificial material [36,74–76] for bioprinting and tissue engineering. It is considered one of the best printable hydrogels due to the nature of micellar-packing gelation, which allows it to be moved and shifted easily. Moreover, the range of its sol-gel transition temperature is broad (10–40 °C), meaning that the viscosity of Pluronic is stable at both room temperature and human body temperature [77–80].

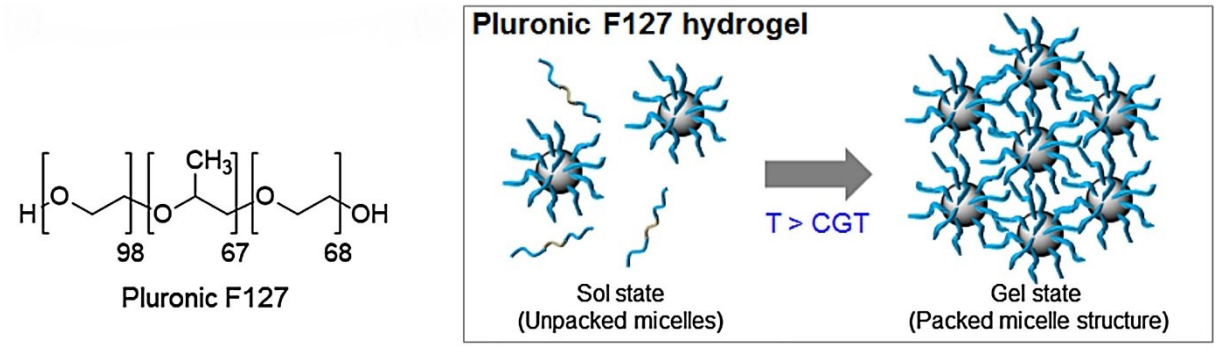

Figure 2.6. *Schematic of Pluronic F127 thermoreversible sol-gel transition; adapted from Jung Y. et al.*

Thermoreversible gelation of the copolymer Pluronic F127 (generic name, poloxamer 407) in water makes it a unique candidate for cell encapsulation applications, either alone or to promote cell seeding and attachment in tissue scaffolds. The ability to induce gelation via a process that is relatively gentle to cells (i.e., increase of temperature to physiological levels rather than chemical cross-linking) makes Pluronic F127 a polymer to explore for cell encapsulation applications [81]. While Pluronic F127 can be modified with photo-crosslinkable acrylate groups to stabilize the hydrogel [82], it still lacks protein or cell binding motifs, resulting in poor cell adhesion [76,77,83,84]. The protocol for the blend requires additional steps with respect to pure GelMA hydrogels protocol, consisting of:

(a) Preparation of Pluronic F127 solutions at different concentrations (0.1%, 0.5%, 1% w/v), at 4 °C;
(b) Filter sterilize using 0.2-µm syringe filter units and mix with pure GelMA solution;
(c) After light-curing, soak GelMA-Plu hydrogel in 1X PBS (usually 3 ml) for 5 min to promote Pluronic F127 dissolution and outflow from the three-dimensional structure.

2.3 GelMA-based hydrogels: characterization

Once the GelMA-based hydrogel samples are prepared, structure characterization analyses are carried out. The aim is to obtain a unique material with fine-tuned properties that can be both printed and can allow encapsulated cells growth and proliferation. The main parameters which characterize hydrogel structures are correlated to its three-dimensional network, and can be evaluated by performing swelling tests and Scanning Electron Microscope (SEM) imaging analysis.

2.3.1 Swelling

Bathing hydrogels in a large volume of water makes them swell up instead of dissolving, effectively retaining large volumes of water within their swollen three-dimensional structure [59]. The ability to display a measurable change in volume in response to external stimuli is a fundamental property of hydrogels [85]: swelling is a way to exhibit this volume change. The degree of crosslinking plays a significant role in the integrity and swelling properties of hydrogels, influencing hydrogel structure and swelling capacity [7,86]. The greater the extent of crosslinking, the less flexible a hydrogel is to shrink, swell or change phase in response to stimuli. The degree of crosslinking influences the area permitted for diffusion across the hydrogel network and, subsequently, the capacity for hydrogels to absorb and retain water [8]. Specifically, swelling can be decreased by decreasing the average molecular weight of the polymer chain segments between crosslinks [86].

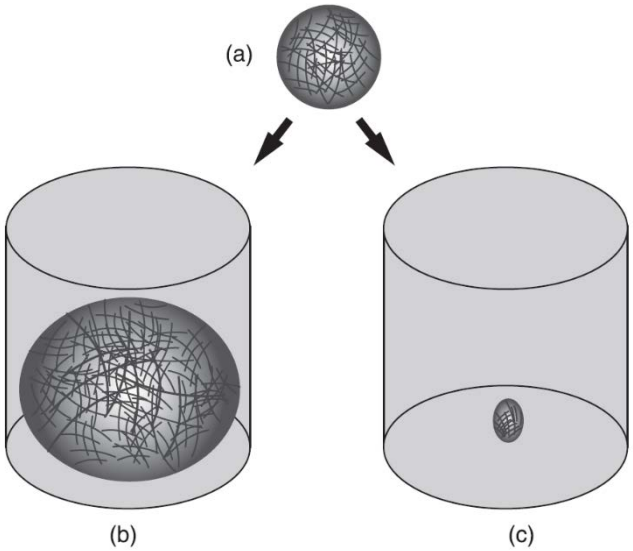

Figure 2.7. *Dehydrated (a), swollen (b), and shrunken (c) hydrogel as the result of small changes in external stimuli, such as pH, temperature and analyte concentration that influence hydrogel hydrophilicity; adapted from Holback et al, 2011.*

In general, hydrogels contain strongly electronegative atoms leading to a charge asymmetry, which promotes hydrogen bonds with water. Polymer-water interactions, electrostatic interactions and osmotic pressure enlarge the hydrogels structure, namely swelling force. The swelling force is counterbalanced by the spring force of the crosslinked structure: if these opposite forces are equal, the swelling equilibrium condition is reached. The swelling degree of hydrogels, and the possibility to retain and exchange aqueous fluids are fundamental factors in biological applications. The swelling degree is defined as the ratio of water uptake of a gel in relation to its dry weight. In chemically crosslinked gels the swelling degree is dependent on the mesh size of the polymer network and the interaction between the polymer and the solvent [87]. The swelling degree evaluation, together with the determination of the hydrogel porosity, can be used to ensure that the encapsulated cells have the necessary nutrients available for their survival, growth, proliferation, and, at the same time, that they can expel waste substances. In fact, several studies show that the ability of pure GelMA-based hydrogels to absorb and retain fluids increase with the decrease of GelMA concentration [2], as well as with the decrease of the DoF. Therefore, in this work the aim was to understand how the addition of a blending material to GelMA could affect the swelling ability of GelMA-based hydrogels. For this purpose, GelMA-based hydrogels samples were prepared, in particular pure GelMA and GelMA-Plu blend at different Pluronic concentrations: 0.1%, 0.5% and 1% (w/v), selected according to the desired biological applications.

Eight cylindrical hydrogel samples for each condition were realized, according to the protocols previously described in 2.2.1. After photo-polymerization, pure GelMA samples were placed

in petri dishes with 1X PBS, and then placed in incubator at 37 °C, in a controlled atmosphere of CO_2 (5.2%) and O_2 (20.1%), for 24 hours, required to reach the swelling balance [33]. GelMA-Plu samples are soaked in 1X PBS bath, before placing them in incubator, to promote Pluronic dissolution and outflow from the three-dimensional structure. After 24 hours incubation, samples are removed from PBS, softly dried at their surfaces with absorbent paper, weighted, and then let air-dry for three days. After three days, when completely dried, samples are weighted again.

To characterize the swelling degree of hydrogel samples, it was then possible to evaluate the percentage swelling ratio, SR, and the percentage water content, WC, as:

$$SR = \frac{m_s - m_d}{m_d} \cdot 100$$

$$WC = \frac{m_s - m_d}{m_s} \cdot 100$$

Where m_s and m_d are the masses of the swollen and dry samples, respectively.

2.3.2 Scanning Electron Microscope

As already explained, the swelling degree was defined as the ratio of water uptake of a gel in relation to its dry weight. In chemically crosslinked gels the swelling degree is dependent on the mesh size of the polymer network and the interaction between the polymer and the solvent [87]. Hydrogels have a range of porosities that influences the diffusion coefficients involved in mass transfer during swelling. Pore size is dependent on the average molecular weight of polymer chain segments between adjacent crosslinks and acts as a selective barrier with respect to the permeability of substances [8]. For example, the degree of functionalization (DoF) directly influences the highest achievable cross-linking density of the hydrogel matrix, and ultimately the hydrogel porosity and mechanical properties. When other factors remain unchanged, increasing the DoF leads to stiffer hydrogels with a higher cross-linking density and improved shape fidelity [88], whereas the pore size decreases [89]. The study of the morphology and structure of GelMA hydrogels is therefore completed by Scanning Electron Microscopy (SEM) analysis, showing how the pore sizes in GelMA and blended-GelMA hydrogels can be tuned by changing both the DoF and blend typology. GelMA-based hydrogels were prepared according to the protocols explained in 2.2.1, using PDMS annulus molds, with 16 mm diameter, 2 mm height and an overall volume of 500 µl. Samples were then placed in petri dishes with 3 ml of 1X PBS, and then incubated at 37 °C, in a controlled atmosphere of CO_2 (5.2%) and O_2 (20.1%). After 24 hours of incubation, samples were removed from PBS, cooled down to -80 °C and freeze-dried for at least three days; freeze-drying allows to maintain

the hydrogel structure that would instead collapse with simple air drying. Freeze-drying can alter the porosity of the material; however, since the effect of the drying process was the same on all the samples, it was evaluated as negligible according to the main aim of the analysis. For the sake of clarity, the sample conditions are summarized in the Table 2.2:

# Condition	*GelMA [% w/v]*	*Irgacure [% w/v]*	*DoF [%]*	*Agarose [% w/v]*	*Pluronic [% w/v]*
1	8	0.5	25	-	-
2	8	0.5	40	-	-
3	8	0.5	70	-	-
4	8	0.5	25	0.7	-
5	8	0.5	40	0.7	-
6	8	0.5	70	0.7	-
7	8	0.5	25	-	0.1
8	8	0.5	40	-	0.1
9	8	0.5	70	-	0.1
10	8	0.5	25	-	0.5
11	8	0.5	40	-	0.5
12	8	0.5	70	-	0.5
13	8	0.5	25	-	1
14	8	0.5	40	-	1
15	8	0.5	70	-	1

Table 2.2. *Hydrogel conditions tested, depending on DoF, blend typology and concentration.*

Samples are then analyzed using the FEI Quanta 400 Scanning Electron Microscope (SEM), which uses a focused beam of high-energy electrons to generate a variety of signals at the surface of solid specimens. The signals that derive from electron-sample interactions reveal information about the sample including external morphology (texture), chemical composition, and crystalline structure and orientation of materials making up the sample. For these reasons, the samples require a preparation step before the SEM analysis: the samples are attached to the sample stage using a conductive double-sided carbon tape and sputtered with a fine gold and palladium dust, under high vacuum (Figure 2.8).

Figure 2.8. *Freeze-dried hydrogel samples preparation before SEM images acquisition: gold and palladium sputtering under vacuum.*

Finally, the samples are placed in the microscope support, as shown in Figure 2.9, and examined on their upper surface only.

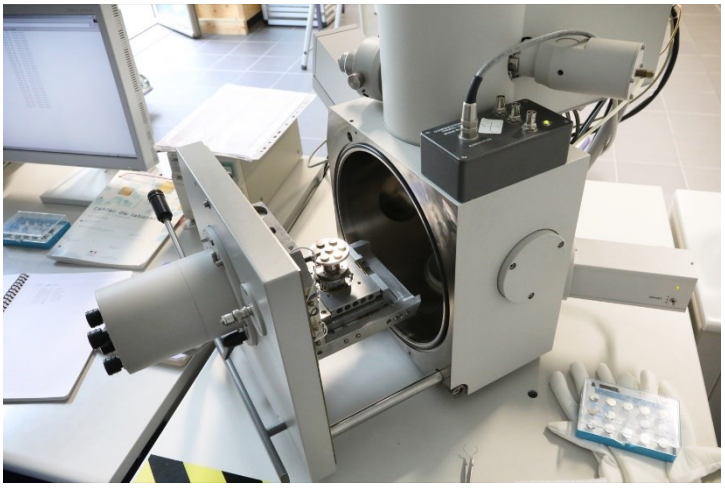

Figure 2.9. *Freeze-dried hydrogel samples, after gold and palladium treatment, introduced into the Scanning Electron Microscope (SEM) support.*

2.3.3 Image processing

Scanning electron microscopy (SEM) coupled with image processing are utilized to determine the porosity and pore size distribution. In the captured images, it is considered that the darker spaces of samples upper surface represent the openings [90]. In this regard, an image processing algorithm was developed in MATLAB, with the following steps, displayed in Figure 2.10:

(a) Binarize the original gray-scale SEM image using Otsu multi-level thresholding method to find the darkest parts of the images, which are segmented in a way that leads to the lowest standard deviation of intensity in each segment (Otsu 1979);
(b) Detect and label all pore spaces within the darker part of the images using watershed segmentation algorithm; it is based on distance transform of a binary image, named city-block and coupled with noise reduction method of median filtering [91,92];
(c) Remove large pores belonging to the samples upper surface, considering an area threshold manually set;
(d) Calculate percent porosity and the equivalent radius of the remaining labelled pores, using it as average pores radius [93].

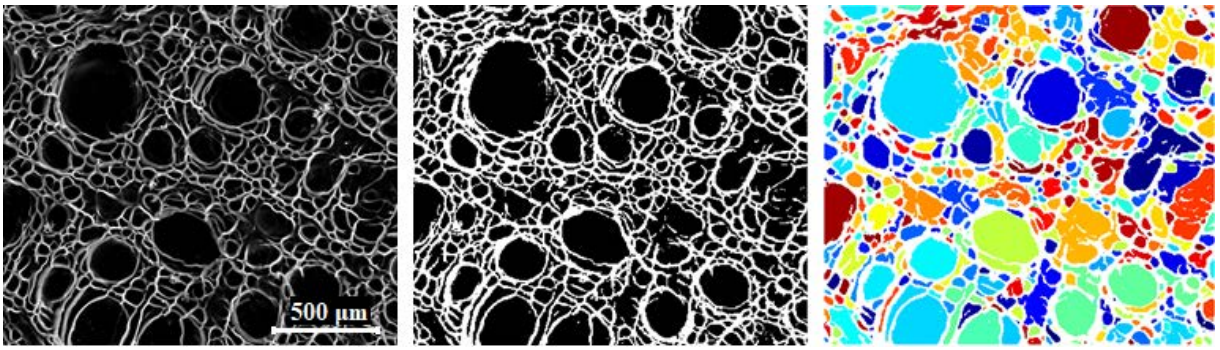

Figure 2.10. *Image processing algorithm sequence. Original SEM image (a); Otsu-binarization application (b); watershed pore-labeling (c).*

2.4 Three-Dimensional Bioprinting

Three-dimensional printing and bioprinting tests were performed with the INKREDIBLE™ bioprinter model, developed and sold by Cellink®, the Swedish biotechnology start-up, officially founded in 2016 by Erik Gatenholm. The INKREDIBLE bioprinter (Figure 2.11), is a pneumatic-based extrusion bioprinter, with dual printerheads and a UV LED curing system. A compressor is used to convey air to the extruders.

Figure 2.11. *Cellink® INKREDIBLE bioprinter.*

The dual-printerheads system allows to print different hydrogels at the same time. This is fundamental for biological applications, not only because it ensures a quicker printing time, but also because it enable the use of different cell types in the same structure without the need to change extruders or to pause the bioprinting process. The UV light-curing system is integrated within the bioprinter; this model is equipped with a 365 nm LED that can be activated

immediately after the print and therefore, by using suitable photo-initiators, it is possible to crosslink a structure without removing it from the printing support. This bioprinter model is not provided with the Cellink's patented Clean Chamber Technology, that allows to operate under sterile conditions; it can however be easily placed under a biological hood. One problem concerning this bioprinter model is the lack of a temperature control system, thus making the use of temperature-sensitive bioinks more difficult. Extruders are sold separately, as well as tips. The nozzle diameters of tips are available in the range from 0.25 mm to 0.41 mm. Both the extruders and tips can be sterilized for biological applications.

2.4.1 G-Code generation

The bioprinter also has an integrated memory where G-Code files are stored, and it can be used even without any computer connected. In this context, structures to be printed were designed with AUTOCAD® 2020, exported as STL files (Stereo Lithography interface format) and then converted into machine language with Slic3r, and saved as G-Codes. Every G-code contains sequences of commands, parameters and instructions, in the form of coordinates, that the printer follows to print objects. For these reasons, the G-code generation can be hand-written (e.g., using Notepad++ software), or by a suitable 3D-printing toolbox. Slic3r is an open-source slicing software that allows to define printing parameters, such as the number of layers for a single structure, their height, the percent infill of a structure and the corresponding fill pattern, the printing speed, the filament dimension, and the number of available extruders. Structures design and printing parameters selection were directly correlated to the type of bioink and to the end-use of structures. Slic3r (as well as most slicing software) slices structures in layers, encoding prints that start from the bottom most layer and proceed by superpositioning a layer on top of the previous one. Instead, writing G-Code by hand lets you encode more complex movements in all three dimensions; while this can get confusing and complicated with bigger structures, it lets you create bridges and oblique filament features – given that a suitable material is used.

2.4.2 3D printing

GelMA hydrogels, obtained as described in §2.2, are used as bioinks for three-dimensional printing and bioprinting applications. In three-dimensional printing, there are constraints on:

(a) GelMA degree of functionalization (DoF), blend typology and concentration;
(b) Operating conditions, such as extrusion temperature and pressure that are related to thermal reversibility and to material viscosity.

In three-dimensional bioprinting applications, in addition to the aforementioned limitations, there are also constraints, on the same parameters, related to the viability of encapsulated cells. Three-dimensional printing tests were performed as trial tests, carried out in order to evaluate the optimal operating conditions for subsequent three-dimensional bioprinting experiments: the main aim was to develop a printable material useful for cells encapsulation, and the identification of optimal printing conditions. To achieve these goals, GelMA hydrogels with a fixed polymer concentration (8% w/v) and with fixed DoF (70%) were used (as described in 2.2) alone and with blending materials (0.7% w/v agarose and 0.1%, 0.5%, 1% w/v Pluronic F127), always ensuring:

(a) Three-dimensional printability of structures with different degrees of complexity and high resolution, avoiding their collapse before light curing and preventing grainy filament conditions;
(b) No clogging of the printer-heads;
(c) A UV-exposure time equal or lower than 120 s;
(d) Printing pressures below 200 kPa;
(e) Sustained printing speed (≤ 4 mm/s), to limit the influence of temperature on the viscosity of the hydrogel.

Since GelMA-based hydrogels are highly sensible to temperature, viscosity was at first optimized by varying the refrigeration time prior to printing. In fact, above and below specific temperature values, depending on the type and concentration of polymers in the hydrogel, gel-sol and sol-gel transitions occur. If temperature is above the gel-sol transition, viscosity is too low and the material is not printable; if temperature is below the sol-gel transition and viscosity is too high, the hydrogel is printed in grainy filaments and printheads clog frequently. Bioinks for 3D bioprinting are partially composed of cells homogeneously suspended in their growth medium, which can change the overall material viscosity. The optimization performed with GelMA-based hydrogels without encapsulated cells is fundamental to determine printing parameters such as the infill percent and fill pattern, the printing speed, and UV exposure time for light curing. The refrigeration time prior to printing, and printing pressure cannot be pre-determined for bioprinting and need to be re-optimized. According to previous results, the concentration of GelMA in hydrogels was fixed at 8% (w/v); although this concentration does not allow 3D structures with high print resolution [2], in hydrogels characterized by such a concentration of GelMA, cells should experience a normal life cycle, come into contact with surrounding cells, not being restricted to a rounded shape because of the high density of the surrounding environment, and migrate [94]. To verify cell viability within our different hydrogels, we performed a series of tests both bioprinting cylindrical scaffolds and comparing them with casted scaffolds obtained with annulus molds made of PDMS, as described in 2.2.

2.4.3 3D printing protocol

The protocol used for 3D printing of structures with one extruder follows: GelMA-based hydrogels are prepared as described in 2.2, to which 25 µl of cell culture media is added. To avoid excessive viscosity alteration, a hydrogel-medium ratio is chosen and kept fixed: 1 ml of hydrogel contains 25 µl of cell culture media. The hydrogel is then stored into test tubes and kept in liquid state at 37 °C; it is subsequently moved into a disposable extruder with a syringe (avoiding the formation of air bubbles) and treated with different thermal cycles, depending on blend typology. After refrigeration, when the hydrogel is viscous enough but not grainy (i.e., in the transition phase between sol and gel state), the extruder is loaded on the printer. A tip with an appropriate nozzle diameter is selected according to the structure to be printed. The desired printing support (a petri dish, a multiwall plate, or a glass slide) is placed on the printbed of the printer. At this point, the instrument is calibrated and the compressor is activated. The G-Code of the desired structure, loaded on the bioprinter integrated memory, is selected. Printing pressure is manually set up by the operator, by means of two knobs located on the printer side, one for each extruder. Every designed structure presents an external control perimeter (i.e., a skirt in 3D printing jargon), with the aim of manual pressure calibration before the actual printing. Once the structure is printed, light curing can be performed with the bioprinter UV LED curing system.

From now on, unless differently stated, a petri dish was selected as printing support; one structure per petri dish plate was printed, with the goal of printing three structures at a time to have at least three technical replicates of the same test; the structures were printed with one extruder, a nozzle with internal diameter of 0.25 mm and a printing speed of 4 mm/s; the maximum applied printing pressure was kept below 200 kPa; UV exposure always lasted 60 seconds.

3D printing of GelMA-hydrogels without encapsulated cells was performed to optimize printing parameters, depending on the bioink typology. For GelMA and GelMA-Agarose blended hydrogels, the structure represented in Figure 2.12 was designed: Figure 2.12.a shows the structure designed with AutoCAD (the larger and the smaller squares have a side length of 12 mm and 6 mm, respectively); Figure 2.12.b shows the virtual printing preview of the overall structure, obtained according to all the parameter set with the software; finally, the structure is composed of two layers, each 0.3 mm high, with a circular infill set to 40%. Table 2.3 summarizes the printing parameters:

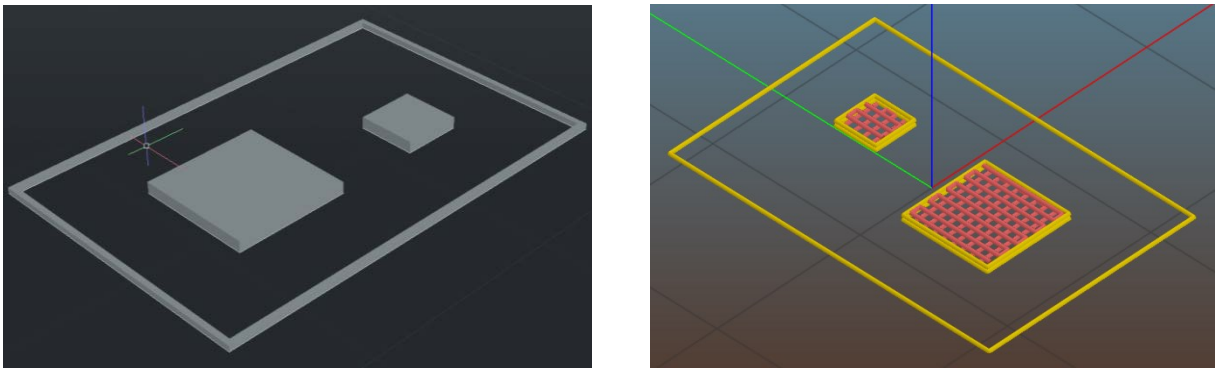

(a) (b)

Figure 2.12. *First structure designed for printing GelMA and GelMA-Agarose hydrogels, with AutoCAD (a) and G-Code generation with Slic3r (b).*

	GelMA	***GelMA - Agarose***
Thermal treatment	7 min at 4 °C	4 min at 4 °C
Extrusion pressure [kPa]	50 ÷ 60	60 ÷ 90
Printing time [s]	~ 120	~ 120

Table 2.3. *Optimized printing parameters for GelMA and GelMA-Agarose hydrogels.*

A second structure was then designed to test hydrogel viscosity over a longer printing time. A more complex structure was designed, composed of nine squares with a side length of 6 mm, and made of one layer 0.3 mm high. For this structure (Figure 2.13), also GelMA-Pluronic 0.5% w/v blend was tested, and the optimized printing parameters are summarized in Table 2.4:

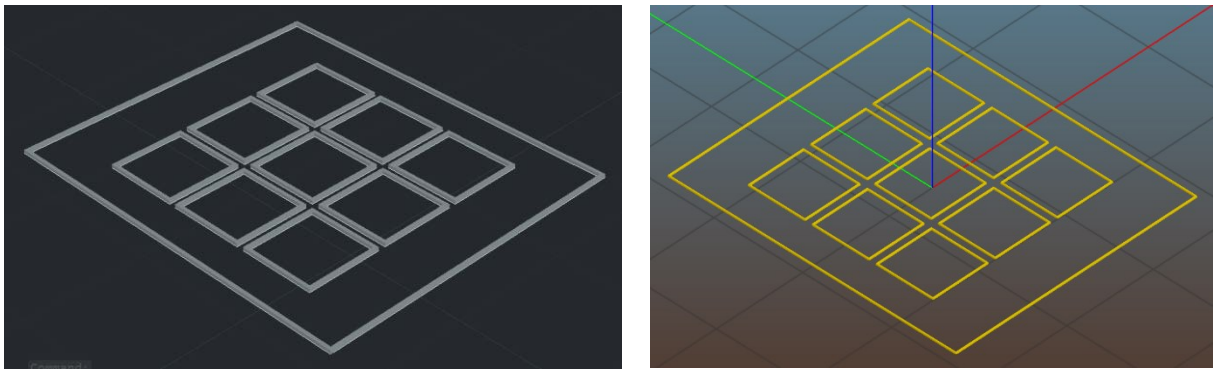

(a) (b)

Figure 2.13. *Second structure designed for printing GelMA, GelMA-Agarose and GelMA-Pluronic 0.5% w/v hydrogels, with AutoCAD (a) and G-code generation with Slic3r (b).*

	GelMA	*GelMA - Agarose*	*GelMA - Plu 0.5% w/v*
Thermal treatment	7 min at 4 °C	4 min at 4 °C	15 min at 20 °C 4 min at 4 °C
Extrusion pressure [kPa]	50 ÷ 60	60 ÷ 90	20 ÷ 30
Printing time [s]	~ 120	~ 120	~ 120

Table 2.4. *Optimized printing parameters for GelMA, GelMA-Agarose and GelMA-Pluronic 0.5% w/v hydrogels.*

A third structure was then designed to perform printing test on GelMA-Pluronic 0.5% w/v hydrogels only. The main aim was to optimize viscosity by regulating the thermal treatment, in order to minimize both the cooling time at 4 °C and extrusion pressure, since it is fundamental to use physical parameters that simulate physiological conditions. The structure is shown in Figure 2.14 and composed of three lines 20 mm long and made of three layers 0.3 mm long, so that the overall structure is 0.9 mm high. Table 2.5 summarizes the optimized printing parameters:

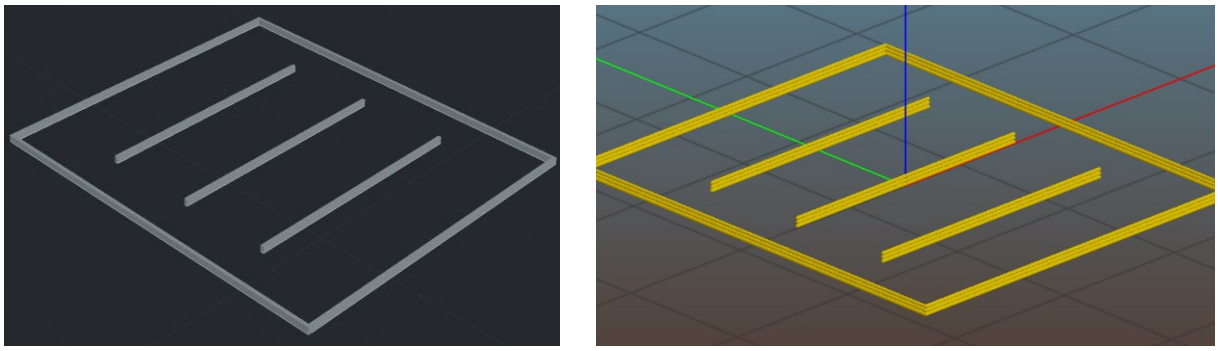

(a) (b)

Figure 2.14. *Third structure designed for printing GelMA-Pluronic 0.5% w/v hydrogels, with AutoCAD (a) and G-code generation with Slic3r (b).*

	GelMA - Pluronic 0.5% w/v
Thermal treatment	15 min at 20 °C, 4 min at 4 °C
Extrusion pressure [kPa]	20 ÷ 30
Printing time [min]	~ 4

Table 2.5. *Optimized printing parameters for GelMA-Pluronic 0.5% w/v hydrogels.*

2.4.4 3D bioprinting with encapsulated cells

3D bioprinting of GelMA-hydrogels with encapsulated neuroblastoma cells (SK-N-AS) and mesenchymal stem cells (MSC) was performed to evaluate cellular viability inside 3D hydrogel structures. The bioink used is composed of: GelMA-Pluronic 0.5% w/v blend, 25 µl cell culture medium for every ml of hydrogel, containing $5 \cdot 10^6$ SK-N-AS cells or $4 \cdot 10^5$ MSC cells. These ratios are based on the experimental results by Santi, Mantovani [2,95]. The optimized structure was designed to have a parallel with the casting method explained in 2.2 and shown in Figure 2.15: a circular geometry with 8 mm radius is displayed in Figure 2.15.a; circular infill at 40% and two layers, each 0.3 mm high, are displayed in Figure 2.15.b. Table 2.6 summarizes the printing parameters:

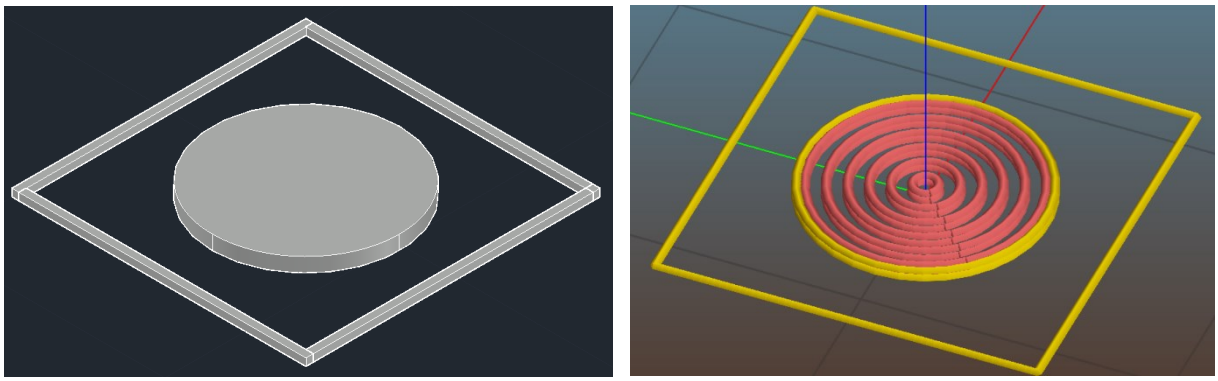

(a) (b)

Figure 2.15. *Optimized circular structure for printing GelMA-Pluronic 0.5% w/v hydrogels with encapsulated SK-N-AS and MSC cells.*

	GelMA - Pluronic 0.5% w/v
Thermal treatment	15 min at 20 °C, 4 min at 4 °C
Extrusion pressure [kPa]	20 ÷ 30
Printing time [s]	~ 60

Table 2.6. *Optimized printing parameters for GelMA-Pluronic 0.5% w/v hydrogels.*

Even for bioprinting experiments, this structure was printed with the same procedure explained in 2.4.3, with the goal of printing five structures at a time to have at least five technical replicates of the same test for biological validation.

To bioprint 3D structures with encapsulated cells, it is necessary to work in sterile conditions, to avoid any type of contamination and therefore to prevent testing failure. The bioprinter was therefore always used under the biological hood, and the necessary extruders, syringes, nozzles, were sterilized before using by autoclaving at 121 °C for 40 minutes. After bioprinting,

structures were transferred in multiwell culture plates and covered with growth medium to study the viability of encapsulated cells immediately after printing, and after 3 and 7 days of incubation. The test is performed in parallel with casting method. The analysis of these structures is carried out by fluorescence markers, as explained in 2.5.2.

2.5 Biological validation

GelMA-based hydrogels were used as scaffolds to perform cellular tests with neuroblastoma cells (SK-N-AS) and mesenchymal stem cells (MSC). The tests were performed in order to evaluate cell viability when encapsulated in 3D hydrogel scaffolds.
The cell lines used to carry out the experiments, were grown in conventional 2D cell culture, using T-flask with vented caps; particularly, T-25, T-75, or T-150 were used according to the necessary area for the cell culture, of 25 cm^2, 75 cm^2, 150 cm^2, respectively. Cell cultures were maintained in a controlled atmosphere (20% of O_2, 5% CO_2) at the physiological temperature of 37°C. Different cells types require different growth media, with the necessary nutrients for their survival and growth, in controlled pH conditions. SK-N-AS requires a growth medium made of 87% Dulbecco's Modified Eagle Medium (DMEM), 10% Fetal Bovine Serum (FBS), 1% Penicillin-Streptomycin, 1% Glutamine and 1% of Mineral Essential Medium (MEM). The growth medium for bone marrow derived MSC cell culture, is made of 90% MesenCult™ MSC Basal Medium (Human) and 10% MesenCult™ MSC Stimulatory Supplement (Human). Culture media also include phenol red, $(C_6H_4OH)_2C_7H_4SO_3$, whose color is sensible to pH: in alkaline solutions red phenol takes on a red color, it turns orange in neutral ones, and yellow in acid ones. The color shift of the growth medium from red to yellow is due to the attack of carbohydrates by microorganisms and makes it possible for the operator to understand when it is necessary to substitute it.

2.5 3D cell culture

The complete protocol followed for biological tests, regardless of the cell line used, assuming the use of T-75 flasks, is reported below; all these steps are performed in sterile conditions:

(a) Once 80-90% cells confluence is reached inside a T-75 flask, the growth medium is removed, and a light washing with 7 ml of 1X PBS is performed in order to remove dead cells, cellular debris and waste;
(b) 1X PBS is removed and 3 ml of 0.04% trypsin are used to detach the cells from the culture flask, that is placed in the incubator for 5 minutes; 0.04% trypsin is a dilute solution of the enzyme trypsin, a pancreatic serine protease, used in order to detach cells

from cell cultivation plates. The time limit of 5 minutes is set to avoid damage to cell membranes;

(c) After 5 minutes, cells detachment is verified, and the trypsin solution is deactivated by adding at least 6 ml of cellular medium; at least a double volume of medium with respect to the trypsin one is actually necessary for its deactivation;

(d) The resulting solution, made of cells suspended in growth medium and trypsin, with an overall volume V, is removed from the T-flask and placed inside a falcon tube; 1 ml of the solution is set aside for cell count, while the remaining volume is centrifuged at 1500 rpm for 5 minutes (soft deceleration activated) in order to obtain a pellet of cells;

(e) Cell count is performed in the spin time. The 1 ml solution, set apart for cell count, can also be diluted with growth medium to simplify this step. Anyway, 10 µl of the original solution (or of the diluted one) are mixed with 10 µl of Trypan Blue solution (0.4%), a stain used to quantify live cells by labelling dead cells exclusively. Especially, Trypan Blue cannot penetrate the cell membrane of live cells, while it can pass through the porous cell membrane of dead cells, entering and staining in blue their cytoplasm. Bürker chamber can be used to determine the average number of live cells per volume unit of the resulting solution of Trypan Blue and medium, N_c. The number of cells in the original volume V, can be evaluated as:

$$N_{cells} = N_c \cdot 2 \cdot V \cdot 10^4$$

where 2 is a dilution factor that derives from the dilution with Trypan Blue solution, and 10^4 is a correction factor for the Bürker chamber;

(f) Once the centrifuge cycle is completed, the solution of trypsin and growth medium is separated from the cellular pellet, settled at the bottom of the falcon tube. The pellet is subsequently re-suspended in fresh growth medium. This step is performed gently and slowly in order to limit cell death and air-bubbles formation, but, at the same time, ensuring the break of clusters of cells. The re-suspension is carried out with a volume of medium that depends on the number of cells previously evaluated, on the number of cells desired per ml of hydrogel, and on the maximum amount of medium that can be added to the hydrogel to avoid excessive variation in its viscosity, such as not to compromise bioprinting performances. Specifically, the number of cells encapsulated per ml of hydrogel was varied between $4 \cdot 10^5$ and $6 \cdot 10^6$, always maintaining a medium-hydrogel volumetric ratio $\leq$ 1:25;

(g) The solution of growth medium and cells is slowly added to liquid hydrogel, at 37 °C, and appropriately mixed obtaining a homogenous solution.

Up to this point, the hydrogel solution with encapsulated cells can be used for both bioprinting and casting applications, as explained in 2.2 and 2.4.4. If it is necessary to repeat the bioprinting procedure to have more technical replicates for the same experiment, the hydrogel solution with encapsulated cells can be thermal-treated again, according to the protocol. Hydrogel thermal treatment can be performed no more than three times to avoid cell death.

2.5.2 Fluorescent imaging

To verify cell viability and migration whitin the 3D bioprinted structures, or with the cylindrical scaffolds realized with PDMS annulus molds, fluorescent dyes were used and fluorescence microscopy analyses were performed. Hoechst 33342 and Calcein AM were used: Hoechst 33432 is a fluorescent stain for detecting DNA in fluorescence microscopy, flow cytometry and immunohistochemistry applications. Hoechst 33432 emits blue fluorescence (λ = 461 nm) when bound to DNA of both live and dead cells nuclei, therefore allowing to determine all the cells encapsulated in the hydrogels. Figure 2.16 shows the chemical structure of Hoechst dye.

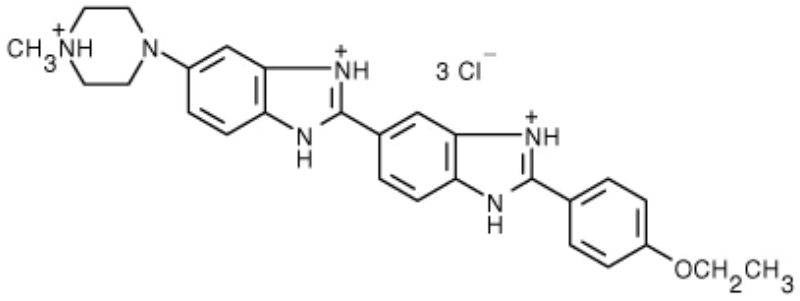

Figure 2.16. *Chemical structure of Hoechst dyes.*

Calcein AM is a fluorogenic, cell-permeant dye, used to determine cell viability in most eukaryotic cells, as it only stains the cytoplasm of live cells. When the acetoxymethyl ester is intact, this probe is non-fluorescent; in live cells instead the non-fluorescent Calcein AM is converted to green-fluorescent Calcein, thanks to the acetoxymethyl ester hydrolysis by intracellular esterases. The probe, whose chemical structure is shown in Figure 2.17, emits at 520 nm with a signal that is proportional to cell viability.

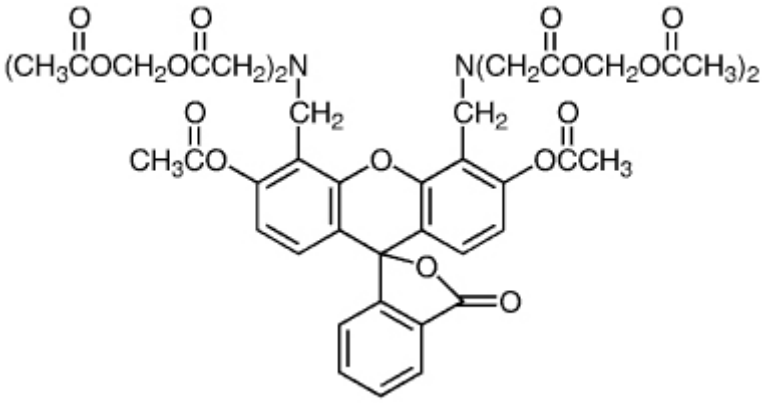

Figure 2.17. *Chemical structure of Calcein AM.*

Hoechst 33342 and Calcein AM are soluble in water and organic solvents. Especially, staining solutions for the analysis of bioprinted structures were prepared with the following composition: in a total volume of 1X PBS or DMEM without FBS, Hoechst 33342 and Calcein AM are added in a volume ratio of 1:1000. After the estabilished incubation time, every single structure to be analyzed, was washed with 1X PBS for at least 3 minutes. Then, after 1X PBS was discarded, it was covered with the staining solution and placed in the incubator for at least 40 minutes before being analyzed with an EVOS fluorescent microscope and ZEISS LSM 800 confocal microscope; this time interval was necessary to allow the solution to permeate inside the structure. Every structure was analyzed in different areas, in order to have at least three images representing all the encapsulated cells, the three corresponding images with live cells only, and, possibly, also the three images with dead cells only.

Chapter 3

Experimental Results

In this Chapter, the efficiency of the synthesis and purification methods applied to obtain GelMA in the desired DoF range is discussed; results of all the characterization analysis carried out on GelMA-based hydrogels are reported and commented. Finally, results of all cellular tests are outlined and discussed.

3.1 GelMA characterization

The method of synthesis described in Chapter 2 was used to obtain GelMA with three different DoF (i.e., 25%, 40%, 70%), depending on the amount of MAA added (i.e., 15, 25, 50 µl per gram of gelatin, respectively). The results are based on H NMR analysis, performed by Professor Sgarbossa's research team, with the aim to verify the method replicability; they are schematically reported in Figure 3.1, while HNM R analysis graphs are shown in Appendix:

Batch number	***DoF expected [%]***	***DoF obtained [%]***
1	70	70 ± 10
2	25	25 ± 10
3	40	42 ± 10
4	70	55 ± 10
5	70	70 ± 10
6	70	64 ± 10

Figure 3.1. *Degree of functionalization of GelMA samples from different batches, obtained with HNM R analysis.*

The uncertainty on DoF values was reasonably fixed to the 10% because measurements are obtained from the analysis of a weak signal, that decreases as the degree of methacrylation increases. According to functionalization results, the synthesis method replicability is verified, since it allows to easily obtain GelMA at desired DoFs, for biological applications. The purification method, based on dialysis of the solution obtained after methacrylation against

deionized water, was successful. The complete removal of salts, unreacted anhydride and methacrylic acid, was at first evident in the variation of the transparency of the solution after 72 hours of dialysis, and was then confirmed by H NMR analysis, given that impurities were not detected in the freeze-dried material. It results that the purification method, followed by the filter-sterilization of the solution and freeze-drying, allows to obtain a pure, dried, and sterile material (Figure 3.2):

Figure 3.2. *GelMA after dialysis, filter-sterilization and freeze-drying.*

3.2 GelMA-based hydrogels

GelMA and GelMA-blended hydrogels, prepared for biological applications, were analyzed in terms of swelling and porosity; analysis results are reported and discussed in the following paragraphs. The main aim was not only to characterize these materials, but also to verify their suitability as scaffolds for cells encapsulation and, if necessary, to study how to optimize them for biological applications. For the sake of clarity, the following Table 3.1 schematically identifies and summarizes the different combinations of materials used for preparing GelMA-based hydrogels:

ID	*Composition [w/v]*	*GelMA DoF*
G25	GelMA 8%	25
G40	GelMA 8%	40
G70	GelMA 8%	70
G25-A	GelMA 8% - Agarose 0.7%	25
G40-A	GelMA 8% - Agarose 0.7%	40
G70-A	GelMA 8% - Agarose 0.7%	70
G25-P0.1	GelMA 8% - Pluronic 0.1%	25
G40-P0.1	GelMA 8% - Pluronic 0.1%	40
G70-P0.1	GelMA 8% - Pluronic 0.1%	70
G25-P0.5	GelMA 8% - Pluronic 0.5%	25
G40-P0.5	GelMA 8% - Pluronic 0.5%	40
G70-P0.5	GelMA 8% - Pluronic 0.5%	70
G25-P1	GelMA 8% - Pluronic 1%	25
G40-P1	GelMA 8% - Pluronic 1%	40
G70-P1	GelMA 8% - Pluronic 1%	70

Table 3.1. *Summary of all combinations of prepared hydrogel and nomenclatures; the first capital letter refers to the base material (GelMA), followed by its DoF value; the first capital letter after the dash refers to the blended material, followed by its concentration if not fixed.*

3.2.1 Swelling

Swelling tests were performed on GelMA-based hydrogel samples - prepared according to the protocol in 2.2 - to evaluate the influence of a blending material on the capability of the material to absorb and retain aqueous solutions. Table 3.2 shows the percentage swelling ratio and water retention evaluated for GelMA and GelMA-Pluronic (at three different concentrations) hydrogels. The tests were performed using GelMA with a fixed DoF of 70%:

ID	*Swelling ratio [%]*	*Water content [%]*
G70	1075 ± 89	91 ± 0.6
G70-P0.1	571 ± 92	85 ± 2
G70-P0.5	1207 ± 115	92 ± 7
G70-P1	1085 ± 141	91 ± 0.8

Table 3.2. *Results of swelling tests performed on hydrogels samples with different Pluronic concentrations.*

The influence of Pluronic concentration, used as blending material, on the overall morphology of hydrogels polymeric network can be inferred on the variation of swelling ratio and water retention. According to the fractional increase of hydrogels weight due to water absorption and retention, Pluronic concentration does not significantly affect the swelling behaviour, compared to G70 samples, prepared with GelMA only. It must be considered that the three Pluronic concentrations chosen are generally low, also compared with GelMA concentration (i.e., GelMA-Pluronic ratios are 1:80, 1:16, 1:8, respectively), so we could anticipate that Pluronic dissolution in water, and consequent outflow from the samples, would not significantly modify the overall morphology of hydrogels. We however observed an opacification phenomenon on G70-P1 samples after photo-polymerization, suggesting a relatively high concentration of Pluronic (Figure 3.3).

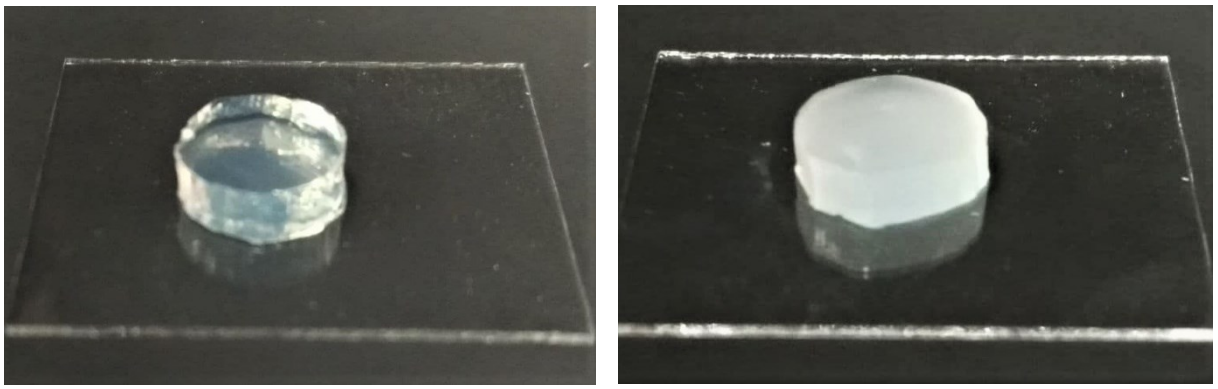

(a) (b)

Figure 3.3. *Optical comparison between GelMA hydrogel samples for swelling, containing 0.5 % w/v (a) and 1% w/v (b) of Pluronic concentration, respectively.*

Finally, considering the high swelling ratio and water content values, evidence shows that both hydrogels with a specified (i.e, 8% w/v) GelMA concentration and blended with Pluronic at low concentration (i.e., 0.1 and 0.5 % w/v) are best suited to ensure the exchange of fluids, providing the appropriate microenvironment for cells growth in 3D.

3.2.2 Porosity evaluation

The porous structure of freeze-dried hydrogels was analyzed with scanning electron microscopy (SEM), as described in Scanning Electron Microscope2.3.2, to determine how both GelMA degree of methacrylation and blending-materials affect hydrogel samples morphology. The analysis is carried out to study the possibility to control micro-architectural features of these materials. For every condition, at least two samples were analyzed and at least four images for sample are taken, using two different magnifications (i.e., 150x and 500x).

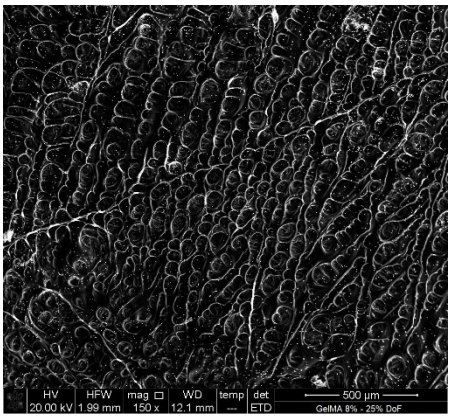

(a)

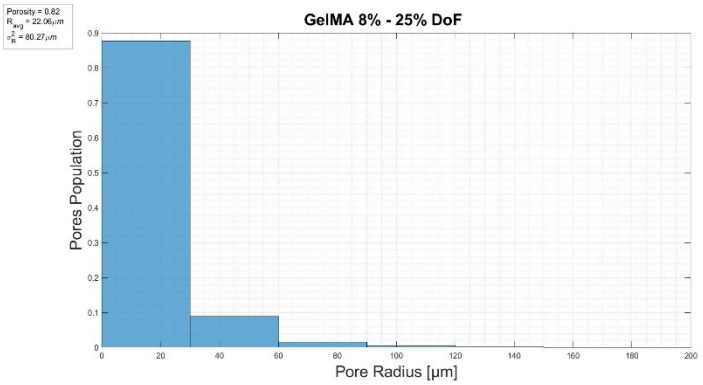

(d)

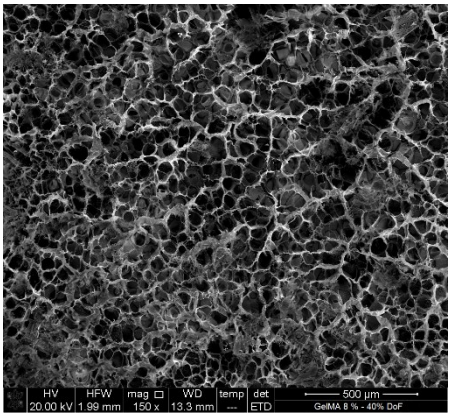

(b)

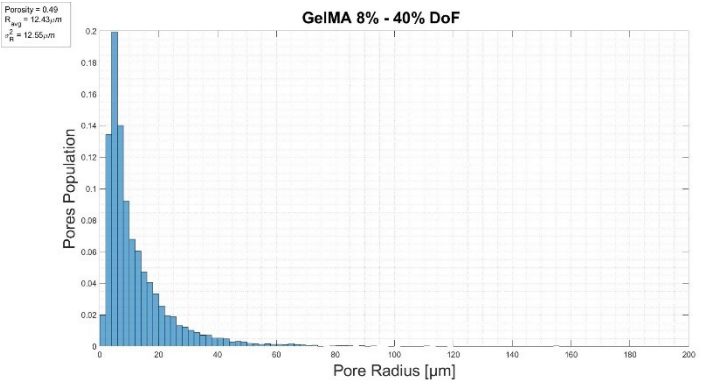

(e)

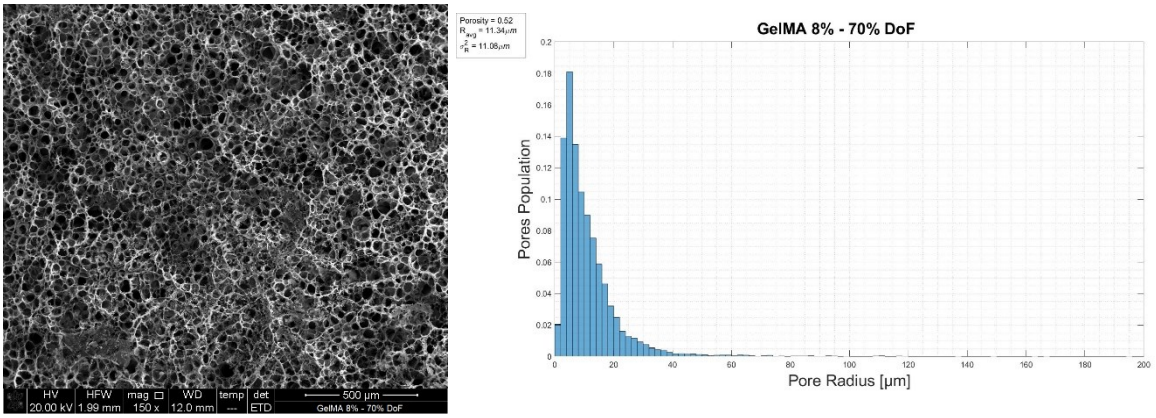

Figure 3.4. *Representative SEM images of freeze-dried hydrogel samples at 8% (w/v) GelMA concentration and 25%, 40%, 70% DoF (a-c) and corresponding pores diameter relative distributions (d-f), analyzed by MATLAB algorithm.*

Image analysis revealed that freeze-dried hydrogels are characterized by a honeycomb-like super-porous structure, with interconnected pores in a defined range of diameter. According to frequency distribution plots and observing SEM images (Figure 3.4), we can conclude that the GelMA DoF affects hydrogel morphology. In particular, for pure GelMA hydrogels (i.e., G25, G40, G70), we can observe a progressive decrease of pore radius, as well as its standard deviation; the overall porosity value is anyway similar for G40 and G70 samples (Figure 3.4.e-f), and much higher for G25 samples (Figure 3.4.d). The polymeric network formation depends on the DoF, resulting in more complex and stronger crosslinks with increasing functionalization. We can identify a threshold DoF value of 40% for an adequately formed network, while values below 25% result in fewer and weaker crosslinks, which are also affected by the freeze-drying process during the sample preparation (i.e., 72 hours of freeze-drying). Statistical data further confirm these considerations: G25 samples have a higher porosity and higher standard deviation. These results were expected based on the observations of the SEM imaging, which was difficult for G25 samples, and resulted in consequent issues to properly detect pores by MATLAB algorithm. This explains the high values in terms of porosity and pore radius standard deviation.

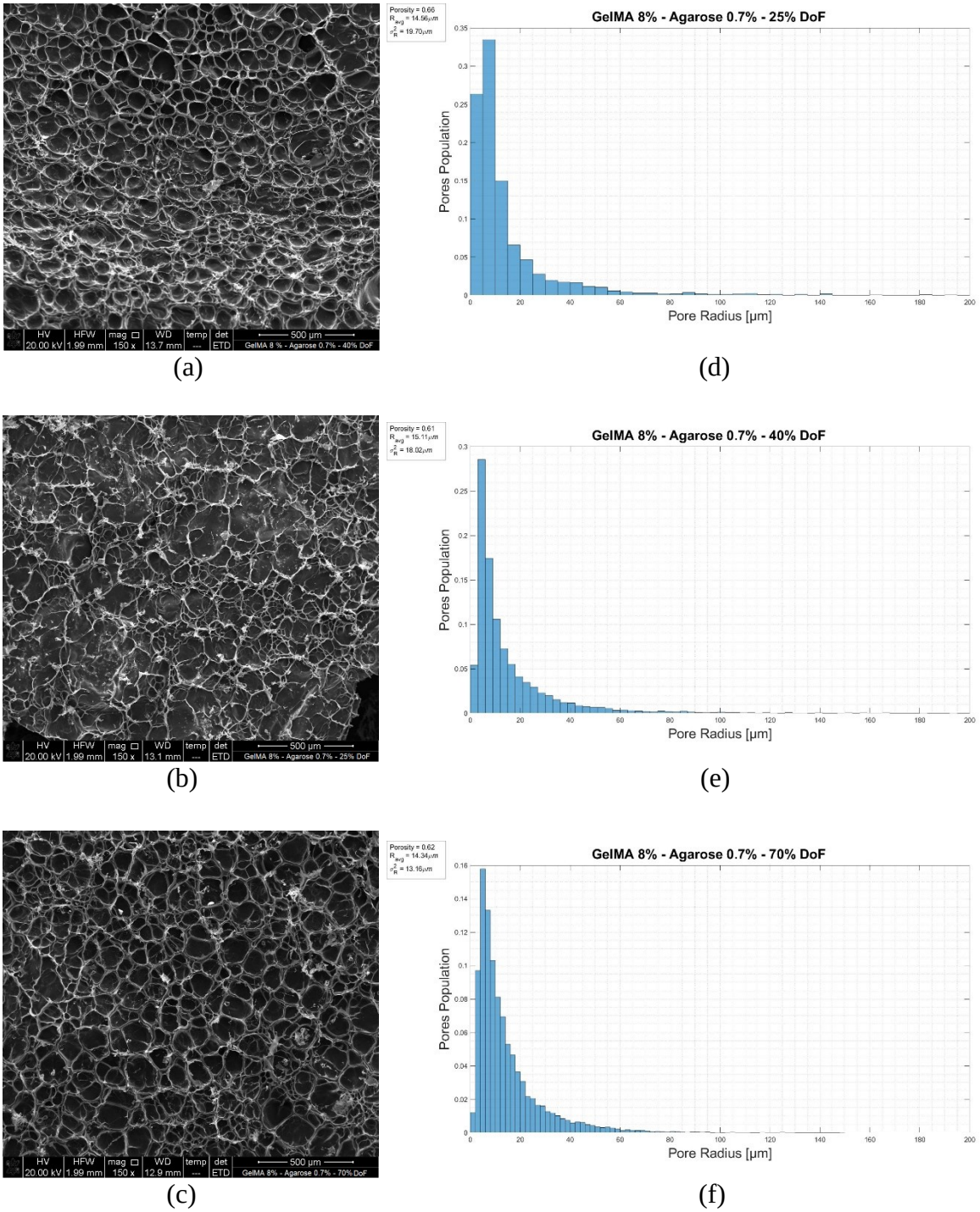

Figure 3.5. *Representative SEM images of freeze-dried hydrogel samples at 8% (w/v) GelMA concentration with 25%, 40%, 70% DoF, and 0.7% (w/v) Agarose concentration (a-c); the corresponding pores diameter relative distributions (d-f), analyzed by MATLAB algorithm.*

Figure 3.5 shows the results for G25-A, G40-A, G70-A blended-hydrogels. If we compare these results to the ones obtained with pure GelMA, agarose addition (0.7% w/v roughly corresponds to 1:11 ratio with respect to 8% w/v GelMA) led to an increase in both percent porosity and

pore radius values, for all the three DoF. However, we can still observe that the polymeric network is more stable and complex at higher DoFs, according to the standard deviation values (Figure 3.5.e-f). The slight increase in the percent porosity and pore radius, together with the superior agarose biocompatibility (promoting cellular adhesion, proliferation and activity) makes GelMA-Agarose blended-hydrogels suitable for cell encapsulation. If encapsulated in such materials, cells can enter the hydrogels porous framework, maintaining their natural 3D shapes and experiencing a normal life cycle, interacting with adjacent cells to create tissue-like structures.

Moreover, DoF influence on the nature of crosslinks is also observed in statistical analysis, since it was easier to perform SEM imaging (i.e., higher number of images taken) and pore detection with MATLAB algorithm (i.e., more precise and reliable detection) at DoF higher than 40%; for this reason, for GelMA-Pluronic hydrogels porosity evaluation, we performed test on GelMA functionalized at 40% and 70% only, as shown in Figure 3.6:

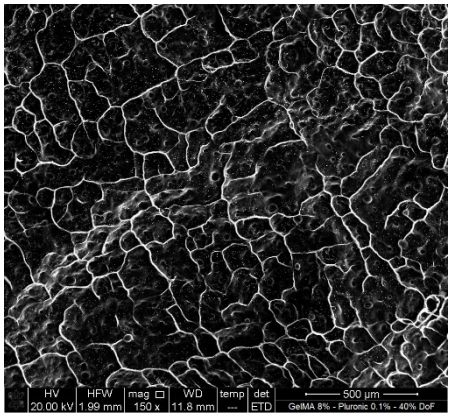

(a)

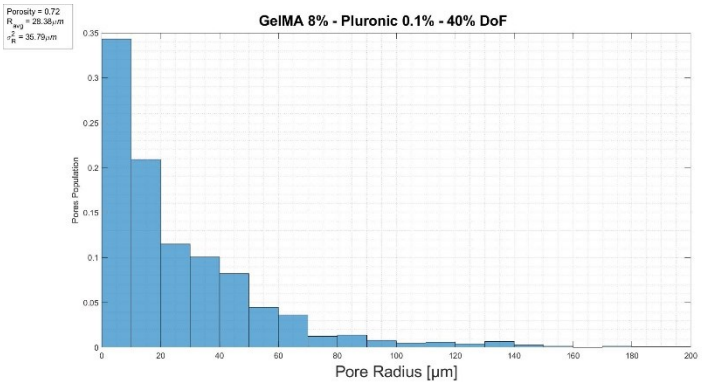

(g)

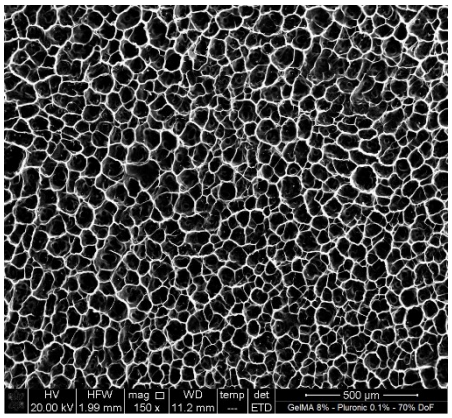

(b)

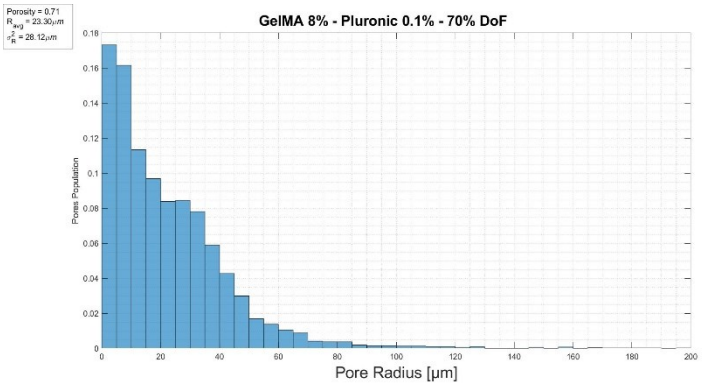

(h)

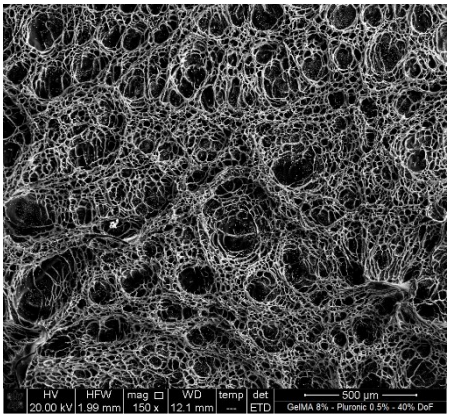
Porosity = 0.61
R_{avg} = 11.73 µm
r_R^2 = 16.95 µm
HV 20.00 kV
HFW 1.99 mm
mag 150 x
WD 12.1 mm
temp ---
det ETD
500 µm
GelMA 8% - Pluronic 0.5% - 40% DoF

(c)

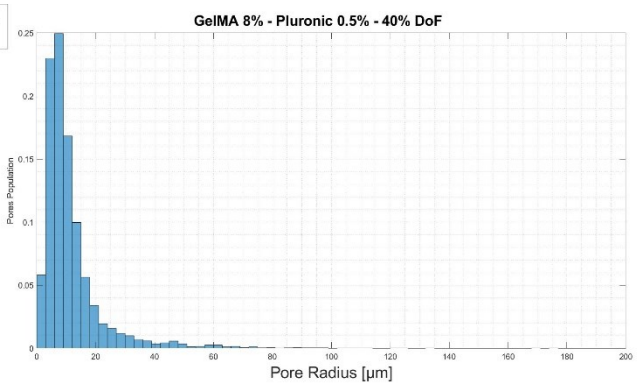
GelMA 8% - Pluronic 0.5% - 40% DoF
Pores Population
Pore Radius [µm]

(i)

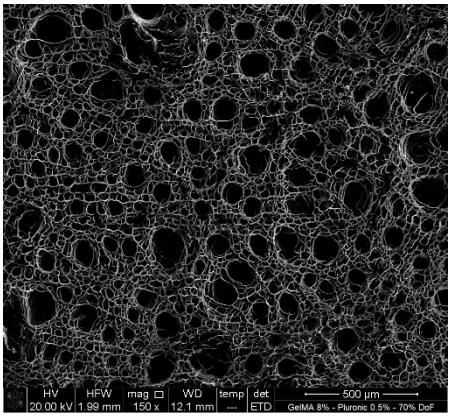
Porosity = 0.72
R_{avg} = 14.88 µm
r_R^2 = 27.26 µm
HV 20.00 kV
HFW 1.99 mm
mag 150 x
WD 12.1 mm
temp ---
det ETD
500 µm
GelMA 8% - Pluronic 0.5% - 70% DoF

(d)

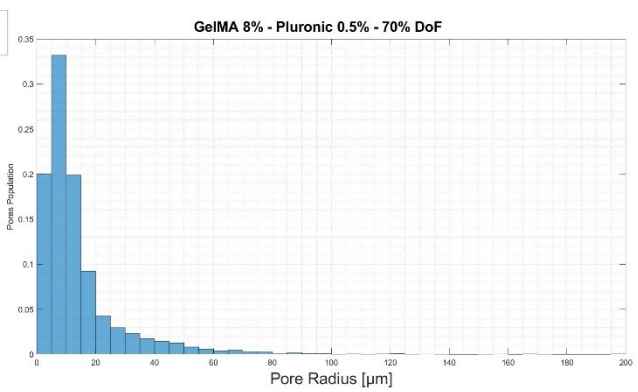
GelMA 8% - Pluronic 0.5% - 70% DoF
Pores Population
Pore Radius [µm]

(j)

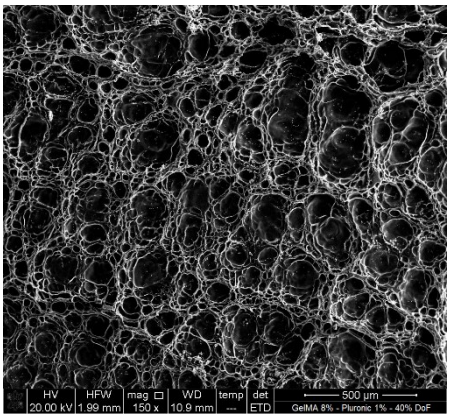
Porosity = 0.67
R_{avg} = 18.91 µm
r_R^2 = 26.79 µm
HV 20.00 kV
HFW 1.99 mm
mag 150 x
WD 10.9 mm
temp ---
det ETD
500 µm
GelMA 8% - Pluronic 1% - 40% DoF

(e)

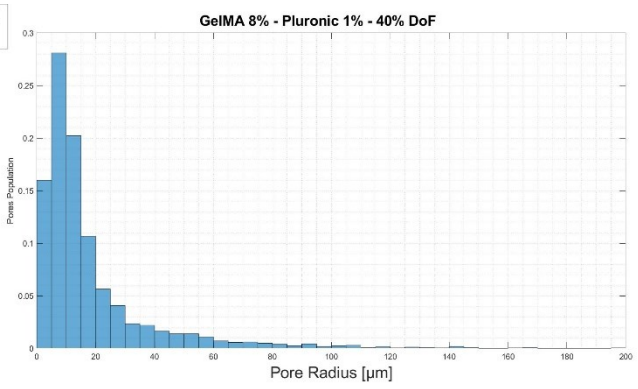
GelMA 8% - Pluronic 1% - 40% DoF
Pores Population
Pore Radius [µm]

(k)

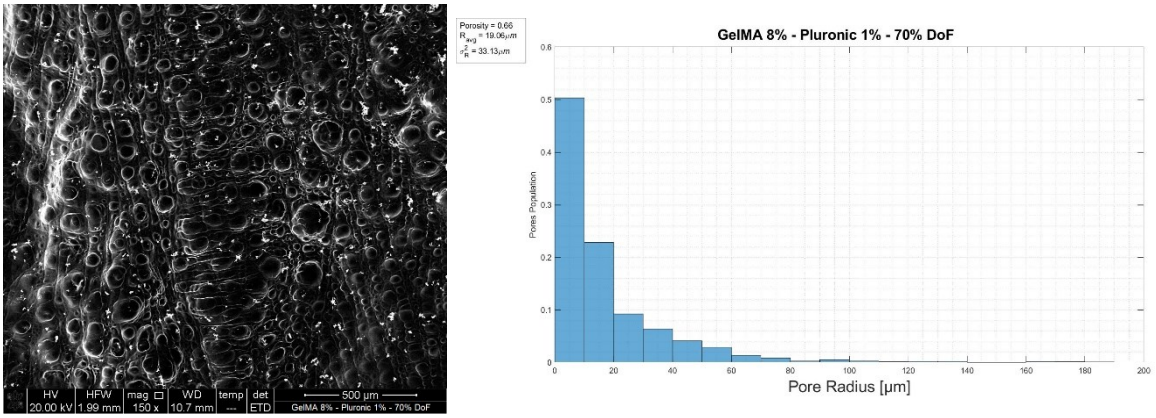

Figure 3.6. *Representative SEM images of freeze-dried hydrogel samples at 8% (w/v) GelMA concentration with 40%, 70% DoF, and 0.1% (a-b), 0.5% (c-d), 1% (e-f) (w/v) Pluronic concentration; the corresponding pores diameter relative distributions (g-l), analyzed by MATLAB algorithm.*

By analyzing the results of GelMA-Pluronic blended-hydrogels, we can see the influence of both DoF and Pluronic concentration on the hydrogels morphology, porosity and pore radius. Since Pluronic is water-soluble, the protocol described in 2.2 ensures its dissolution in an aqueous solution bath and promotes dissolved Pluronic outflow from the structure. The idea behind the adoption of Pluronic as a blending polymer was to enlarge the hydrogels mesh size by generating Pluronic micelles around which GelMA would crosslink, and that would solubilize in aqueous solution, after photoactivation; this would leave bigger holes in the hydrogels structure. In this way, we also expect higher permeability to cell culture media and an overall improved cells mobility and progression in the cell cycle. At the same time, however, Pluronic can alter the morphology in terms of crosslinks regularity, making it thus even more important to choose the correct concentration, as well as to conveniently mix it with GelMA to obtain a homogeneous solution before light-curing.

The results evidence a high variability in terms of standard deviation in all the cases (G40-P0.1, G70-P.01, G40-P0.5, G70-P0.5, G40-P1, G70-P1). The samples with a Pluronic concentration of 0.1% w/v behaves differently than we expected, even if compared with other concentrations (Figure 3.6.i-l). In addition, pores were detected by MATLAB algorithm with difficulties, so we must state that these results are not reliable. The samples with a Pluronic concentration of 0.5% w/v resulted in porosity and pore radius values higher than pure GelMA samples and similar to GelMA-Agarose ones. In particular, G70-P0.5 samples show a high variability in pore radius; it is a good result because in SEM imaging and plots (Figure 3.6.j) we observed the super-porous structure characterized by smaller holes (pore radius of 9÷10 µm), with scattered larger holes (pore radius of 60 µm). Finally, GelMA blended-hydrogels with Pluronic concentration of 1% w/v are analyzed in Figure 3.6.k-l: they are characterized by higher pore radius values and high variability, resulting in small pores (radius of 10÷11 µm) and larger

holes (60÷80 µm). Since it was not easy for the MATLAB aalgorithm to detect the pores, a smaller population of pores was obtained in the histograms; furthermore, after light-curing the samples, they appeared white-opaque, suggesting that a high concentration of Pluronic might still be trapped inside the hydrogel - potentially negatively affecting cell viability.
Overall, taking together the results obtained for GelMA-Pluronic blended-hydrogels, the choice for the best suitable materials for cell encapsulation fell on G70-P0.5, for which we expect both good printability and maintenance of cell viability. The following table summarizes the main characteristic parameters for every condition:

ID	***Porosity [%]***	***Pore radius [µm]***
G25	0.82	22.06 ± 80.27
G40	0.49	12.43 ± 12.55
G70	0.52	11.34 ± 11.08
G25-A	0.66	14.56 ± 19.70
G40-A	0.61	15.01 ± 18.02
G70-A	0.62	14.34 ± 13.16
G40-P0.1	0.72	28.38 ± 35.79
G70-P0.1	0.71	23.30 ± 28.12
G40-P0.5	0.61	11.73 ± 15.95
G70-P0.5	0.72	14.88 ± 27.26
G40-P1	0.67	18.91 ± 25.79
G70-P1	0.66	19.06 ± 33.13

Table 3.3. *Results of porosity evaluation tests performed by SEM and analyzed using MATLAB.*

3.3 3D bioprinting

As explained in 2.4, 3D bioprinting is possible with an appropriate bioink choice. Before the addition of cells dissolved in culture media, it is required to optimize the printing parameters. Therefore, preliminary tests were done without cells to regulate and fine-tune the extrusion pressure and print temperature for every type of hydrogel, being printability strongly affected by material viscosity. To obtain a good print, grainy filaments must be avoided (i.e., too much viscous solution), as well as liquid filaments (i.e., viscosity is too low) which can lead to structural collapse, as shown in Figure 3.7

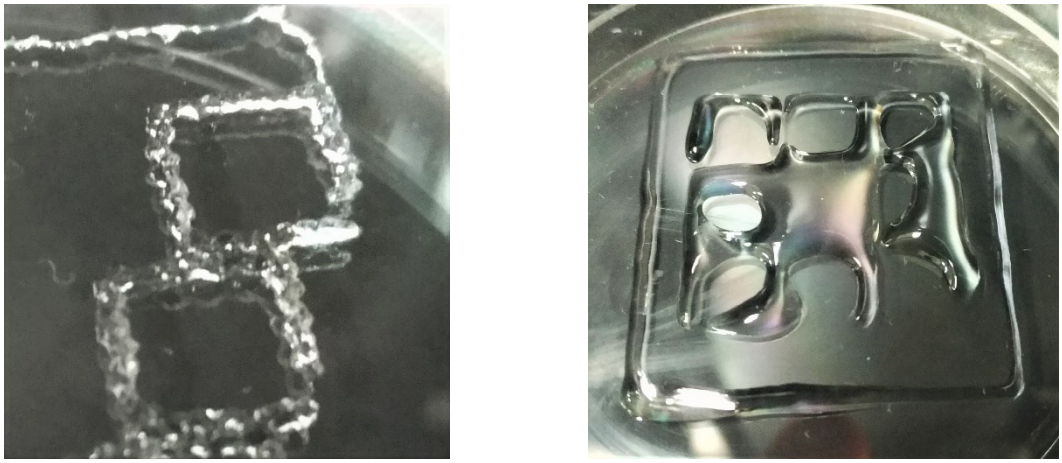

(a) (b)

Figure 3.7. *Examples of wrong choice of bioprinting parameters; grainy filaments obtained with excessive cooling time, resulting in increase in viscosity and extrusion pressure (a); liquid filaments obtained with insufficient cooling time, resulting in low viscosity and extrusion pressure values (b).*

Accordingly, different structures were designed and printed with G70, G70-A and G70-P0.5 hydrogels; Table 3.4 recaps the optimized printing parameters for the three hydrogel solutions:

	G70	***G70-A***	***G70-P0.5***
Thermal treatment	7 min at 4 °C	4 min at 4 °C	15 min at 20 °C 4 min at 4 °C
Extrusion pressure [kPa]	50 ÷ 60	60 ÷ 90	20 ÷ 30

Table 3.4. *Optimized printing parameters for GelMA, GelMA-Agarose and GelMA-Pluronic 0.5% w/v hydrogels.*

All the solutions were cooled down starting from liquid phase (i.e., 37°C, same temperature of standard cell culture incubators and, in general, the physiological human body temperature), in order to reach the appropriate material viscosity. Since cells are highly stressed if kept away from their ideal environment, the thermal treatment and the related extrusion pressure are also chosen according to biological constraints. In particular, when the solution is cooled down in the fridge at 4°C, a long-time exposure to this low temperature can induce cell apoptosis and therefore death, as well as a high extrusion pressure if the solution is too viscous. Also, the bioink choice has to be done in order to ensure a quite-constant viscosity during the entire printing time, otherwise the material cannot be finely printed. Even if results from the porosity analysis pointed at G70-A and G70-P0.5 as suitable materials for 3D bioprinting, preliminary printing tests were also done on G70 hydrogels to have an idea of the thermal treatment for GelMA at 8% w/v, and therefore the extrusion pressure during the print.

The best printing results are obtained with G70-P0.5 hydrogels, in which the thermal treatment at low temperature is minimized, as well as the extrusion pressure, thanks to Pluronic inverse

thermoreversibility (i.e., it completely reaches liquid state at 4°C). At the same time, during printing time there is only a slight and manageable variation in pressure even after prolonged printing (up to 4 minutes). In contrast, G70-A hydrogel presented a high variation in viscosity, since the cooling down treatment is difficult to implement, with precise cooling time; in addition, significant viscosity variation is observed during the print itself, resulting in an extrusion pressure varying from 60 to 90 kPa, not ideal for cell culture.
After the optimization of 3D printing parameters, the bioink can be prepared as explained in 2.4.4. The 1:25 ratio is not only kept constant for every GelMA-blended hydrogel, but is also chosen in such a way to have the same optimized printing parameters for 3D bioprinting. The cell lines used are:

(a) SK-N-AS, which are human neuroblastoma cells;

(b) Mesenchymal stem cells (MSC), derived from yellow bone marrow, known as fatty tissue.

We decided to characterize the materials and optimize the printing parameters in order to bioprint and perform biological tests on GelMA-blended hydrogels only, since from the results obtained by Santi G. [2], GelMA alone presents issues in terms of permeability and therefore in cell viability.
Based on the porosity results and on optimized printing parameters, we chose G70-P0.5 as the ideal material for 3D bioprinting. Figure 3.8 shows the bioink printed and photopolymerized:

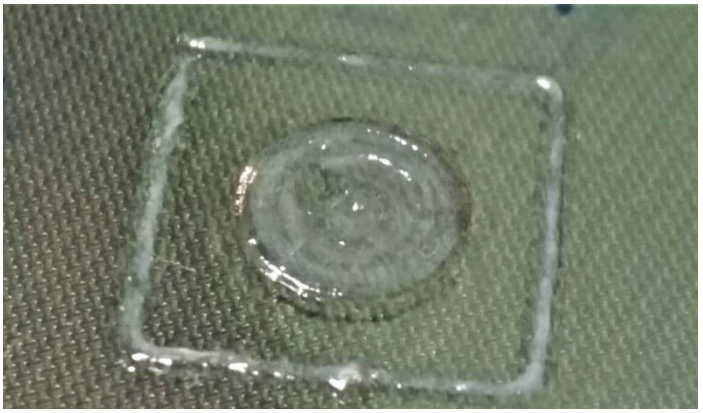

Figure 3.8. *3D bioprinted circular scaffold, using G70-P0.5 material and light-cured for 60 seconds.*

3.4 Biological tests

As discussed in the previous paragraphs, pure GelMA-based hydrogels presents issues in terms of permeability, ultimately limiting the necessary nutrient supply to cells. However, biological tests were also performed on G70 hydrogels as further supporting evidence. Initially, cylindrical cellularized scaffolds were prepared with casting method, according to the protocol described in 2.5. Samples containing SK-N-AS cells were then placed in incubator and analyzed via immunofluorescence staining (i.e., using Hoechst and Calcein) after one day of incubation. Although most experiments failed due to contamination, we observed low concentrations of tracers in the bulk of the scaffold, highlighting the super-porosity of GelMA structure and its low permeability.

The same cell line was then cultured in G70-A hydrogels. Initially, we decided to perform preliminary biological tests on cylindrical scaffolds prepared with the same casting method employed above 2.2, and to conduct fluorescent analysis after 24 hours of incubation.

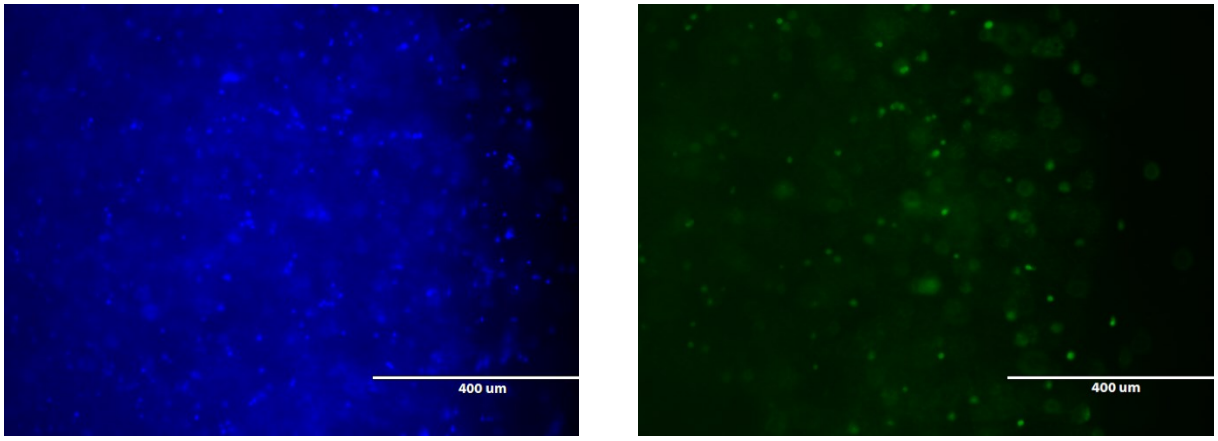

(a) (b)

Figure 3.9. *Results of test with fluorescent markers on G70-A sample prepared with casting method, after 24 hours from incubation: SK-N-AS nuclei marked in blue by Hoecst(a), SK-N-AS cytoplasm marked in green by Calcein (b); 10X magnification.*

Figure 3.9.a shows shows a stitching of several images across the cylinder section where all cells nuclei are marked in blue by Hoechst, while Figure 3.9.b shows the cytoplasm of live cells in the same areas, marked in green with Calcein. We can clearly observe poor diffusion and high autofluorescence of proteins inside the scaffold, which made difficult the interpretation of images.

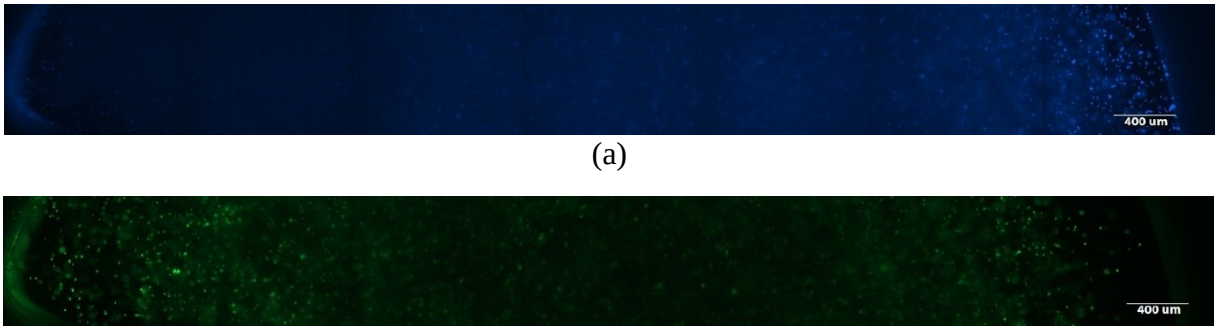

(a)

(b)

Figure 3.10. *Results of test with fluorescent markers on G70-A sample prepared with casting method, after 72 hours from incubation: SK-N-AS nuclei marked in blue by Hoecst(a), SK-N-AS cytoplasm marked in green by Calcein (b); 10X magnification.*

Given that, Figure 3.10 shows the horizontal view of the entire sample, the permeability issues are further highlighted: cells are correctly exposed to fluorescent markers - and therefore to cell culture media - at the interface area (i.e., sample edges), while a definitely lower concentration of markers is detected in the bulk (i.e., sample center). In general, the experiments failed due to bacterial contamination, typically detected after three days of incubation. Agarose may be responsible for the contamination, since it provides nutrients for cells, but also promotes bacterial activity, both in terms of growth and proliferation.

According to both porosity and printing parameters results, G70-P0.5 hydrogels (GelMA-Pluronic blend) are chosen as the most suitable materials for 3D bioprinting. The biological tests with fluorescent markers were conducted for both bioprinted and cast scaffolds, simultaneously. The material was also tested with both cell lines, SK-N-AS and MSC.

(a)

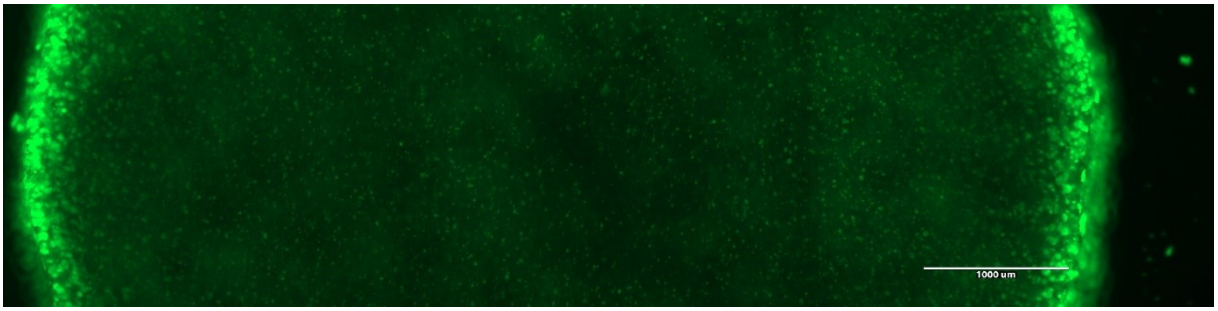

(b)

Figure 3.11. *Results of test with fluorescent markers on G70-P0.5 sample prepared with casting method, after 7 days from incubation: SK-N-AS nuclei marked in blue by Hoechst (a), SK-N-AS cytoplasm marked in green by Calcein (b); 4X magnification.*

Figure 3.11 shows the entire field width of a cast sample, containing SK-N-AS, and analyzed with Hoechst (Figure 3.11.a) and Calcein (Figure 3.11.b) after 7 days of incubation. We can observe good permeability in both cases: although the sample exhibits a low color gradient in the interface-bulk range, the bulk is clearly visible. In this case, we can state that Pluronic dissolution after casting and photo-curing promotes a correct flow of liquid solutions in which the scaffold is soaked. Also, the experiment provides a confirmation of the porosity results obtained, proving that the mesh size is larger. Moreover, low autofluorescence can be observed, which is always inevitable because the cells overlap on layers at different height. Finally, after day 7 of cell culture, SK-N-AS appear alive and correctly progressing in their cell cycle and, above all, no bacterial contamination was detected.

Another experiment was carried out to simultaneously evaluate cell viability in scaffolds obtained with bioprinting and casting method. The results are collected after 10 days of incubation, using the Hoechst and Calcein immunostaining:

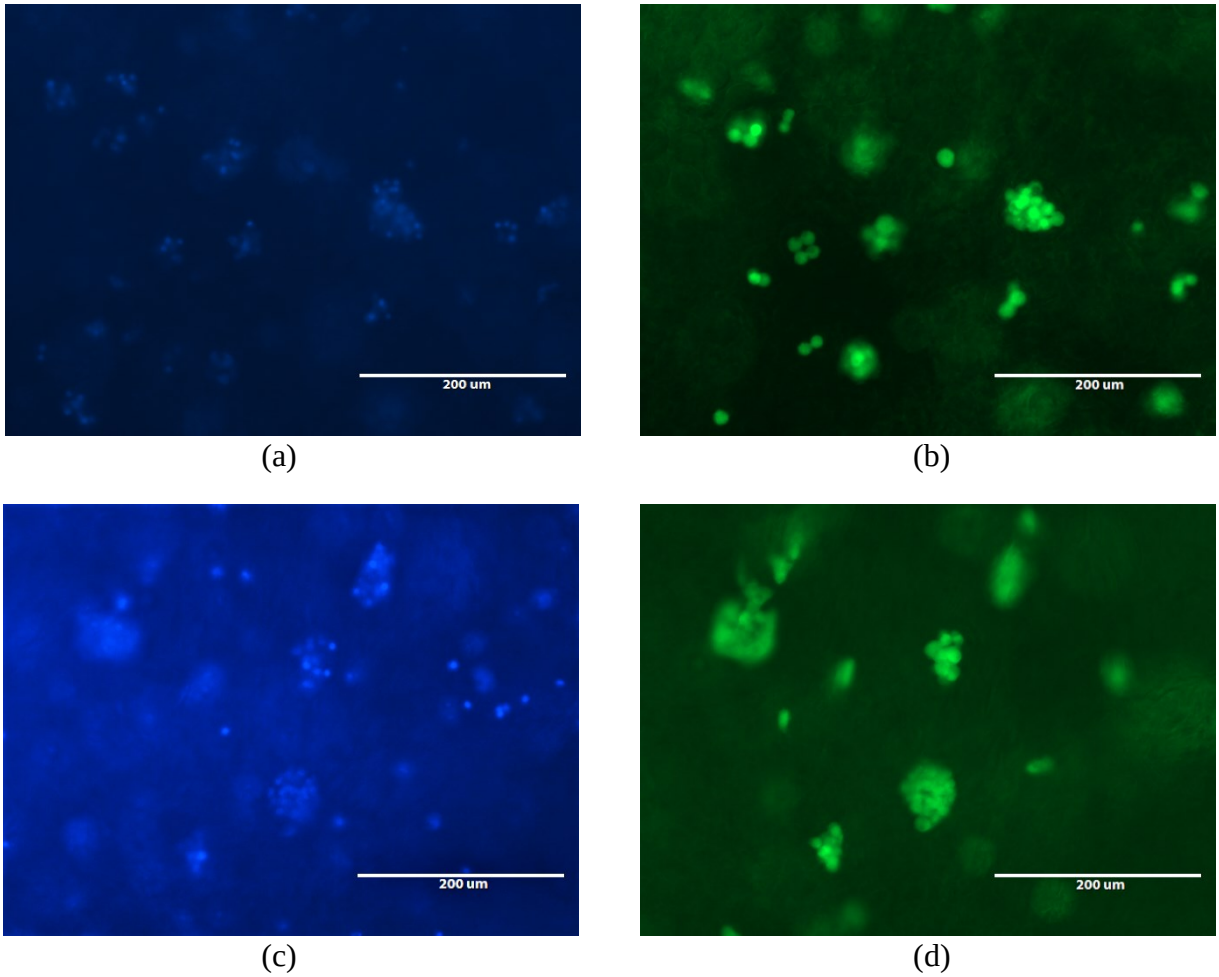

Figure 3.12. *Results of test with fluorescent markers on G70-P0.5 sample prepared with casting method (a-b), and bioprinting (c-d) after 10 days from incubation: SK-N-AS nuclei marked in blue by Hoechst (a, c), SK-N-AS cytoplasm marked in green by Calcein (b, d); 20X magnification.*

Figure 3.12 shows the natural behavior of SK-N-AS cells, which tend to move through the network and form aggregates composed by several cells. This is a very important result, because simultaneously proves a good mass transfer between culture media and cells, and supports the Pluronic influence on GelMA porosity, all leading to an improved cell viability. In general, we observed better results for cast samples with respect to bioprinted scaffolds: a reason can be found in the thermal treatment and pressure to which the cells are nonetheless subjected during the printing procedures.

However, to better observe the SK-N-AS cells behavior, another experiment was carried out to perform fluorescent analysis using confocal microscopy, which is an optical imaging technique for increased optical resolution and contrast of a micrograph. Briefly, confocal microscopes use a spatial pinhole to block out-of-focus light in image formation [96], and therefore reduce autofluorescence.

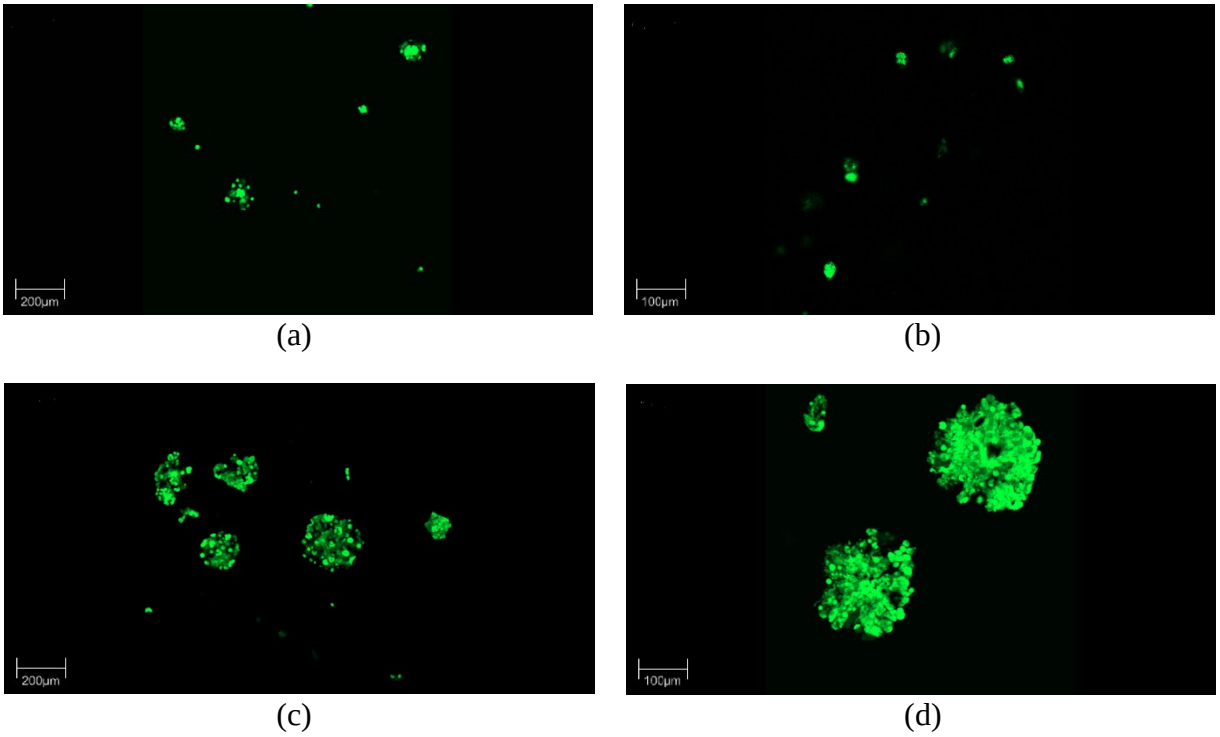

Figure 3.13. *Results of tests on G70-P0.5 samples prepared with casting method, analyzed with confocal microscopy after 2 (a-b) and 10 days from incubation: SK-N-AS cytoplasm marked in green by Calcein.*

Figure 3.13 shows images representative of samples obtained with both casting and bioprinting methods, analyzed after two (Figure 3.13.a-b) and ten (Figure 3.13.c-d) days of incubation, stained with Calcein marker. Images better underline SK-N-AS behavior, showing rounded cells with the tendency of forming clusters. Furthermore, SK-N-AS clusters are better defined after 10 days, proving a good microbiological environment for cells. If we compare these results with those obtained using pure GelMA [2] and GelMA-Agarose hydrogels, we observe the absence of cells clusters. It is clearly evident that the voids left by Pluronic dissolution are now occupied by SK-N-AS cells, which are free to move through the entire network and to form clusters. Again, cast samples allows a better life cycle with respect to bioprinting. Finally, no bacteriological contamination was detected.

The promising results encouraged the addition of MSC cell line, which are generally more fragile than SK-N-AS, and the growth rate is quite low.

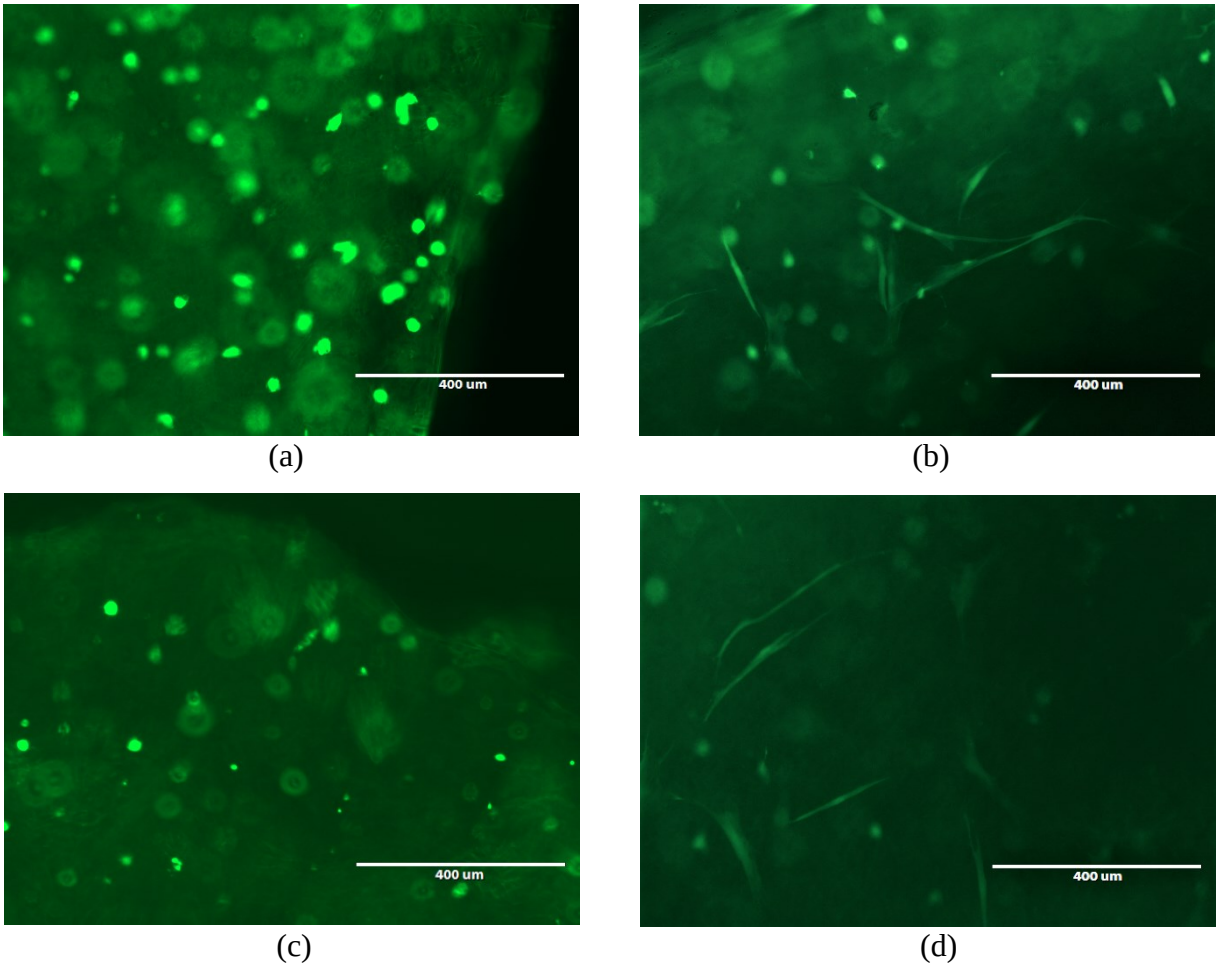

(a) (b)

(c) (d)

Figure 3.14. *Results of test with Calcein on G70-P0.5 sample prepared with casting method (a-b), and bioprinting (c-d) after 2 (a, c) and 8 (b, d) days from incubation; 10X magnification.*

Figure 3.14 shows samples prepared with both casting and bioprinting method and analyzed after 2 and 8 days of incubation, with Calcein marker. As expected, after two days MSCs retain a rounded shape and are in quite good conditions in the cast sample (Figure 3.14.a), while we observed higher autofluorescence and worse conditions in the bioprinted sample (Figure 3.14-c). The same situation occurred after 8 days (Figure 3.14.b, Figure 3.14.d); however, we observed the natural behavior of MSCs: they are less motile than SK-N-AS, but tend to stretch their cytoplasm along the porous structure.

To better visualize MSC behaviour, an experiment was carried out after 12 days of cell culture and analyzed with confocal microscopy (Figure 3.15), where we clearly observed the extended cytoplasm filaments of MSC. Cell viability differences between casting and bioprinting are still detected: one of the reasons may be ascribed to the cell culture media used. In particular, an aged culture media was the only available, which lead to a change in color from red to magenta, and therefore corresponds to a change in pH, fundamental for a good life cycle for cells.

However, after 12 days cellular activity is confirmed, as well as the absence of bacteriological contamination.

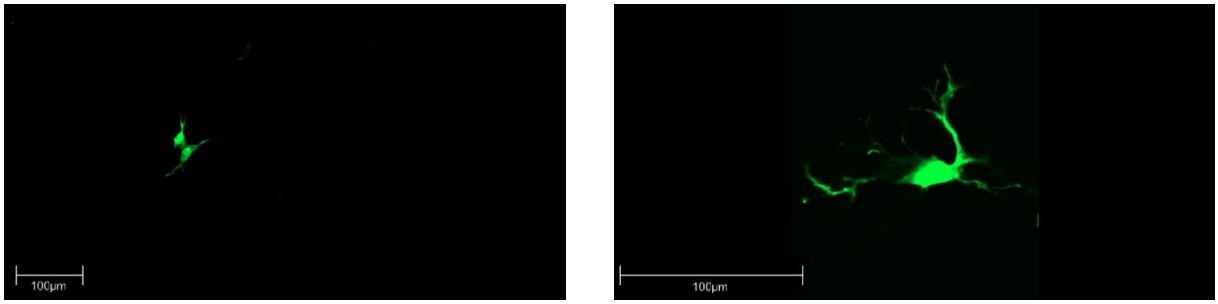

(a) (b)

Figure 3.15. *Results of tests on G70-P0.5 samples prepared with casting (a) and bioprinting (b) method, analyzed with confocal microscopy after 12 days from incubation: SK-N-AS cytoplasm marked in green by Calcein.*

From a biological standpoint, independently of the tested different cellular lines, high cells viability was verified even after 3 days of incubation in every sample; especially, vesicular apoptotic bodies, resulting from cells disassembly, were identified in samples with MSCs only. It should be anyway repeated that cell culture media may be the responsible for the low cellular activity. In fluorescence analysis images, cells nuclei and cytoplasm were clearly distinguished, suggesting that cells were encapsulated in a microenvironment favorable to their survival. Neuroblastoma cells (SK-N-AS) arranged in clusters even after 3 days of incubation, while yellow bone marrow-derived cells (MSC), showed extended cytoplasm after 8 days.

Conclusion

The aim of this thesis was the development of three-dimensional polymeric structures for studies on neuroblastoma cancer cells, through the production of printable gelatin methacrylate hydrogels and using micro extrusion bioprinting technologies.
GelMA-based hydrogels are widely used in biological applications of tissue engineering and cell culture studies in general. GelMA-based hydrogels were thus selected as suitable materials to replicate a favourable environment for growth and proliferation of two cell lines: neuroblastoma human cells (SK-N-AS) and yellow marrow bone-derived mesenchymal stem cells (MSC).

Starting from previous results [2], several subtargets were set and pursued. First, we showed how GelMA degree of functionalization (DoF) can be opportunely fine-tuned with selected changes in concentration of methacrylic acid (MAA), demonstrating the synthesis replicability, and overall protocol efficiency. In addition, we studied how the blending with different materials (i.e., Agarose, Pluronic F127), both natural and synthetic, could affect the morphology and behaviour of the hydrogels.

We characterized the swelling behavior and porosity of the hydrogels at varying DoF and when blended with secondary materials. Overall, 70% functionalized GelMA provides the best hydrogels in terms of crosslinks formation, stability and homogeneity. Swelling analysis showed no specific influence of Pluronic concentration tested (i.e., 0.1, 0.5, 1 %w/v) with respect to pure GelMA hydrogels.

Porosity analysis was then carried out using SEM imaging and analyzed in MATLAB, where an appropriate algorithm was set up to detect the mesh pores, with the aim of representing the pore size distribution and of estimating percent porosity. Results confirmed the influence of GelMA DoF on hydrogel morphology, showing an inverse corelation between DoF and mesh size (i.e., an increase in DoF corresponds to a decrease in pore size). Moreover, we showed how the super-porous honeycomb-like mesh can be enlarged with the addition of Agarose and Pluronic F127 at the three different concentrations reported above. Comparing pure GelMA hydrogels (with a 70% DoF) with the blends, we measured that the average of pore size radius increased from 11 μm, up to 15 μm (Agarose) and 19 μm (1% w/v Pluronic F127); the results refer to 70% functionalized GelMA, which provides the best hydrogels in terms of crosslinks

formation, stability and homogeneity. Also, the MATLAB algorithm performed poorly when analyzing hydrogels prepared with low DoF GelMA, suggesting both the need to improve the software and the lack of clearly defined pores in the materials.

While agarose was chosen for its high biocompatibility, Pluronic F127 was chosen for its reverse thermoreversibility and water-soluble properties. The main idea behind its use was to induce the formation of larger void structures in the hydrogel left by the dissolution of Pluronic micelles when immersed in an aqueous solution.
Among all three different concentrations, GelMA containing 0.5% w/v of Pluronic was chosen as the most suitable for 3D bioprinting.

Concerning bioprinting, an accurate fine-tuning of printing parameters was performed: the aim was to obtain a material with well-defined and appropriate viscosity, since mild extrusion pressure and long printing times are required. A thermal treatment was optimized, considering short cooling time and the desired viscosity. Extrusion pressures and cooling times must be optimized respecting all requirements necessary to avoid cell apoptosis. Optimized printing parameters confirmed GelMA-Pluronic hydrogels as an optimal material for 3D bioprinting, since they respect the required low extrusion pressures and cooling time.

We concluded that the GelMA super-porous structure led to permeability and cell viability issues for both pure GelMA and GelMA-Agarose blended-hydrogels. Moreover, bacterial contamination was detected in both cases, stimulating further investigations on the original synthesis protocol [2]. The proposed modifications allowed us to bypass all contamination issues and to preserve biological sterility.
The permeability issues were investigated with the use of GelMA-Pluronic 0.5% w/v samples prepared with both casting and bioprinting methods - comparing cell viability in both cases. Analysis with fluorescent markers of cell nuclei and cytoplasm were carried out with an optical microscope for up to 12 days of culture; cells were also observed with confocal microscopy. Results showed improvement in hydrogels permeability, which promoted the natural behaviour of the two different cell lines: after 10 days, SK-N-AS inclination to migrate and form clusters - possibly in the large voids left by Pluronic dissolution - is clearly observed; MSCs showed stretched cytoplasm after 8 days, with cytoplasmic filaments clearly observed after 12 days.

In general, better cell viability results were obtained for samples prepared with casting method, suggesting that further improvement in the bioprinting protocol is needed, together with a more in-depth investigation in cell viability tests with the use of supplementary fluorescent markers (e.g., Propidium Iodide, F-actin).

Appendix

A.1 H NMR spectra

The H NMR spectra, result of the analysis of GelMA samples from three synthesis batch, purified through dialysis and freeze-dried, are shown in . HNM R analysis and the estimation of degree of methacrylation were kindly performed by Professor Sgarbossa's research team.

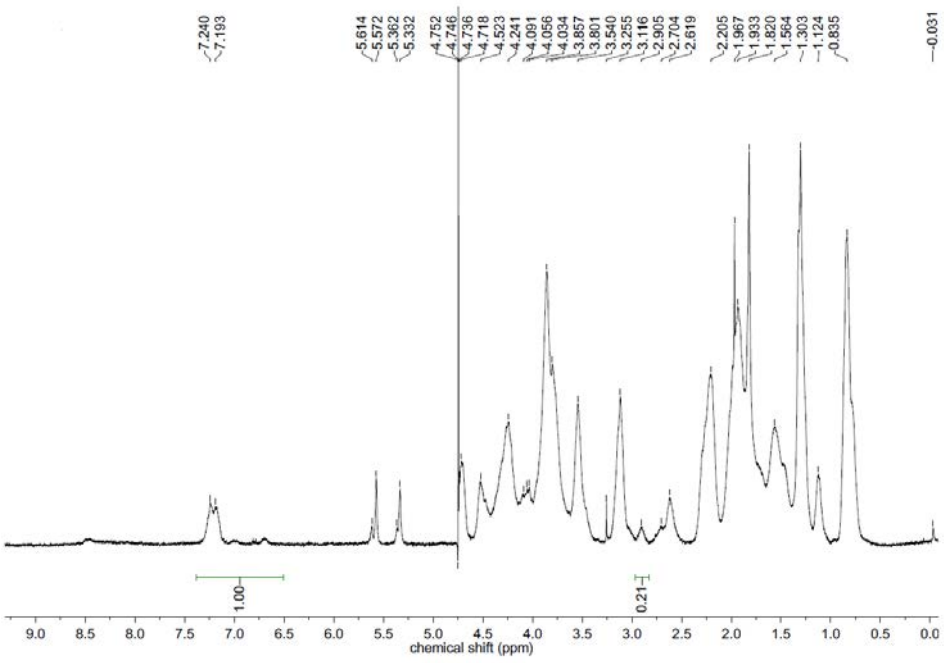

Figure A.1.1. *H NMR spectrum of synthetized GelMA from batch 1, purified through dialysis and freeze-dried. The estimated degree of functionalization of gelatin molecules is 70 ± 10%.*

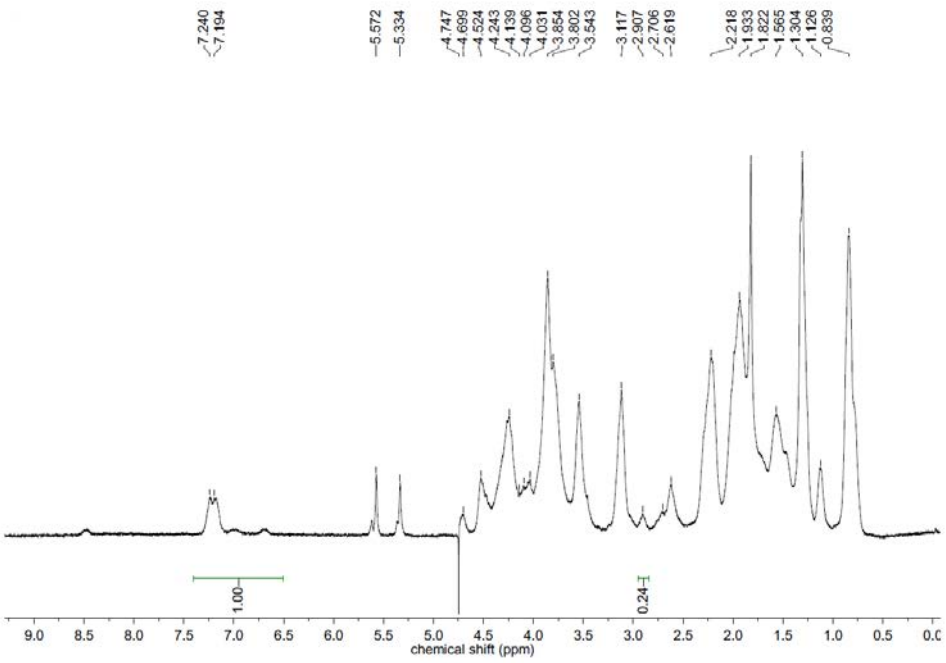

Figure A.1.2. *H NMR spectrum of synthetized GelMA from batch 1, purified through dialysis and freeze-dried. The estimated degree of functionalization of gelatin molecules is 66 ± 10%.*

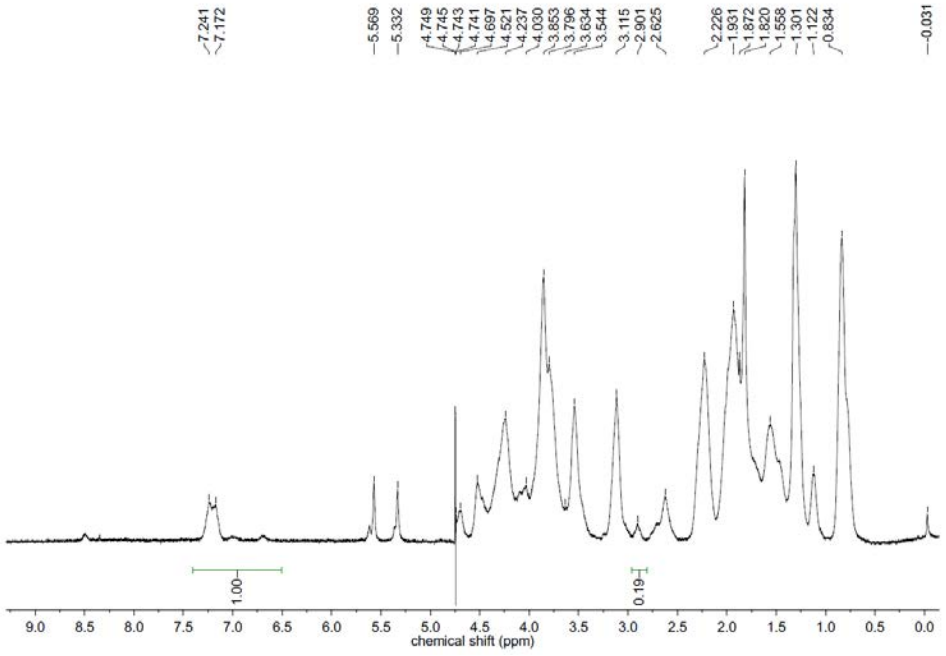

Figure A.1.3. *H NMR spectrum of synthetized GelMA from batch 2, purified through dialysis and freeze-dried. The estimated degree of functionalization of gelatin molecules is 73 ± 10%.*

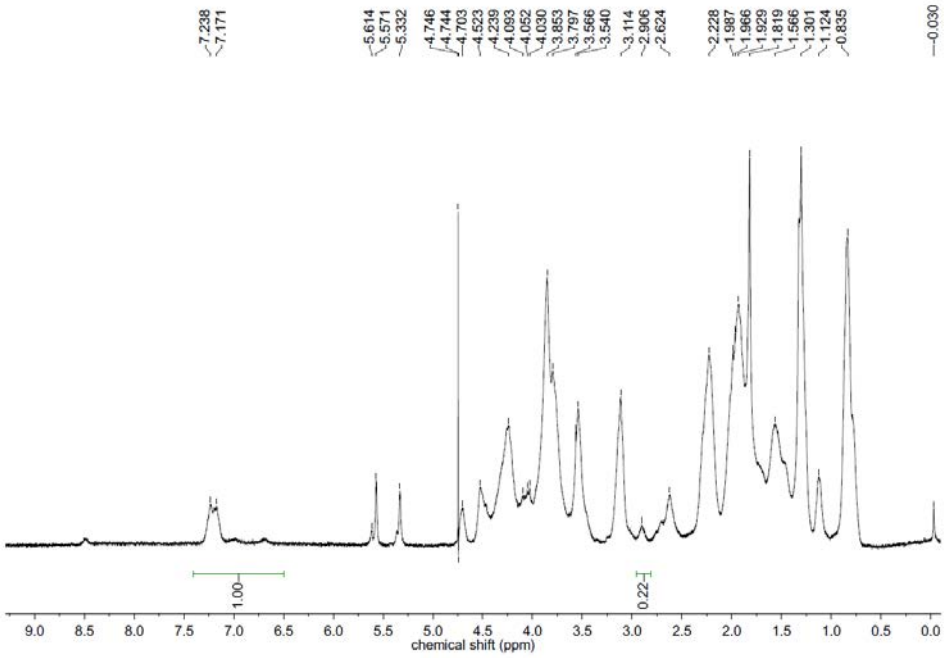

Figure A.1.4. *H NMR spectrum of synthetized GelMA from batch 2, purified through dialysis and freeze-dried. The estimated degree of functionalization of gelatin molecules is 69 ± 10%.*

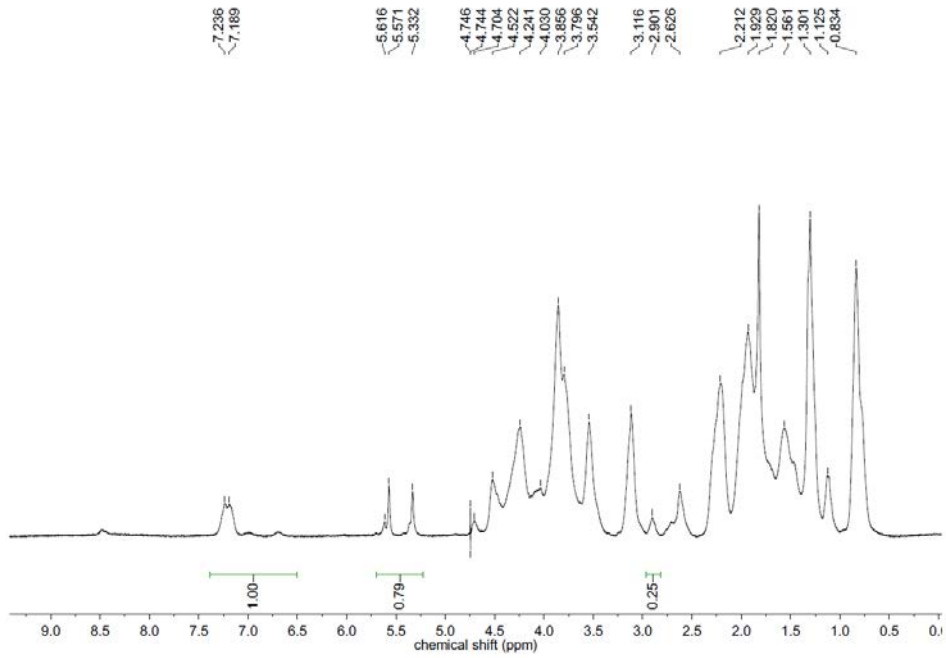

Figure A.1.5. *H NMR spectrum of synthetized GelMA from batch 3, purified through dialysis and freeze-dried. The estimated degree of functionalization of gelatin molecules is 64 ± 10%.*

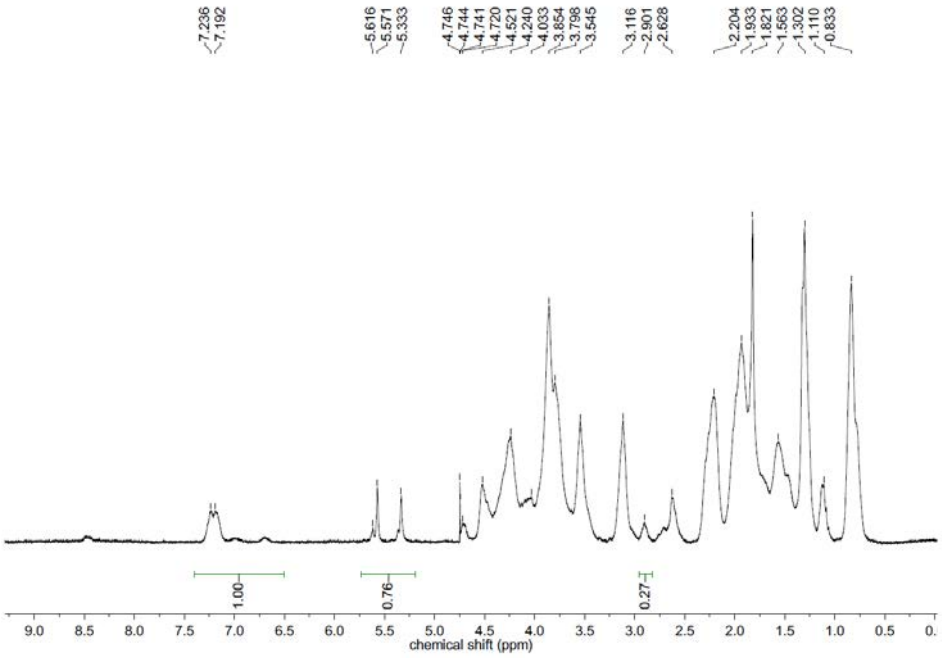

Figure A.1.6. *H NMR spectrum of synthetized GelMA from batch 3, purified through dialysis and freeze-dried. The estimated degree of functionalization of gelatin molecules is 61 ± 10%.*

Bibliography

[1] D. Lv, Z. Hu, L. Lu, H. Lu, X. Xu, Three-dimensional cell culture: A powerful tool in tumor research and drug discovery, Oncol. Lett. 14 (2017) 6999–7010. https://doi.org/10.3892/ol.2017.7134.

[2] G. Santi, PRODUCTION OF GELATIN METHACRYLATE, Master Thesis. Univ. Padua. (2020).

[3] E.M. Ahmed, Hydrogel: Preparation, characterization, and applications: A review, J. Adv. Res. 6 (2015) 105–121. https://doi.org/10.1016/j.jare.2013.07.006.

[4] F. Ganji, S. Vasheghani-Farahani, E. Vasheghani-Farahani, Theoretical description of hydrogel swelling: A review, Iran. Polym. J. (English Ed. 19 (2010) 375–398.

[5] S. Hernandez, D. Davenport, Nanocomposite Membranes for Water Purification Dibakar Bhattacharyya , PhD, (2015).

[6] S. Cai, Y. Hu, X. Zhao, Z. Suo, Poroelasticity of a covalently crosslinked alginate hydrogel under compression, J. Appl. Phys. 108 (2010). https://doi.org/10.1063/1.3517146.

[7] P.J. Flory, J. Rehner, Statistical mechanics of cross-linked polymer networks II. Swelling, J. Chem. Phys. 11 (1943) 521–526. https://doi.org/10.1063/1.1723792.

[8] N.A. Peppas, P. Bures, W. Leobandung, H. Ichikawa, Hydrogels in pharmaceutical formulations, Eur. J. Pharm. Biopharm. 50 (2000) 27–46. https://doi.org/10.1016/S0939-6411(00)00090-4.

[9] F. Ganji, M.J. Abdekhodaie, Synthesis and characterization of a new thermosensitive chitosan-PEG diblock copolymer, Carbohydr. Polym. 74 (2008) 435–441. https://doi.org/10.1016/j.carbpol.2008.03.017.

[10] H. Hosseinkhani, M. Hosseinkhani, Biodegradable Polymer-Metal Complexes for Gene and Drug Delivery, Curr. Drug Saf. 4 (2009) 79–83. https://doi.org/10.2174/157488609787354477.

[11] H. Hosseinkhani, M. Hosseinkhani, H. Kobayashi, Design of tissue-engineered nanoscaffold through self-assembly of peptide amphiphile, J. Bioact. Compat. Polym. 21 (2006) 277–296. https://doi.org/10.1177/0883911506066934.

[12] H. Hosseinkhani, M. Hosseinkhani, A. Khademhosseini, H. Kobayashi, Y. Tabata, Enhanced angiogenesis through controlled release of basic fibroblast growth factor from peptide amphiphile for tissue regeneration, Biomaterials. 27 (2006) 5836–5844. https://doi.org/10.1016/j.biomaterials.2006.08.003.

[13] D. Gao, H. Xu, M.A. Philbert, R. Kopelman, Ultrafine hydrogel nanoparticles: Synthetic approach and therapeutic application in living cells, Angew. Chemie - Int. Ed. 46 (2007) 2224–2227. https://doi.org/10.1002/anie.200603927.

[14] E. Vasheghani-Farahani, D.G. Cooper, J.H. Vera, M.E. Weber, Concentration of large biomolecules with hydrogels, Chem. Eng. Sci. 47 (1992) 31–40. https://doi.org/10.1016/0009-2509(92)80197-K.

[15] R. Panahi, E. Vasheghani-Farahani, S.A. Shojaosadati, Separation of l-lysine from dilute aqueous solution using molecular imprinting technique, Biochem. Eng. J. 35 (2007) 352–356. https://doi.org/10.1016/j.bej.2007.01.027.

[16] J. Aalaie, E. Vasheghani-Farahani, A. Rahmatpour, M.A. Semsarzadeh, Effect of montmorillonite on gelation and swelling behavior of sulfonated polyacrylamide nanocomposite hydrogels in electrolyte solutions, Eur. Polym. J. 44 (2008) 2024–2031. https://doi.org/10.1016/j.eurpolymj.2008.04.031.

[17] J. Aalaie, A. Rahmatpour, E. Vasheghani-Farahani, Rheological and swelling behavior of semi-interpenetrating networks of polyacrylamide and scleroglucan, Polym. Adv. Technol. 20 (2009) 1102–1106. https://doi.org/10.1002/pat.1369.

[18] L. Yang, J.S. Chu, J.A. Fix, Colon-specific drug delivery: New approaches and in vitro/in vivo evaluation, Int. J. Pharm. 235 (2002) 1–15. https://doi.org/10.1016/S0378-5173(02)00004-2.

[19] Z. Maolin, L. Jun, Y. Min, H. Hongfei, The swelling behavior of radiation prepared semi-interpenetrating polymer networks composed of polyNIPAAm and hydrophilic polymers, Radiat. Phys. Chem. 58 (2000) 397–400. https://doi.org/10.1016/S0969-806X(99)00491-0.

[20] H. Omidian, K. Park, Biomedical Applications of Hydrogels Handbook, Biomed. Appl. Hydrogels Handb. (2010) 1–16. https://doi.org/10.1007/978-1-4419-5919-5.

[21] M.W. Tibbitt, K.S. Anseth, Hydrogels as extracellular matrix mimics for 3D cell culture, Biotechnol. Bioeng. 103 (2009) 655–663. https://doi.org/10.1002/bit.22361.

[22] M.C. Catoira, L. Fusaro, D. Di Francesco, M. Ramella, F. Boccafoschi, Overview of natural hydrogels for regenerative medicine applications, J. Mater. Sci. Mater. Med. 30 (2019). https://doi.org/10.1007/s10856-019-6318-7.

[23] G.-F. Xiong, R. Xu, Function of cancer cell-derived extracellular matrix in tumor progression, J. Cancer Metastasis Treat. 2 (2016) 357. https://doi.org/10.20517/2394-4722.2016.08.

[24] R.J. Seager, C. Hajal, F. Spill, R.D. Kamm, M.H. Zaman, Dynamic interplay between tumour, stroma and immune system can drive or prevent tumour progression, ArXiv. (2017). https://doi.org/10.1088/2057-1739/aa7e86.

[25] R.F. Pereira, P.J. Bártolo, Manufacturing of advanced biodegradable polymeric components, J. Appl. Polym. Sci. 132 (2015). https://doi.org/10.1002/app.42889.

[26] S. V. Murphy, A. Atala, 3D bioprinting of tissues and organs, Nat. Biotechnol. 32 (2014) 773–785. https://doi.org/10.1038/nbt.2958.

[27] V. Keriquel, H. Oliveira, M. Rémy, S. Ziane, S. Delmond, B. Rousseau, S. Rey, S. Catros, J. Amédée, F. Guillemot, J.C. Fricain, In situ printing of mesenchymal stromal cells, by laser-assisted bioprinting, for in vivo bone regeneration applications, Sci. Rep. 7 (2017) 1–10. https://doi.org/10.1038/s41598-017-01914-x.

[28] G. Cidonio, M. Glinka, J.I. Dawson, R.O.C. Oreffo, The cell in the ink: Improving biofabrication by printing stem cells for skeletal regenerative medicine, Biomaterials. 209 (2019) 10–24. https://doi.org/10.1016/j.biomaterials.2019.04.009.

[29] K. Yue, G. Trujillo-de Santiago, M.M. Alvarez, A. Tamayol, N. Annabi, A. Khademhosseini, Synthesis, properties, and biomedical applications of gelatin methacryloyl (GelMA) hydrogels, Biomaterials. 73 (2015) 254–271. https://doi.org/10.1016/j.biomaterials.2015.08.045.

[30] G. Ying, N. Jiang, C. Yu, Y.S. Zhang, Three-dimensional bioprinting of gelatin methacryloyl (GelMA), Bio-Design Manuf. 1 (2018) 215–224. https://doi.org/10.1007/s42242-018-0028-8.

[31] W. Jia, P.S. Gungor-Ozkerim, Y.S. Zhang, K. Yue, K. Zhu, W. Liu, Q. Pi, B. Byambaa, M.R. Dokmeci, S.R. Shin, A. Khademhosseini, Direct 3D bioprinting of perfusable vascular constructs using a blend bioink, Biomaterials. 106 (2016) 58–68. https://doi.org/10.1016/j.biomaterials.2016.07.038.

[32] H.W. Kang, S.J. Lee, I.K. Ko, C. Kengla, J.J. Yoo, A. Atala, A 3D bioprinting system to produce human-scale tissue constructs with structural integrity, Nat. Biotechnol. 34 (2016) 312–319. https://doi.org/10.1038/nbt.3413.

[33] P.S. Gungor-Ozkerim, I. Inci, Y.S. Zhang, A. Khademhosseini, M.R. Dokmeci, Bioinks for 3D bioprinting: An overview, Biomater. Sci. 6 (2018) 915–946. https://doi.org/10.1039/c7bm00765e.

[34] H.J. Lee, Y.B. Kim, S.H. Ahn, J.S. Lee, C.H. Jang, H. Yoon, W. Chun, G.H. Kim, A New Approach for Fabricating Collagen/ECM-Based Bioinks Using Preosteoblasts and Human Adipose Stem Cells, Adv. Healthc. Mater. 4 (2015) 1359–1368. https://doi.org/10.1002/adhm.201500193.

[35] Y. Loo, A. Lakshmanan, M. Ni, L.L. Toh, S. Wang, C.A.E. Hauser, Peptide Bioink: Self-Assembling Nanofibrous Scaffolds for Three-Dimensional Organotypic Cultures, Nano Lett. 15 (2015) 6919–6925. https://doi.org/10.1021/acs.nanolett.5b02859.

[36] D.B. Kolesky, K.A. Homan, M.A. Skylar-Scott, J.A. Lewis, Three-dimensional bioprinting of thick vascularized tissues, Proc. Natl. Acad. Sci. U. S. A. 113 (2016) 3179–3184. https://doi.org/10.1073/pnas.1521342113.

[37] A. Ribeiro, M.M. Blokzijl, R. Levato, C.W. Visser, M. Castilho, W.E. Hennink, T. Vermonden, J. Malda, Assessing bioink shape fidelity to aid material development in 3D bioprinting, Biofabrication. 10 (2018) 0–21. https://doi.org/10.1088/1758-5090/aa90e2.

[38] T. Ahlfeld, G. Cidonio, D. Kilian, S. Duin, A.R. Akkineni, J.I. Dawson, S. Yang, A. Lode, R.O.C. Oreffo, M. Gelinsky, Development of a clay based bioink for 3D cell printing for skeletal application, Biofabrication. 9 (2017). https://doi.org/10.1088/1758-5090/aa7e96.

[39] D. Chimene, C.W. Peak, J.L. Gentry, J.K. Carrow, L.M. Cross, E. Mondragon, G.B. Cardoso, R. Kaunas, A.K. Gaharwar, Nanoengineered Ionic-Covalent Entanglement (NICE) Bioinks for 3D Bioprinting, ACS Appl. Mater. Interfaces. 10 (2018) 9957–9968. https://doi.org/10.1021/acsami.7b19808.

[40] J. Yin, M. Yan, Y. Wang, J. Fu, H. Suo, 3D Bioprinting of Low-Concentration Cell-Laden Gelatin Methacrylate (GelMA) Bioinks with a Two-Step Cross-linking Strategy, ACS Appl. Mater. Interfaces. 10 (2018) 6849–6857. https://doi.org/10.1021/acsami.7b16059.

[41] W. Liu, M.A. Heinrich, Y. Zhou, A. Akpek, N. Hu, X. Liu, X. Guan, Z. Zhong, X. Jin, A. Khademhosseini, Y.S. Zhang, Extrusion Bioprinting of Shear-Thinning Gelatin Methacryloyl Bioinks, Adv. Healthc. Mater. 6 (2017) 1–11. https://doi.org/10.1002/adhm.201601451.

[42] Z. Wang, H. Kumar, Z. Tian, X. Jin, J.F. Holzman, F. Menard, K. Kim, Visible Light Photoinitiation of Cell-Adhesive Gelatin Methacryloyl Hydrogels for Stereolithography 3D Bioprinting, ACS Appl. Mater. Interfaces. 10 (2018) 26859–26869. https://doi.org/10.1021/acsami.8b06607.

[43] B.J. Klotz, D. Gawlitta, A.J.W.P. Rosenberg, J. Malda, F.P.W. Melchels, Gelatin-Methacryloyl Hydrogels : Towards Biofabrication-Based Tissue Repair, xx (2016) 1–14.

[44] D. Wu, Y. Yu, J. Tan, L. Huang, B. Luo, L. Lu, C. Zhou, 3D bioprinting of gellan gum and poly (ethylene glycol) diacrylate based hydrogels to produce human-scale constructs with high-fidelity, Mater. Des. 160 (2018) 486–495. https://doi.org/10.1016/j.matdes.2018.09.040.

[45] Y. Huang, X.F. Zhang, G. Gao, T. Yonezawa, X. Cui, 3D bioprinting and the current applications in tissue engineering, Biotechnol. J. 12 (2017). https://doi.org/10.1002/biot.201600734.

[46] E. Axpe, M.L. Oyen, Applications of alginate-based bioinks in 3D bioprinting, Int. J. Mol. Sci. 17 (2016). https://doi.org/10.3390/ijms17121976.

[47] Y. Luo, G. Luo, M. Gelinsky, P. Huang, C. Ruan, 3D bioprinting scaffold using alginate/polyvinyl alcohol bioinks, Mater. Lett. 189 (2017) 295–298. https://doi.org/10.1016/j.matlet.2016.12.009.

[48] A.C. Daly, S.E. Critchley, E.M. Rencsok, D.J. Kelly, A comparison of different bioinks for 3D bioprinting of

fibrocartilage and hyaline cartilage, Biofabrication. 8 (2016) 1–10. https://doi.org/10.1088/1758-5090/8/4/045002.

[49] H. Lee, D.W. Cho, One-step fabrication of an organ-on-a-chip with spatial heterogeneity using a 3D bioprinting technology, Lab Chip. 16 (2016) 2618–2625. https://doi.org/10.1039/c6lc00450d.

[50] W. Liu, Y.S. Zhang, M.A. Heinrich, F. De Ferrari, H.L. Jang, S.M. Bakht, M.M. Alvarez, J. Yang, Y.C. Li, G. Trujillo-de Santiago, A.K. Miri, K. Zhu, P. Khoshakhlagh, G. Prakash, H. Cheng, X. Guan, Z. Zhong, J. Ju, G.H. Zhu, X. Jin, S.R. Shin, M.R. Dokmeci, A. Khademhosseini, Rapid Continuous Multimaterial Extrusion Bioprinting, Adv. Mater. 29 (2017) 1–8. https://doi.org/10.1002/adma.201604630.

[51] I.T. Ozbolat, M. Hospodiuk, Current advances and future perspectives in extrusion-based bioprinting, Biomaterials. 76 (2016) 321–343. https://doi.org/10.1016/j.biomaterials.2015.10.076.

[52] T. Jungst, W. Smolan, K. Schacht, T. Scheibel, J. Groll, Strategies and Molecular Design Criteria for 3D Printable Hydrogels, Chem. Rev. 116 (2016) 1496–1539. https://doi.org/10.1021/acs.chemrev.5b00303.

[53] Q. Chai, Y. Jiao, X. Yu, Hydrogels for Biomedical Applications: Their Characteristics and the Mechanisms behind Them, Gels. 3 (2017) 6. https://doi.org/10.3390/gels3010006.

[54] B.H. Lee, H. Shirahama, N.J. Cho, L.P. Tan, Efficient and controllable synthesis of highly substituted gelatin methacrylamide for mechanically stiff hydrogels, RSC Adv. 5 (2015) 106094–106097. https://doi.org/10.1039/c5ra22028a.

[55] P.A. Levett, F.P.W. Melchels, K. Schrobback, D.W. Hutmacher, J. Malda, T.J. Klein, A biomimetic extracellular matrix for cartilage tissue engineering centered on photocurable gelatin, hyaluronic acid and chondroitin sulfate, Acta Biomater. 10 (2014) 214–223. https://doi.org/10.1016/j.actbio.2013.10.005.

[56] H. Wang, L. Zhou, J. Liao, Y. Tan, K. Ouyang, C. Ning, G. Ni, G. Tan, Cell-laden photocrosslinked GelMA-DexMA copolymer hydrogels with tunable mechanical properties for tissue engineering, J. Mater. Sci. Mater. Med. 25 (2014) 2173–2183. https://doi.org/10.1007/s10856-014-5261-x.

[57] S.R. Shin, S.M. Jung, M. Zalabany, K. Kim, P. Zorlutuna, S.B. Kim, M. Nikkhah, M. Khabiry, M. Azize, J. Kong, K.T. Wan, T. Palacios, M.R. Dokmeci, H. Bae, X. Tang, A. Khademhosseini, Carbon-nanotube-embedded hydrogel sheets for engineering cardiac constructs and bioactuators, ACS Nano. 7 (2013) 2369–2380. https://doi.org/10.1021/nn305559j.

[58] S.R. Shin, B. Aghaei-Ghareh-Bolagh, T.T. Dang, S.N. Topkaya, X. Gao, S.Y. Yang, S.M. Jung, J.H. Oh, M.R. Dokmeci, X. Tang, A. Khademhosseini, Cell-laden microengineered and mechanically tunable hybrid hydrogels of gelatin and graphene oxide, Adv. Mater. 25 (2013) 6385–6391. https://doi.org/10.1002/adma.201301082.

[59] A.I. Van Den Bulcke, B. Bogdanov, N. De Rooze, E.H. Schacht, M. Cornelissen, H. Berghmans, Structural and rheological properties of methacrylamide modified gelatin hydrogels, Biomacromolecules. 1 (2000) 31–38. https://doi.org/10.1021/bm990017d.

[60] H. Shirahama, B.H. Lee, L.P. Tan, N.J. Cho, Precise tuning of facile one-pot gelatin methacryloyl (GelMA) synthesis, Sci. Rep. 6 (2016) 1–11. https://doi.org/10.1038/srep31036.

[61] M.C. Gomez-Guillen, B. Gimenez, M.E. Lopez-Caballero, M.P. Montero, Functional and bioactive properties of collagen and gelatin from alternative sources: A review, Food Hydrocoll. 25 (2011) 1813–1827. https://doi.org/10.1016/j.foodhyd.2011.02.007.

[62] Y.H. Bae, S.W. Kim, Hydrogel delivery systems based on polymer blends, block co-polymers or interpenetrating networks, Adv. Drug Deliv. Rev. 11 (1993) 109–135. https://doi.org/10.1016/0169-409X(93)90029-4.

[63] D. Velasco, E. Tumarkin, E. Kumacheva, Microfluidic encapsulation of cells in polymer microgels, Small. 8 (2012)

1633–1642. https://doi.org/10.1002/smll.201102464.

[64] H. Iwata, T. Takagi, H. Amemiya, H. Shimizu, K. Yamashita, K. Kobayashi, T. Akutsu, Agarose for a bioartificial pancreas, J. Biomed. Mater. Res. 26 (1992) 967–977. https://doi.org/10.1002/jbm.820260711.

[65] J.Y. Xiong, J. Narayanan, X.Y. Liu, T.K. Chong, S.B. Chen, T.S. Chung, Topology evolution and gelation mechanism of agarose gel, J. Phys. Chem. B. 109 (2005) 5638–5643. https://doi.org/10.1021/jp044473u.

[66] M.A. Salati, J. Khazai, A.M. Tahmuri, A. Samadi, A. Taghizadeh, M. Taghizadeh, P. Zarrintaj, J.D. Ramsey, S. Habibzadeh, F. Seidi, M.R. Saeb, M. Mozafari, Agarose-Based biomaterials: Opportunities and challenges in cartilage tissue engineering, Polymers (Basel). 12 (2020) 1–15. https://doi.org/10.3390/POLYM12051150.

[67] J.M. Anderson, Biocompatibility and Bioresponse to Biomaterials, Elsevier Inc., 2019. https://doi.org/10.1016/b978-0-12-809880-6.00039-4.

[68] F. Sefat, T.I. Raja, M.S. Zafar, Z. Khurshid, S. Najeeb, S. Zohaib, E.D. Ahmadi, M. Rahmati, M. Mozafari, Nanoengineered biomaterials for cartilage repair, Elsevier Inc., 2018. https://doi.org/10.1016/B978-0-12-813355-2.00003-X.

[69] B.D. Ulery, L.S. Nair, C.T. Laurencin, Biomedical applications of biodegradable polymers, J. Polym. Sci. Part B Polym. Phys. 49 (2011) 832–864. https://doi.org/10.1002/polb.22259.

[70] L.S. Nair, C.T. Laurencin, Biodegradable polymers as biomaterials, Prog. Polym. Sci. 32 (2007) 762–798. https://doi.org/10.1016/j.progpolymsci.2007.05.017.

[71] C. Bougault, A. Paumier, E. Aubert-Foucher, F. Mallein-Gerin, Investigating conversion of mechanical force into biochemical signaling in three-dimensional chondrocyte cultures, Nat. Protoc. 4 (2009) 928–938. https://doi.org/10.1038/nprot.2009.63.

[72] J.M. Lee, W.Y. Yeong, Design and Printing Strategies in 3D Bioprinting of Cell-Hydrogels: A Review, Adv. Healthc. Mater. 5 (2016) 2856–2865. https://doi.org/10.1002/adhm.201600435.

[73] W.L. Ng, S. Wang, W.Y. Yeong, M.W. Naing, Erratum: Skin Bioprinting: Impending Reality or Fantasy? (Trends in Biotechnology (2016) 34(9) (689–699)(S0167779916300257)(10.1016/j.tibtech.2016.04.006)), Trends Biotechnol. 35 (2017) 278. https://doi.org/10.1016/j.tibtech.2016.08.009.

[74] D.B. Kolesky, R.L. Truby, A.S. Gladman, T.A. Busbee, K.A. Homan, J.A. Lewis, 3D bioprinting of vascularized, heterogeneous cell-laden tissue constructs, Adv. Mater. 26 (2014) 3124–3130. https://doi.org/10.1002/adma.201305506.

[75] M. Müller, J. Becher, M. Schnabelrauch, M. Zenobi-Wong, Printing thermoresponsive reverse molds for the creation of patterned two-component hydrogels for 3D cell culture., J. Vis. Exp. 99 (2013) 1–9. https://doi.org/10.3791/50632.

[76] M.E. Prendergast, R.D. Solorzano, D. Cabrera, Bioinks for biofabrication: current state and future perspectives, J. 3D Print. Med. 1 (2017) 49–62. https://doi.org/10.2217/3dp-2016-0002.

[77] R. Suntornnond, E.Y.S. Tan, J. An, C.K. Chua, A highly printable and biocompatible hydrogel composite for direct printing of soft and perfusable vasculature-like structures, Sci. Rep. 7 (2017) 1–11. https://doi.org/10.1038/s41598-017-17198-0.

[78] R. Suntornnond, J. An, C.K. Chua, Bioprinting of Thermoresponsive Hydrogels for Next Generation Tissue Engineering: A Review, Macromol. Mater. Eng. 302 (2017) 1–15. https://doi.org/10.1002/mame.201600266.

[79] M.R. Matanović, J. Kristl, P.A. Grabnar, Thermoresponsive polymers: Insights into decisive hydrogel characteristics,

mechanisms of gelation, and promising biomedical applications, Int. J. Pharm. 472 (2014) 262–275. https://doi.org/10.1016/j.ijpharm.2014.06.029.

[80] E. Gioffredi, M. Boffito, S. Calzone, S.M. Giannitelli, A. Rainer, M. Trombetta, P. Mozetic, V. Chiono, Pluronic F127 Hydrogel Characterization and Biofabrication in Cellularized Constructs for Tissue Engineering Applications, Procedia CIRP. 49 (2016) 125–132. https://doi.org/10.1016/j.procir.2015.11.001.

[81] S.F. Khattak, S.R. Bhatia, S.C. Roberts, Pluronic F127 as a cell encapsulation material: Utilization of membrane-stabilizing agents, Tissue Eng. 11 (2005) 974–983. https://doi.org/10.1089/ten.2005.11.974.

[82] W. Wu, A. Deconinck, J.A. Lewis, Omnidirectional printing of 3D microvascular networks, Adv. Mater. 23 (2011) 178–183. https://doi.org/10.1002/adma.201004625.

[83] L. Klouda, Thermoresponsive hydrogels in biomedical applications A seven-year update, Eur. J. Pharm. Biopharm. 97 (2015) 338–349. https://doi.org/10.1016/j.ejpb.2015.05.017.

[84] C.C. Chang, E.D. Boland, S.K. Williams, J.B. Hoying, Direct-write bioprinting three-dimensional biohybrid systems for future regenerative therapies, J. Biomed. Mater. Res. - Part B Appl. Biomater. 98 B (2011) 160–170. https://doi.org/10.1002/jbm.b.31831.

[85] S.J. Lee, K. Park, Synthesis and Characterization of Sol-Gel Phase-reversible Hydrogels Sensitive to Glucose, J. Mol. Recognit. 9 (1996) 549–557. https://doi.org/10.1002/(SICI)1099-1352(199634/12)9:5/6<549::AID-JMR299>3.0.CO;2-C.

[86] L. Brannon-Peppas, N.A. Peppas, Equilibrium swelling behavior of dilute ionic hydrogels in electrolytic solutions, J. Control. Release. 16 (1991) 319–329. https://doi.org/10.1016/0168-3659(91)90009-3.

[87] E. Hoch, C. Schuh, T. Hirth, G.E.M. Tovar, K. Borchers, Stiff gelatin hydrogels can be photo-chemically synthesized from low viscous gelatin solutions using molecularly functionalized gelatin with a high degree of methacrylation, J. Mater. Sci. Mater. Med. 23 (2012) 2607–2617. https://doi.org/10.1007/s10856-012-4731-2.

[88] W. Schuurman, P.A. Levett, M.W. Pot, P.R. van Weeren, W.J.A. Dhert, D.W. Hutmacher, F.P.W. Melchels, T.J. Klein, J. Malda, Gelatin-methacrylamide hydrogels as potential biomaterials for fabrication of tissue-engineered cartilage constructs, Macromol. Biosci. 13 (2013) 551–561. https://doi.org/10.1002/mabi.201200471.

[89] Y.C. Chen, R.Z. Lin, H. Qi, Y. Yang, H. Bae, J.M. Melero-Martin, A. Khademhosseini, Functional human vascular network generated in photocrosslinkable gelatin methacrylate hydrogels, Adv. Funct. Mater. 22 (2012) 2027–2039. https://doi.org/10.1002/adfm.201101662.

[90] A. Rabbani, S. Salehi, Dynamic modeling of the formation damage and mud cake deposition using filtration theories coupled with SEM image processing, J. Nat. Gas Sci. Eng. 42 (2017) 157–168. https://doi.org/10.1016/j.jngse.2017.02.047.

[91] A. Rabbani, S. Ayatollahi, R. Kharrat, N. Dashti, Estimation of 3-D pore network coordination number of rocks from watershed segmentation of a single 2-D image, Adv. Water Resour. 94 (2016) 264–277. https://doi.org/10.1016/j.advwatres.2016.05.020.

[92] A. Rabbani, S. Jamshidi, S. Salehi, An automated simple algorithm for realistic pore network extraction from micro-tomography images, J. Pet. Sci. Eng. 123 (2014) 164–171. https://doi.org/10.1016/j.petrol.2014.08.020.

[93] C.P. Ezeakacha, A. Rabbani, S. Salehi, A. Ghalambor, Integrated image processing and computational techniques to characterize formation damage, Proc. - SPE Int. Symp. Form. Damage Control. 2018-Febru (2018). https://doi.org/10.2118/189509-ms.

[94] I. Pepelanova, K. Kruppa, T. Scheper, A. Lavrentieva, Gelatin-methacryloyl (GelMA) hydrogels with defined degree

of functionalization as a versatile toolkit for 3D cell culture and extrusion bioprinting, Bioengineering. 5 (2018). https://doi.org/10.3390/bioengineering5030055.

[95] M. Mantovani, Synthesis , optimization and 3D bioprinting of gelatin methacrylate hydrogels for cell culture studies, 2019.

[96] J.B. Pawley, Handbook of biological confocal microscopy: Third edition, 2006. https://doi.org/10.1007/978-0-387-45524-2.